DEVELOPMENT AND ANALYSIS OF SOLAR ENERGY BASED MULTIGENERATION SYSTEMS

By

Sinan Ozlu

A Thesis Submitted in Partial Fulfillment

Of the Requirements for the Degree of Doctor of Philosophy

in

Mechanical Engineering

Faculty of Engineering and Applied Science

University of Ontario Institute of Technology (UOIT)

Oshawa, Ontario, Canada

© Sinan Ozlu, May 2015

Abstract

To reach sustainable development, humankind needs to be focused towards a low-carbon society. For this reason, there is a growing interest in optimizing the design of urban settlements by means of the exploitation of natural sources of energy such as solar, wind, geothermal and biomass energy. Research on multigeneration systems has been the subject of increasing interest in the last few decades in order to reduce energy consumption and achieve more sustainable and economic energy generation. A multigeneration energy production process refers to a system with more than three different purposes, including electricity, hydrogen, oxygen, cooling, heating, hot water, fresh water and air, synthetic fuels, and chemicals with same sources of the input energy.

In this thesis three novel multigeneration energy systems are introduced based on renewable resources such as solar and wind energy. In the hybrid system of solar and wind energy (System 1), energy is used for domestic hot water as well as for cooling by means of an absorption chiller. Electricity produced from a turbine in a Rankine cycle and wind turbine supply a multi-unit building, in addition to feeding an electrolyzer to produce hydrogen. In the second system (System 2), solar energy is used to feed a two stage Rankine cycle to supply domestic hot water for a multi-unit building and electricity for an electrolyzer to produce hydrogen. The waste heat of the steam Rankine cycle is used in ammonia-water Rankine cycle. Rankine cycle supplies electricity to the house and helps sea water desalination. In the third system (System 3), solar energy is used to produce electricity for a multi-unit building by Kalina cycle. A four stage absorption chiller runs on excessive energy for cooling. An electrolyzer produces hydrogen from the unused electricity. In addition, domestic hot water is also obtained from the system.

To analyze and compare these systems, a comprehensive thermodynamic model of each multigeneration system is defined, the second-law efficiencies, associated with the overall system and its components are determined and the effect of different configurations and operating conditions is analyzed. Exergoeconomic and exergoenvironmental analyses are conducted to understand the effects of key variables on the cost and the environment.

The results of the analyses show that, System 1 has a maximum energy efficiency of 43% and a maximum exergy efficiency of 65%, based on the produced maximum power of 48 kW which results in a CO_2 reduction of 1613 tons per year which a minimum cost of $236,024 using renewable energy as a source. System 2 has a maximum energy efficiency of 36% and a maximum exergy efficiency of 44% while producing a maximum power of 116 kW and reducing 4873 tons

of CO_2 per year at a minimum cost of $160,596. System 3 has a maximum energy efficiency of 47%, a maximum exergy efficiency of 88%, a 164 kW maximum power production and a CO_2 reduction of 2897 tons per year at a cost of $133,021.

Each system has different strengths and can be chosen according to the main purpose of the multigeneration system. This study undertook a comprehensive analysis and comparison of three systems powered by renewable resources. The study shows that it is possible to maintain a building utilizing these systems. Use of the systems in the future will also contribute eliminating fossil fuels and helping the environment.

Acknowledgement

I would like to thank Dr. Ibrahim Dincer for accepting me as his student and in particular for providing unwavering support and motivating me to pursue my research. His office has always been open to me, and on many occasions he has amended his schedule to accommodate my requests for assistance and support. He has always encouraged me to do better, even when I was less than satisfactory. I am deeply honored to know him as a person, as a mentor and above all as a teacher. His ability to impart knowledge makes him perhaps the finest example of a teacher I ever had the pleasure to know.

I am especially grateful to my friends Tahir Ratlamwala and Hasan Ozcan for helping me in the development of the EES code for an absorption chiller, Calin Zamfirescu for guiding me with his deep knowledge and Md. Ali Tarique for supplying me his experimental data about his experimental trigeneration cycle.

I sincerely appreciate Colm Doyle's help in correcting the grammatical errors of my thesis.

Last but not least I would like to thank three wonderful women in my life; my wife Svetlana, my mother Fethiye and my grandmother Mebrure for their continuous support and blessings during my research and continuing professional development.

Table of Contents

List of Tables

List of Figures

Nomenclature

A	area, m^2
c	specific heat, kJ/kgK
C	power coefficient
$\dot{C}$	cost rate, $/h
d	cost per exergy, $/kWh
D	diameter, m
E	heat removal factor
$\dot{Ex}$	exergy rate, kW
f	flashing temperature, K
F	view factor;
F'	collector efficiency factor
g	gravitational acceleration, 9.81 m/s^2
G	solar radiation rate, W/m^2
h	specific enthalpy, kJ/kg
H	heat transfer coefficient, W/m^2K
k	conductivity of the absorber tube material, W/mK
K	condenser cost constant
I	solar flux, W/m^2
l	length, m
L	latent heat, kJ/kg
$\dot{m}$	mass flow rate, kg/s
N	number of stages
$\dot{p}$	power, kW
P	pressure, kPa
Q	heat, kJ
$\dot{Q}$	heat transfer rate, kW
s	specific entropy, kJ/kgK
S	absorbed solar radiation per unit aperture area, W/m^2
$\dot{S}$	entropy rate, kW
t	time, s

T	temperature, K
U	heat transfer coefficient, W/m^2K
v	volume flow rate, m^3/kg
V	velocity, m/s
w	width, m
W	work, kJ
$\dot{W}$	work rate, kW
x	ammonia mass fraction
z	elevation, m
Z	expenses of investment, $

Greek letters

α	absorptivity
β	capital recovery factor
η	efficiency
γ	operating and maintenance costs excluding fuel, $
τ	annual system operation time at the nominal capacity, h
ξ	insulation thickness, m
ρ	density, kg/m^3

Subscripts

abs	absorption
ap	aperture
ch	chemical
chx	condenser heat exchanger
coll	collector
con	condenser
cv	control volume
d	destructed
dt	distillate
dwh	domestic water heater

e	exit stream
elec	electrolyzer
en	energy
eva	evaporator
ex	exergy
exp	expander
f	feed
gen	generator
he	heat exchanger
hhx	high temperature heat exchanger
hp	high pressure
hs	hot storage
htg	high temperature generator
in	inlet
j	index for exit streams
k	index for inlet streams
kc	Kalina cycle
L	overall
lhx	low temperature heat exchanger
ln	logarithmic
lp	low pressure
ltg	low temperature generator
mtg	medium temperature generator
out	outlet
p	pump
ph	physical
pr	pressure
Q	heat
r	Rankine
rb	recirculated brine
rc	ammonia-water Rankine cycle

re	receiver
s	storage
sc	solar cycle
st	steam
t	turbine
tb	top brine
te	tube
th	throttle
ts	thermal storage
u	unshaded
v	vaporization
vhhx	very high temperature heat exchanger
vlhx	very low temperature heat exchanger
vhth	very high temperature generator
vltg	very low temperature generator
w	wind
wt	wind turbine
0	ambient or reference condition
1..70	state numbers

Acronyms

CHP	combined heat and power
CHX	condenser heat exchanger
CTHX	cold temperature heat exchanger
COP	coefficient of performance
EES	Engineering Equation Solver
HAWT	horizontal axis wind turbine
HTHX	high temperature heat exchanger
HD	humidification-dehumidification
HHV	higher heating value
HTG	high temperature generator

LHX	low temperature heat exchanger
LTG	low temperature generator
MED	multi-effect distillation
MM	molar mass
MSF	multi-stage-flash
MTG	medium temperature generator
MTHX	medium temperature heat exchanger
MVC	mechanical vapor compression
ORC	organic Rankine cycle
PEM	proton exchange membrane
PR, PPR	pump pressure ratio
PV	photovoltaic
SOFC	solid oxide fuel cell
TES	Thermal Energy Storage
VAWT	vertical axis wind turbine
VHHX	very high temperature heat exchanger
VHTG	very high temperature generation

Chapter 1: Introduction

1.1 Overview

Energy in the world has become more important as we strive to develop new technologies which help make our lives easier and more productive. Energy is needed everywhere, from transportation to housing, and plays a fundamental role in the world today. Civilization began when people found out how to use fire extensively. They burned wood and obtained high temperatures for melting metals, cooking and heating. Since wood was unable to meet the fuel demand, the industrial revolution began with the use of fossil fuels, e.g. oil, coal and gas [1]. Currently, much of the world's energy is derived from fossil fuels which are unsustainable resources [2]. Fossil fuel depletion and global warming are the two important concerns for the sustainability of energy systems in the future.

The demand for energy has been steadily rising despite limited availability of non-renewable fuel resources [3]. There are alternative energy options to fossil fuels, such as solar, geothermal, hydropower, wind and biomass energy. Most energy supplies on earth derive from the sun, which continually warms us and supports plant growth via photosynthesis. Solar energy heats the land and sea differentially causing winds and consequently waves. Solar energy also drives evaporation, which leads to rain and in turn hydropower [4]. Solar energy is a free renewable energy source with no gas emissions. The number of power plants operated partially or completely by solar energy has been increasing significantly [5]. The current use of solar energy for electricity generation is less than 1% of the global energy consumption. Despite tremendous efforts toward development of photovoltaic systems, high capital cost, modest conversion efficiency, and intermittency are major drawbacks for dominant use of solar energy [6]. Solar energy can be used to obtain electrical power directly through photovoltaic solar cells or indirectly through a solar thermal system.

A thermal system that produces cooling, heating, and power simultaneously from the same energy source is defined as a trigeneration system [7]. In trigeneration systems, the waste heat from a plant's prime mover, such as a gas turbine or a low temperature heat source such as solar energy is used for power generation, heating and cooling. Recently researchers have gone beyond trigeneration to produce more purposes like hot water, hydrogen and potable water using the same

prime mover. A system that can produce more than three purposes is called multigeneration energy system. It is completely reasonable that efficiency for multigeneration energy systems is higher than trigeneration because of producing hydrogen, potable and hot water [8]. Efforts to develop more efficient energy systems are becoming increasingly significant.

1.2 Exergetic and Environmental Aspects

Exergy analysis is a technique that uses the conservation of mass and conservation of energy principles together with the second law of thermodynamics for the analysis, design and improvement of energy and other systems [9].

Exergy is defined as the maximum amount of work that a system can produce in order to bring it to equilibrium with a reference environment through reversible processes [10]. Exergy is a measure to evaluate the potential of a system. Energy analysis, which is based on the first law of thermodynamics, often does not provide a clear picture of thermodynamic efficiency and losses [11]. Energy efficiencies are often misleading in that they do not always provide a measure of how nearly the performance of a system approaches optimum. Further, the thermodynamic losses which occur within a system (i.e., those factors which cause performance to deviate from optimum) often are not accurately identified and assessed with energy analysis. The results of energy analysis can indicate incorrect sections of the system where the main inefficiencies can be found, and a state of technological efficiency different than actually exists [12]. Exergy is not conserved like energy but rather it is destructed during the process. In addition, exergy consumption during the process is proportional to the entropy created due to irreversibilities. Exergy analysis is a useful tool because exergy efficiencies are a measure of how nearly the efficiency of a process approaches the ideal or optimum state. Therefore it is considered that exergy analysis is a more powerful tool than energy analysis [4].

Many environmental issues are caused by or related to the production, transformation and use of energy. Researchers and others can play a vital role in our planet's evolution by guiding the development of industrial society, in part by using exergy as a tool to reduce energy consumption and environmental degradation. Energy and exergy efficiencies have received increasing attention over the last couple of decades [12]. Increasing system efficiency minimizes environmental impacts. Following on this, the optimization of thermal systems has been an important subject in

recent years as an increase in the efficiency decreases the amount of fuel used and especially the release of carbon dioxide, which is one of the main components of the greenhouse gases [13].

1.3 Motivation

In the developed world, human life heavily depends on fossil fuels. Basic needs like heating, electricity, transportation are highly dependent on energy supplied by fossil fuels. The burning of fossil fuels causes the emissions of gases that pollute the environment and create global warming. Moreover, fossil fuels will be depleted one day. Other sources of energy need to be created if a global crisis of involving energy and the environment is to be avoided. Nuclear energy is an alternative but, as a result of a tsunami near Japan and the resultant 2011 Fukushima nuclear disaster, serious environmental concerns persist. Recycling nuclear waste continues to be a problem.

Renewable energy sources are the only clean and continuous energy solution to satisfy requirements. The main focus of researchers is the utilization of solar, wind and geothermal energy in the most efficient manner. Multigeneration systems that use renewable sources combine the power of clean energy with high efficiency. These systems are relatively new and expensive. As a result, very little research information is available. Integration of energy systems is expected to increase the thermal efficiency of the system, and help to supply different needs of a public unit. The lack of study, especially totally renewable based multigeneration energy systems to produce electricity, cooling, heating, hot water, hydrogen, oxygen and fresh water simultaneously has made the proposed systems quite interesting.

In this Ph.D. thesis, a comprehensive analysis is conducted on the three newly developed multigeneration energy systems based on renewable energy source. Each system is modeled thermodynamically to obtain the optimal energy and exergy efficiencies for the overall system. To have a better understanding of the system performance analysis, exergy analysis is a potential tool. Exergy analysis can investigate the areas of irreversibilities and recommend ways to improve the overall efficiency of the system. The optimal solution of altering the thermodynamic parameters is considered. The most efficient system by comparing various configurations for the same outcomes is proposed. Moreover, greenhouse gas emissions caused by the conventional energy systems that produce the same outcomes is calculated and compared with the studied systems.

The three systems utilize different subsystems to compare and evaluate the interaction of each. Subsystems that are studied are: Single and quadruple effect absorption chillers, steam and ammonia-water Rankine cycles, desalination system, electrolyzer, Kalina cycle, domestic water heater and thermal storage. For example although Kalina cycle is more efficient that Rankine cycle, it is less popular. As a result, less research results are available. To my knowledge, exergy analysis of these configurations has not previously been conducted. These systems will assist other system designers and this dissertation should prove a useful tool for future research.

1.4 Objectives

The originality of this Ph.D. research is to undertake comprehensive modeling, analysis and optimization of three novel renewable energy based multigeneration energy systems which have not been the subject of past research. This thesis consists of some main objectives as follows:

1. To build a model for three novel solar based multigeneration energy systems:
    - Thermodynamic modeling of a solar and wind based multigeneration system with hot and warm storage tanks, a single effect absorption chiller, ammonia-water Rankine cycle, domestic water heater and electrolyzer for hydrogen production.
    - Thermodynamic modeling of a solar based multigeneration system with hot storage tank, two stage steam Rankine cycle, two stage ammonia-water Rankine cycle, an electrolyzer for hydrogen production, sea water desalination and domestic water heater.
    - Thermodynamic modeling of a solar based multigeneration system with quadruple effect absorption chiller, Kalina cycle, domestic water heater and an electrolyzer for hydrogen production.
2. To carry out energy and exergy analyses of each multigeneration system.
3. To conduct exergoeconomic analyses for each multigeneration system.
    - Determination of cost of each line of the system.
    - Estimation of cost of exergy destruction of each component.
    - Calculation of purchase cost of each component.
    - Reckoning of exergoeconomic factor for each component.

4. To assess the environmental impact of the system. Calculating greenhouse gas emissions from those of conventional energy systems that produce the same outcomes with the systems in operation by giving the emphasis on carbon dioxide and comparing obtained. The objective is to show how much improvement is made by employing multigeneration systems instead of conventional separate units.
5. To perform optimization of multigeneration energy systems to find the best design parameters.
    - Proposing objective functions such as energy efficiency, exergy efficiency, and power output.
    - Applying the optimization methods based on some reasonable constraints.
    - Finding the best decision variables.

Chapter 2: Background and Literature Review

2.1 Introduction

In this chapter background and literature review will be introduced relating to the main concepts referred in this thesis such as cogeneration, trigeneration, multigeneration, solar energy, wind energy, geothermal energy, desalination, absorption chillers and Kalina cycle. Although there are a number of studies than those contained herein, only most recent and pertinent ones are highlighted.

2.2 Cogeneration

Cogeneration (also called combined heat and power generation (CHP)) is by definition the production of more than one useful form of energy (such as process heat and electric power) from the same energy source.

In heat engine cycles a portion of the heat is transferred to the working fluid. The remaining portion of the heat is rejected to rivers, lakes, oceans, or the atmosphere, as waste heat because its quality (or grade) is too low to be of any practical use. However many systems or devices, require energy input in the form of heat. This is generally referred to as process heat. Examples of industries that rely heavily on process heat are chemical, pulp and paper, oil production and refining, steel making, food processing, and textile industries. Process heat in these industries is usually supplied by steam at 500 to 700 kPa and 150 to 200°C. Energy is usually transferred to the steam by burning coal, oil, natural gas, or another fuel in a furnace. Therefore, it makes economical as well as engineering sense to use the already-existing work potential to produce power instead of letting it go to waste. This would result in a plant that produces electricity while meeting the process-heat requirements of certain industrial processes [14]. Figure 2.1 shows an example of an ideal cogeneration plant which uses the heat output for process heating purposes.

Earlier researchers studied cogeneration systems as a base for the further study of multigeneration systems. This section addresses some examples of those studies.

Abusoglu and Kanoglu [15] published a review about exergoeconomic analysis and optimization of combined heat and power production. Main thermodynamic methodologies available in literature are described and their advantages and disadvantages with respect to one another are compared and discussed.

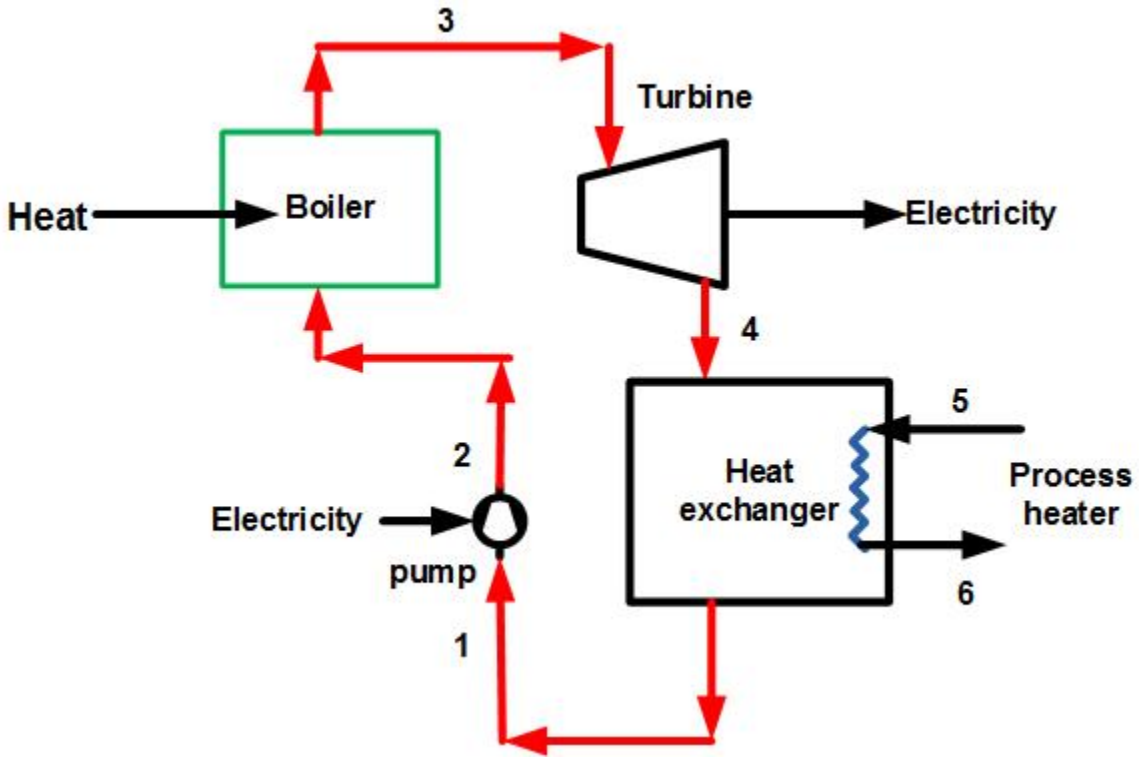

Figure 2.1 An ideal cogeneration plant

Ahmadi and Dincer [16] optimized a combined heat and power plant for cogeneration purposes that produces 50 MW of electricity and 33.3 kg/s of saturated steam at 1.3 MPa. They showed that by increasing the fuel cost, compressor isentropic efficiency, turbine isentropic efficiency and turbine inlet temperature increase.

Pavlas *et al.* [17] integrated renewable sources of energy into an existing combined heat and power system. After considering the technical and economic factors of the various design solutions obtained, and taking into account additional criteria such as the global trend of the price of crude oil and natural gas, electricity costs, and the political support for electric production from renewable sources, they determined two best alternatives. The preferred design utilizes an energy production plant with a biomass boiler. An alternative choice includes the use of a combined heat

and power energy plant that utilizes biomass as a fuel combined with a backpressure steam turbine for extraction.

2.3 Trigeneration

Trigeneration is a type of plant operation wherein the production of power, heating and cooling are all from the same source. In trigeneration plants, the waste heat from the plant prime mover is used to provide the energy needed for heating and cooling. A portion of the waste heat from the prime mover (e.g., gas turbine or diesel engine or organic Rankine cycle), is used for heating, for example to heat water to produce steam. The remaining portion of the waste heat is used for cooling, for example to cool air. The use of waste heat improves overall plant efficiency which, for a trigeneration plant, could reach as high as 80%, EPA-US [18].

Figure 2.2 describes trigeneration energy system which is composed of four major parts as follows:

- A power generation unit which is known as a prime mover (such as a gas turbine);
- A cooling unit, (such as a single-effect absorption chiller);
- A heating unit, such as the plant boiler;
- An electrical generator.

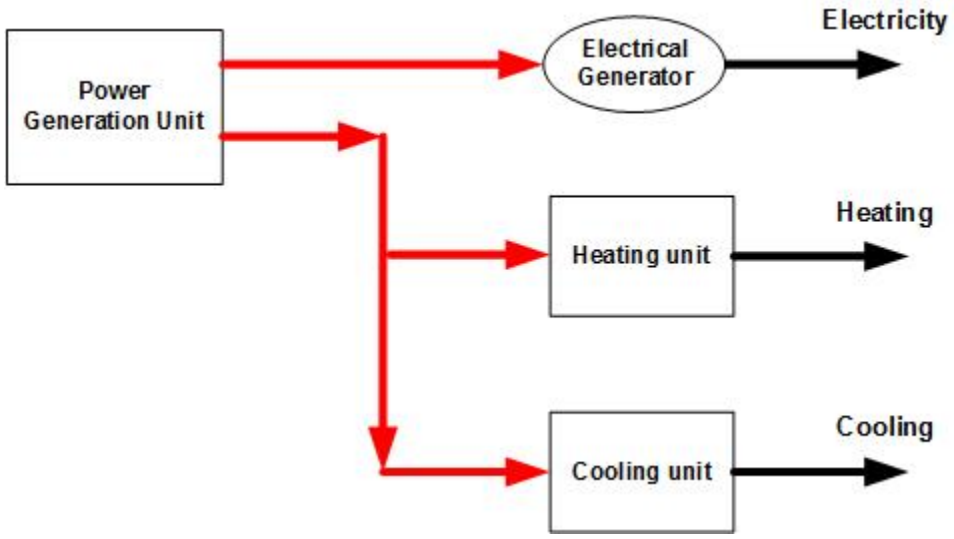

Figure 2.2 Schematic diagram of a typical trigeneration energy system

The energy process in a trigeneration plant can be described as follows:

- Mechanical power is produced from a mechanical power generator unit, such as a gas turbine.
- The mechanical power produced is used to rotate an electrical generator.
- Waste heat from the mechanical generator unit including exhaust gases.

It can be seen from Figure 2.2 that with a same prime mover heating, cooling and electricity can be produced simultaneously.

The results are then compared using a trigeneration system and for this reason, trigeneration systems are an integral part of this study. A detailed explanation of the experimental setup can be found in section 5.4.

Suleiman *et al.* [18] conducted energy analysis of a trigeneration plant based on solid oxide fuel cell (SOFC) and ORC. The results showed that there is at least a 22% gain in efficiency using the trigeneration plant compared with the power cycle (SOFC and ORC). Maximum efficiency of the trigeneration plant is found to be 74%. Maximum output provided by the trigeneration plant was 540 W. They also presented exergy and energy analyses of a biomass trigeneration system using an ORC [19]. They considered four cases for analysis: electrical-power, cooling-cogeneration, heating-cogeneration and trigeneration. The study revealed that there is a significant improvement when trigeneration is used as compared to only electrical power production. Fuel utilization efficiency increased from 12% for electrical power to 88% for trigeneration. Maximum exergy efficiency of the ORC increased from 13% to 28% when trigeneration is used.

Ahmadi *et al.* [3] modeled a trigeneration system for cooling, heating and electricity generation thermodynamically. Trigeneration system consists of a gas turbine cycle, an ORC, a single-effect absorption chiller and a domestic water heater. The exergy efficiency of the trigeneration system is found to be higher than that of typical combined heat and power systems or gas turbine cycles. The results also indicated that the carbon dioxide emissions for the trigeneration system are less than for the aforementioned systems. The parametric investigations showed that the compressor pressure ratio, the gas turbine inlet temperature and the gas turbine isentropic efficiency significantly affect the exergy efficiency and environmental impact of the trigeneration system.

Khaliq [20] analyzed a gas turbine trigeneration system for combined production of power heat and refrigeration. Thermodynamic analysis indicated that exergy destruction in a combustion chamber and heat recovery steam generator is significantly affected by the pressure ratio and turbine inlet temperature, and not at all affected by pressure drop and evaporator temperature.

Ahmadi *et al.* [21] modeled a trigeneration system for cooling, heating and electricity purposes thermodynamically. Trigeneration system consists of a gas turbine cycle, a steam turbine cycle and a single effect absorption chiller. The exergy efficiency is found to be higher than that for typical heat and power systems or gas turbine cycles. Also the carbon dioxide emissions for the trigeneration system are less than those for the compared systems.

Al-Suleiman *et al.* [22] compared three trigeneration systems using ORCs. They are SOFC-trigeneration, biomass-trigeneration and solar-trigeneration systems. The results showed that SOFC-trigeneration system has the highest electrical efficiency among the three systems. The trigeneration efficiencies are found as 76%, 90% and 90% respectively.

Temir and Bilge [23] analyzed a trigeneration plant thermodynamically. The system produces electrical power with a natural gas fed reciprocating engine and by making use of exhaust gases, yields absorption cooling.

2.4 Multigeneration Systems

Recently researchers have gone beyond trigeneration to produce more purposes like hot water, hydrogen and potable water using the same prime mover. The systems that can produce more than three purposes are called multigeneration energy systems.

Figure 2.3 shows an example of a multigeneration system. In this system solar energy is used as a source and heliostat field helps generating more heat. There is an absorption chiller for cooling, a Kalina cycle for electricity output, a domestic water heater and an electrolyzer for hydrogen production. The integrated Kalina cycle-absorption chiller system is equipped with a heliostat field solar collector and electrolyzer. This integrated system uses the heat from the sun, to provide hot water, which then drives a turbine in Kalina cycle to produce electricity. This in turn is used to drive an electrolyzer to produce hydrogen. After passing through the boiler, the

excess heat is used in the absorption chiller system to produce cooling effect. The working fluid is then pumped back to the solar collector, and the cycle is repeated continuously.

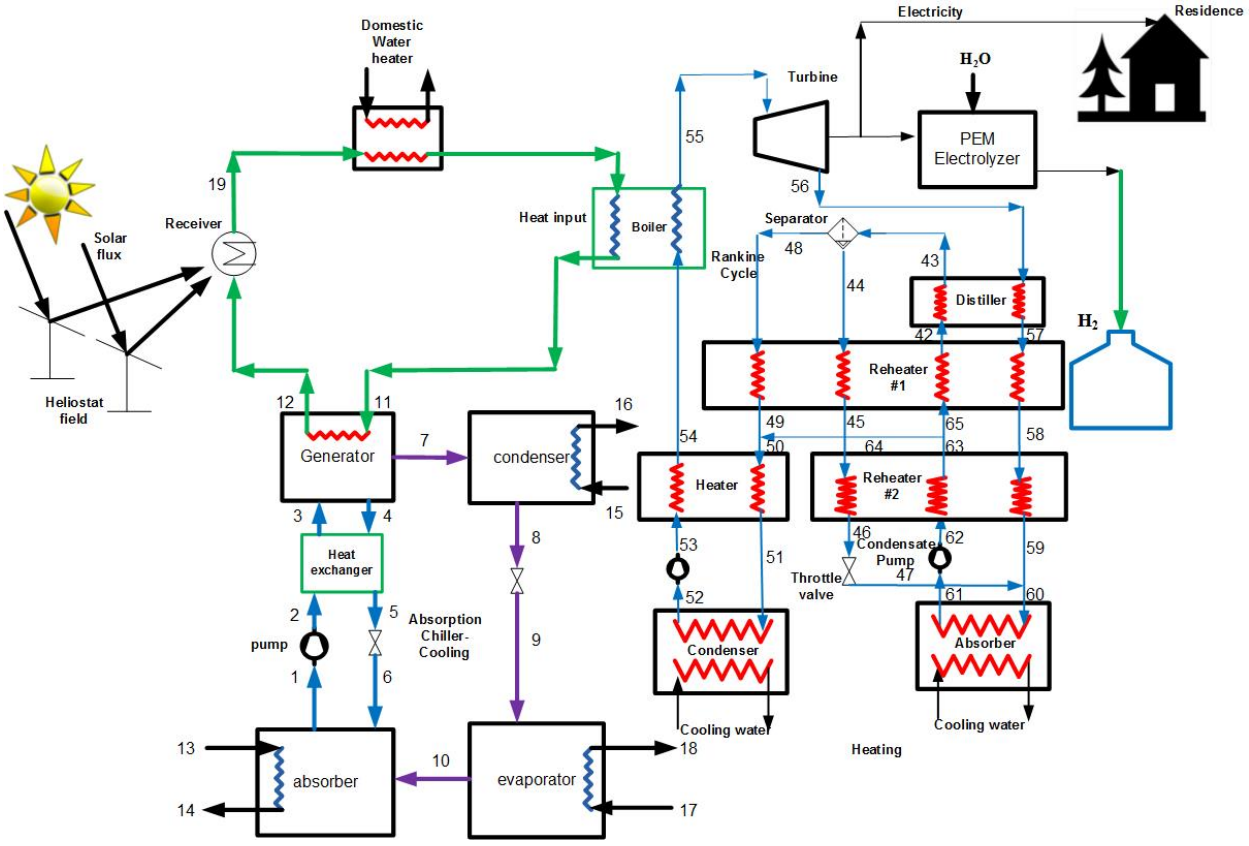

Figure 2.3 Schematic diagram of a multigeneration energy system

2.4.1 Solar Energy Based Multigeneration Systems

The amount of solar energy that reaches earth's upper atmosphere is about 1,350 W/m^2. The atmosphere reflects, scatters and absorbs some of the energy. In Canada, depending on sky conditions, peak solar intensity varies from about 900 W/m^2 to 1,050 W/m^2. Peak solar intensity is at solar noon, when the sun is due south [14].

The amount of the sun's energy reaching the surface of the earth also depends on cloud cover, air pollution, location and the time of year.

An active solar system uses mechanical equipment to collect, store and distribute heat from the sun. Active systems consist of solar collectors, a storage medium and a distribution system. Active solar systems are commonly used for:

- Water heating
- Space conditioning
- Producing electricity
- Processing heat
- Solar mechanical energy

When higher temperatures are required, concentrated solar collectors are used. Solar energy falling on a large reflective surface is reflected onto a smaller area before it is converted into heat. This is done so that the surface absorbing the concentrated energy is smaller than the surface capturing the energy and as a result can attain higher temperatures before heat loss due to radiation and the convection wastes of the energy that has been collected [17].

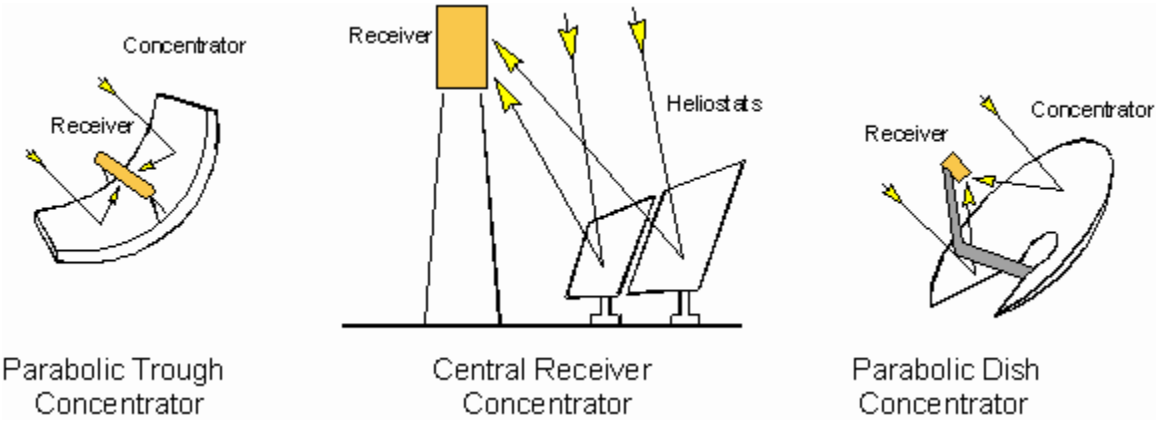

Figure 2.4 Three commonly used reflecting schemes for concentrating solar energy to attain high temperatures (adapted from [18])

Parabolic trough reflector systems use linear parabolic concentrators to focus sunlight onto a solar tubular receiver positioned along their focal line. Parabolic solar trough systems are usually aligned with their long axes from north to south. Solar energy is absorbed by a fluid in pipes located along the focal line. The maximum temperature of the heat transfer fluid does not exceed 450°C, which is insufficient to supply process heat for all steps in a thermochemical cycle. The heliostat solar tower uses arrays of two-axis tracking mirrors to reflect direct insolation onto a receiver/reactor mounted at the top of a centrally located tower. Heliostat solar tower has the

important advantage of reaching large generation capacities in a single unit that concentrates the reflections from thousands of mirrors. The temperature of the heat transfer fluid can reach up to 1000°C. In a parabolic dish system, a point focus collector tracks the sun along two axes, concentrating the insolation onto a receiver located at the focal point of the dish. Temperatures in excess of 1500°C can be achieved. The double concentration system consists of a heliostat field, the reflective tower, and a ground receiver equipped with a secondary concentrator.

PV/T systems which are used produce heat while its PV section produces only electricity and therefore are not a part of this study. Quantifying the performance of PV and PV/T is a challenge because these systems produce different types of energy: electrical and thermal respectively. In most applications, thermal and electrical energy do not have the same value. Thus, it is not straight-forward to compare the performance of two configurations that have different electrical and thermal yields. Delisle and Kummert [101] showed that for a water temperature at the heat exchanger inlet corresponding to 10 °C, PV systems produces 5–29% more equivalent useful thermal energy than the PV/T system

Optical efficiency from thermal measurements gives a maximum optical efficiency of 65%, while the theoretical optical efficiency is 71%, respectively. The difference is explained by thermal losses due to the limited fin-efficiency of the photovoltaic-thermal absorber and to reflector imperfections [103].

Most concentrating collectors can only concentrate the parallel insolation coming directly from the sun's disk (normal beam insolation), and must follow (track) the sun's path across the sky. Four types of solar concentrators are in common use; parabolic troughs, parabolic dishes, central receivers and Fresnel lenses. Figure 2.4 shows three of these concepts schematically [18]. The receiver/reactor on the ground can achieve temperatures in excess of 1300°C [26-28].

Various heat transfer fluids can be used with those solar systems; water, air and molten salt. Molten salt has an outstanding advantage as the heat transfer medium as the solar heat can be stored for tens of hours and used at night, or when sunlight is not available [26].

Ratlamwala *et al.* [29] proposed an integrated system, consisting of a heliostat field, a steam cycle, an ORC and an electrolyzer for hydrogen production. The results showed that the power and rate of hydrogen production increased with an increase in the heliostat field area and solar flux. The optimization study yielded maximum energy and exergy efficiencies and the rate of hydrogen production was 18.74%, 39.6% and 1.57 m^3/s respectively.

Ozturk and Dincer [30] worked on a renewable based multigeneration energy production system producing a number of outputs, such as power, heating, cooling, hot water, hydrogen and oxygen. The solar based multigeneration system which has an exergy efficiency of 57.4% is obtained to be higher than using the sub-systems separately. The parabolic dish collectors had the highest exergy destruction rate among constituent parts of the solar based multigeneration system due to a high temperature difference between the working fluid and collector receivers.

Ratlamwala *et al.* [31] assessed an integrated PV/T and triple effect cooling system for hydrogen and cooling production. The study is based on United Arab Emirates weather data; effect of average solar radiation for different months, operating time of the electrolyzer; air inlet temperature and area of the PV module on power; and rate of heat production, energy and exergy efficiencies, hydrogen production and energetic and exergetic COPs are studied.

Xu *et al.* [32] made an energy and exergy analysis of the solar power tower system using molten salt as the heat transfer fluid. They evaluated both the energy and exergy losses in each component and in the overall system to identify the causes and locations of the thermodynamic imperfections.

Ratlamwala *et al.* [33] conducted a parametric study of the triple effect absorption cooling system integrated with solar photo-voltaic/thermal, geothermal and Linde-Hampson cycle. They studied the effect of different operating parameters on the COPs, ratio ‘n’, amount of hydrogen gas pre-cooled, amount of hydrogen liquefied, and utilization factor of the integrated system.

Wang *et al.* [34] proposed a new combined cooling, heating and power system driven by solar energy. The system combines a Rankine cycle and an ejector refrigeration cycle, which could produce cooling output, heating output and power output simultaneously.

Ozcan and Dincer [35] analyzed and conducted a performance assessment of a solar driven hydrogen production plant running in an MG-Cl cycle through energy and exergy methods.

Ozturk and Dincer [36] addressed the thermodynamic assessment of a solar-based multigeneration system with coal gasification, involving power, heating, cooling, hydrogen, oxygen and hot water production.

Chua *et al.* [37] evaluated the potential of hybridizing renewable technologies to support trigeneration. The developed trigeneration system aimed to be self-sustaining where cooling, heating and power needs of a commercial building are simultaneously fulfilled.

Focus of attention has increased in recent times on solar energy based multigeneration systems and as a result more research is being conducted on these systems every year. This should result in finding new techniques, increase in the efficiencies and a decrease in operating costs.

2.4.2 Solar-Wind Hybrid Energy Based Multigeneration Systems

Electricity can be generated in many ways. In each case, a fuel is used to turn a turbine which drives a generator which in turn feeds the grid. The turbines are designed to suit the particular characteristics of the fuel. Wind generated electricity is no different. The wind is the fuel – unlike fossil fuels it is both free and clean, but otherwise it is just the same. It drives the turbine which generates electricity into a grid [38].

Modern commercial wind energy started in earnest in the early 1980s following the oil crises of the 1970s when issues of security and diversity of energy supply and, to a lesser extent, long-term sustainability, and generated interest in renewable energy sources. However, wind power technology raised questions about:

- Reliability
- Noise
- Efficiency
- Grid impact
- Visual and general environmental impact
- Potential for serious contribution to a national energy supply
- Cost

There are 2 kinds of designs which utilize the main axis of wind turbine, horizontal or vertical axis. Horizontal axis wind turbines (HAWT) are more widely. Vertical axis wind turbines (VAWT) are a new development. They have rotor blades that spin parallel to the ground, so that they can operate anywhere without having to account for the wind direction. This makes areas with volatile wind directions great locations for VAWTs. Because of the axis orientation, the gearbox and generator can be placed near the ground, eliminating the need for a high tower.

- For the same reason as above, VAWTs are easier to maintain since most of them are installed near the ground. HAWTs should be checked constantly so that they face against the wind. Automatic yaw-adjustment mechanisms have eliminated the need for constant maintenance on HAWTs.
- HAWTs require a tower be erect such that the rotor blades are placed in a high enough location that so as to maximize wind speeds, whilst VAWTs require guy cables to ensure that the machine remains stable. HAWTs require lesser land space compared to VAWTs, since tower bases occupy minimal space whilst the need for guy cables for VAWTs would entail occupying a much larger land area.

Utilization of solar and wind power has become increasingly significant, attractive and cost-effective, since the oil crises of the early 1970s. However, a common drawback with solar and wind energy is their unpredictable nature. Standalone photovoltaic (PV) or wind energy systems do not produce usable energy for a considerable portion of time during the year. This is mainly due to dependence on sunshine hours, which are variable. In the former case and on relatively high cut-in wind speeds, which range from 3.5 to 4.5 m/s, in the latter case, result in underutilization of capacity. In general, the variations of solar and wind energy do not match with the time distribution of demand. The independent use of the systems results in considerable over-sizing for system reliability, which in turn makes the design costly. As the advantages of solar and wind energy systems became widely known, system designers have started looking towards their integration [39]. The term hybrid renewable energy system is used to describe any energy system with more than one type of energy source to lower costs and increase reliability, compared to systems which use only one source of alternative energy.

Celik [40] addressed the sizing and techno-economic optimization of an autonomous PV-wind hybrid energy system with battery storage. The level of autonomy, i.e. the fraction of time for which the specified load can be met, and the cost of the system were his design parameters. He showed that the worst month scenarios prove too costly results so he suggested an alternative solution to incorporate a third energy source into the system.

Nema *et al.* [41], reviewed the current state of the design, operation and control requirement of the stand-alone PV solar-wind hybrid energy systems with conventional backup

source i.e. diesel or grid. They also highlighted future developments, which have the potential to increase the economic attractiveness of systems and their acceptance by the user.

Agustin and Lopez [42] revised the simulation and optimization techniques, as well as the existing tools that are needed to simulate and design stand-alone hybrid system for the generation of electricity. They considered stand-alone hybrid renewable energy systems such as PV-Wind-Battery and PV-Diesel-Battery.

Notton *et al.* [43] showed that a precise study of renewable energy potential is indispensable before implementing a renewable energy system. The solar and wind energy potential is presented for five sites distributed in a Mediterranean island and the temporal complementary of these two energy resources is discussed.

Caliskan *et al.* [44] performed exergoeconomic and environmental impact analyses, through energy, exergy and sustainability assessment methods to investigate a hybrid wind-solar based hydrogen and electricity production system.

Kaabeche *et al.* [45] proposed an integrated PV/wind hybrid system optimization model, which utilizes the iterative optimization technique following the deficiency and power supply probability, the relative excess power generated, the total net present cost, the total annualized cost and break-even distance analysis for power reliability and system costs.

Celik [46] addressed the sizing and techno-economic optimization of an autonomous PV-wind hybrid energy system with battery storage. A novel sizing method is introduced. He suggested that instead of increasing the hardware sizes excessively for the worst month, a third energy source be incorporated into the system and showed that this leads to greater techno-economic optimization.

Deshmukh and Deshmukh [47] described methodologies to model hybrid renewable energy systems components, their design and evaluation. They highlighted the issues related to penetration of these systems in the present distribution network.

Erdinc and Uzunoglu [48] provided a detailed analysis of optimum sizing approaches for hybrid renewable energy systems that can make significant contributions to wider renewable energy penetration by enhancing the system applicability in terms of economy.

Solar-wind hybrid systems are studied as these two sources complement each other in that if one is deficient or inactive the other system comes into effect. Optimization of the system by studying the behavior of solar and wind energy has been the main focus of the researchers in this subject.

2.4.3 Geothermal Energy Based Multigeneration Systems

Geothermal energy is an abundant, clean (effectively no green- house gas emissions) and reliable (renewable or sustainable) natural resource. The heat is generated by the natural decay over millions of years of radiogenic elements including uranium, thorium and potassium. Geothermal power has significant benefits. It is environmentally benign, renewable (temperature is renewed by conduction from adjacent hot rocks, heat is generated by natural radiogenic decay), and able to provide base-load power and heat for industrial processes. Geothermal resources that have been utilized, or are under consideration for development, range from shallow ground to hot water and rock several kilometers below the Earth's surface. In the last few years, the concept of geothermal energy has dramatically improved in its development, capabilities and application through the reforming of traditional thought and approaches. The most compelling feature of a geothermal energy process is that it produces zero carbon emissions, potentially making it one of the cleanest sources of energy at our disposal. Another compelling feature is that, unlike other renewable energy sources, it can create a constant 24 hours base-load power. For example, solar energy can only be produced during daylight hours, but is diminished with cloud cover. Similarly, wind turbines are dependent on wind speed which is inherently variable [49].

It is important to consider geothermal energy based multigeneration systems because their source is in the same range of temperature as solar energy or excessive energy from thermal plants and can be modified as appropriate.

Ratlamwala *et al.* [50] proposed a novel integrated geothermal based binary multi-stage power generating and quadruple effect absorption system for cooling, heating, power, and hot water production. It is found that increasing geothermal source temperature and concentration of ammonia in vapor leaving a very high temperature generator results in improved performance of the overall system.

Coskun *et al.* [51] analyzed geothermal based multigeneration systems with seven different combinations for practical applications. The systems considered are examined under two distinct main groups for heating and cooling periods. The analysis results showed that overall system energy and exergy efficiency are increased by 3.40 and 1.12 times for cooling season and 4.25 and 1.25 times for heating season, as compared to the single power generating option.

Desideri and Bidini [52] examined three configurations of the Rankine cycle and compared them to conventional single and dual flash steam power steam plants. The results showed that there is a potential for optimization of performance, by modifying the main parameters, such as turbine inlet pressure and type of fluid.

Ozgener *et al.* [53] reported an exergoeconomic study of geothermal district heating systems through mass, energy, exergy, cost accounting analyses and presented a case study for the Salihli geothermal district heating system in Turkey to illustrate the present method.

Ratlamwala *et al.* [54] undertook a comprehensive study to meet the building heating/cooling and power demand through a sustainable operation by using an integrated polymer electrolyte membrane fuel cell, triple effect absorption refrigeration system and geothermal system.

Ratlamwala *et al.* [55] proposed a novel integrated, geothermal-based double flash power generating, ammonia-water quadruple effect absorption, and electrolyzer sysyem for cooling, heating, power, hot water and hydrogen production. Detailed energy and exergy analyses were carried out, and the effects of geothermal source temperature, geothermal source mass flow rate, geothermal source pressure, effect of ambient temperature were studied parametrically.

Ratlamwala and Dincer [56] focused on a comparative assessment of multi-flush (single to quintuple) geothermal power generating systems integrated with electrolyzers through three definitions of energy and exergy efficiencies. The operating parameters such as ambient temperature and geothermal source temperature were varied to investigate their effects on the respective efficiencies of individual and integrated systems.

2.5 Desalination

Available water resources are not suitable for drinking and daily use as they are strongly mineralized and contaminated part of the population live in small villages or settlements without

infrastructure, and are not connected to a centralized system of electrification and drinking water supply [57].

Available fresh-water resources from rivers and groundwater are presently limited and are being increasingly depleted at an alarming rate in many places. The oceans represent the earth's major water reservoir. About 97% of the earth's water is seawater, while another 2% is locked in icecaps and glaciers. Available fresh water accounts for less than 0.5% of the earth's total water supply. Vast reserves of fresh water lie beneath the earth's surface, but much of it is too deep to access in an economically efficient manner. Additionally, seawater is unsuitable for human consumption and for industrial and agricultural uses.

The locations experiencing water shortages usually have significant solar energy, which can justify the use of solar energy for desalination purposes. By removing salt from the virtually unlimited supply of seawater, desalination has emerged as an important source of fresh water [58]. However, it still requires intensive energy, which is the key parameter affecting the cost. The cost of desalination depends on capacity and type of facility, energy use, feed water, location, labor, and concentrate disposal. The most common methods for desalination are reverse osmosis and multi-stage flash distillation (accounting for 85% of production worldwide) [59].

Recent applications on solar desalination processes are small-scale and decentralized. On the contrary, concentrated solar power plants are suitable for large scale desalination. From an environmental point of view, it can be utilized as an alternative source of fresh water to prevent over-exploitation of groundwater. It can be useful, either by thermal or membrane process, with volumetric flow rates up to several 100,000 m^3/day. It is expected that in twenty years, energy from solar thermal power plants will become the least expensive option for electricity generation (below 4 ¢/kWh) and desalinated water (below 0.4 \$/m^3) [60].

Houcine *et al.* [61] tested and optimized a solar desalination unit working with an air multiple-effect humidification-dehumidification technique.

Yildirim and Solmus [62] investigated the theoretical performance of a solar powered humidification-dehumidification desalination system for various operating and design parameters in accordance with the existing climatic conditions of Antalya, Turkey. They developed the mathematical model of the system and numerically solved governing conservation equations. They also calculated daily and annual yields for different configurations of the system.

Franchini and Perdichizzi [63] developed a computer code to simulate the operation of a low-temperature thermally driven desalination system, based on the HD (humidification-dehumidification) process. The code was used to analyze an HD desalination unit in Abu Dhabi (United Arab Emirates) with fresh water production of about 200 liters per hour.

Fernandez-Lopez *et al.* [60] worked on a seawater integrated desalination plant without brine discharge and powered by renewable energy systems. They analyzed an integrated desalination scheme consisting of two sequential systems: a multi-effect distillation (MED) plant and a mechanical vapour compression (MVC) system based on evaporator equipment.

Trieb and Muller – Steinhagen [64] presented a long-term scenario for the demand of freshwater in the Middle East and North Africa and showed how it may be addressed by a better use of the existing renewable water sources and by sea water desalination powered with solar energy.

Trieb *et al*. [65] showed the principles and the state of the art of concentrating solar power technology and explained the option for seawater desalination, either using electricity or steam, generated in such plants.

Mabrouk *et al.* [66] presented a thermoeconomic analysis of widely used and existing desalination processes. The results show that both mechanical vapor compression and reverse osmosis systems are in competition and give lower unit product costs.

Sharqawy *et al.* [67] studied exergy calculations of seawater with applications in desalination systems. They investigated the effect of the system properties as well as the environment dead state on the exergy and flow exergy variation.

The subject of desalination is studied mostly in the Mediterranean, middle-eastern and Arabic countries where solar radiation is abundant and fresh water sources are scarce. In addition, most of the experimental systems are developed in this region. This trend is likely to continue in the future.

2.6 Kalina Cycle

Kalina cycle utilizes a mixture of ammonia and water as the working fluid in a vapor power cycle. When the liquid mixture is heated, the more volatile ammonia tends to vaporize first and at a lower temperature than pure water. This property of ammonia-water mixtures makes possible a

better match to the enthalpy-temperature curve of a hot gas heat source, such as a gas turbine exhaust and also permits circulation of fluids of different composition in different parts of the cycle. Taking advantage of the latter feature, condensation (absorption) can be attained at slightly above atmospheric pressure with a low concentration of ammonia, while heat input is at a higher concentration for optimum cycle performance [68].

Figure 2.5 shows the simplified Kalina cycle. The numbers in the parentheses in this paragraph show the state points. This is a bottoming cycle fed by exhaust gases (1, 2) to the boiler. Superheated ammonia-water vapor (3) is expanded in a turbine to generate work (4). The turbine exhaust (5) is cooled (6, 7, 8), diluted with ammonia-poor liquid (9, 10) and condensed (11) in the absorber by cooling water (12, 13). The saturated liquid leaving the absorber is compressed (14) to an intermediate pressure and heated (15, 16, 17, 18). The saturated mixture is separated into an ammonia-poor liquid (19) which is cooled (20, 21) and depressurized in a throttle and ammonia-rich vapor (22) is cooled (23) and some of the original condensate (24) is added to the nearly pure ammonia vapor to obtain an ammonia concentration of about 70% in the working fluid (25). The mixture is then cooled (26), condensed (27) by cooling water (28, 29), compressed (30), and sent to the boiler via a regenerative feed water heater (31).

Nad and Gupta [69] analyzed the Kalina cycle thermodynamically and developed a general code for the calculation of thermodynamic properties of the mixture. The effects of the parameters on the exergy loss of each component have also been studied.

Marston [68] made a parametric analysis of the Kalina cycle. He used computer models to optimize a simplified form of the cycle and developed a method of balancing the cycle. He optimized the key parameters of the cycle identified.

Wall *et al.* [70] made an exergy study of the Kalina cycle. They proved that the Kalina cycle is 10% more efficient than the Rankine cycle and the cycle is very well optimized when the cycle is optimized.

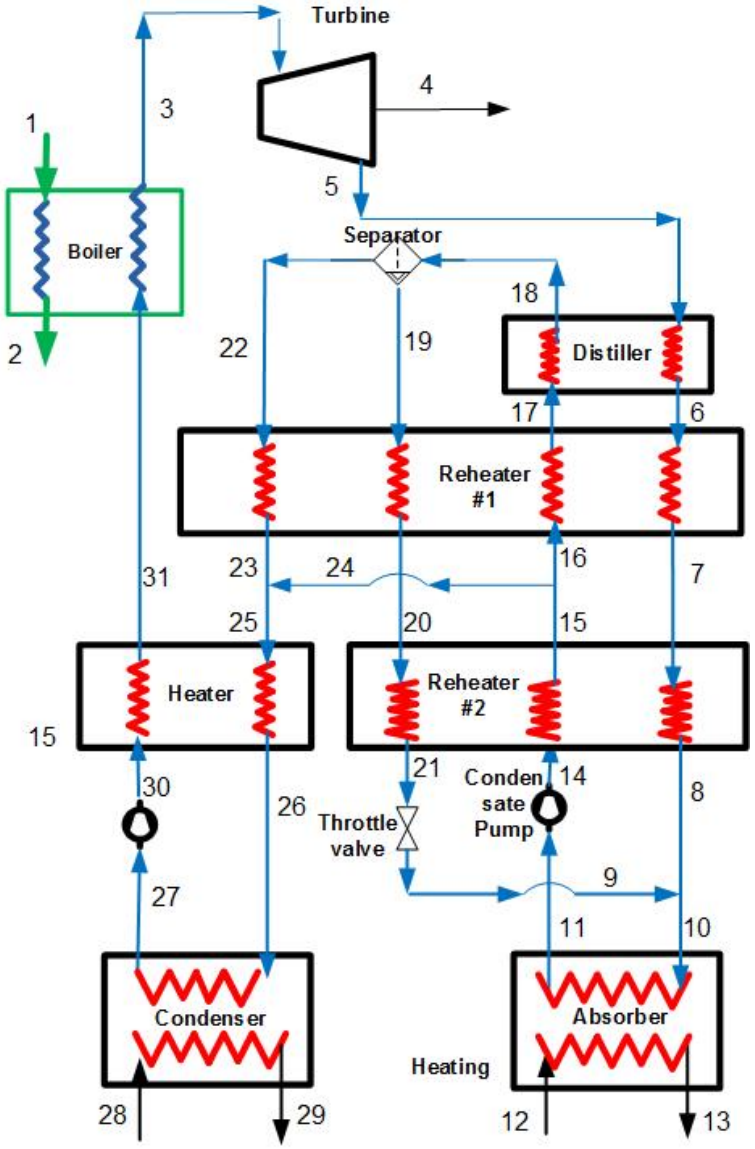

Figure 2.5 Simplified Kalina cycle (adapted from [68])

Jones [71] studied the Kalina cycle system and compared it with an organic Rankine cycle in his thesis. He found that with a source temperature of 200°C, the Kalina cycle can achieve thermal efficiencies in excess of 30%.

Lolos and Rogdakis [72] investigated a Kalina cycle using low-temperature heat sources to produce power. The main heat source of the cycle is provided from flat solar collectors. For given conditions, an optimum range of vapor mass fractions and operating pressures have been identified that result in optimum cycle performance.

Ogriseck [73] integrated the Kalina cycle process in a combined heat and power (CHP) plant for improvement of efficiency. He calculated the net efficiency of an integrated Kalina plant varies between 12.3% and 17.1%.

Wang *et al.* [74] examined a solar-driven Kalina cycle to utilize solar energy effectively by using ammonia-water's varied temperature vaporizing characteristic. In order to ensure a continuous and stable operation for the system, a thermal storage system is introduced to store the collected solar energy and provide stable power when solar radiation is insufficient.

Zhang *et al.* [75] reviewed the research on the Kalina cycle including the comparison of the Rankine and Kalina cycle, energy and exergy analysis on the Kalina cycle, different Kalina systems and their different applications.

Wang *et al.* [76] examined a solar-driven Kalina cycle to utilize solar energy effectively, using ammonia-water's varied temperature vaporizing characteristic.

Although its efficiency is higher, Kalina cycle has not been studied as extensively as Rankine cycle in the research literature. For this reason, it has been selected to be studied in this thesis.

2.7 Absorption Chillers

Absorption chillers use heat, instead of mechanical energy, to provide cooling. The mechanical vapor compressor is replaced by a thermal compressor that consists of an absorber, a generator, a pump, and a throttling device.

Figure 2.6 shows the basic vapour compression cycle, while Figure 2.7 shows the basic absorption cooling cycle. The two cycles are the same between each other than that the basic vapour compression cycle is operated with electricity, while the basic absorption cooling cycle is operated by heat. The refrigerant vapor in the basic absorption cooling cycle from the evaporator is absorbed by a solution mixture in the absorber. This solution is then pumped to the generator where the refrigerant is re-vaporized using a waste steam heat source. The refrigerant-depleted solution is then returned to the absorber via a throttling device. The two most common refrigerant/absorbent mixtures used in absorption chillers are water/lithium bromide and ammonia/water [77].

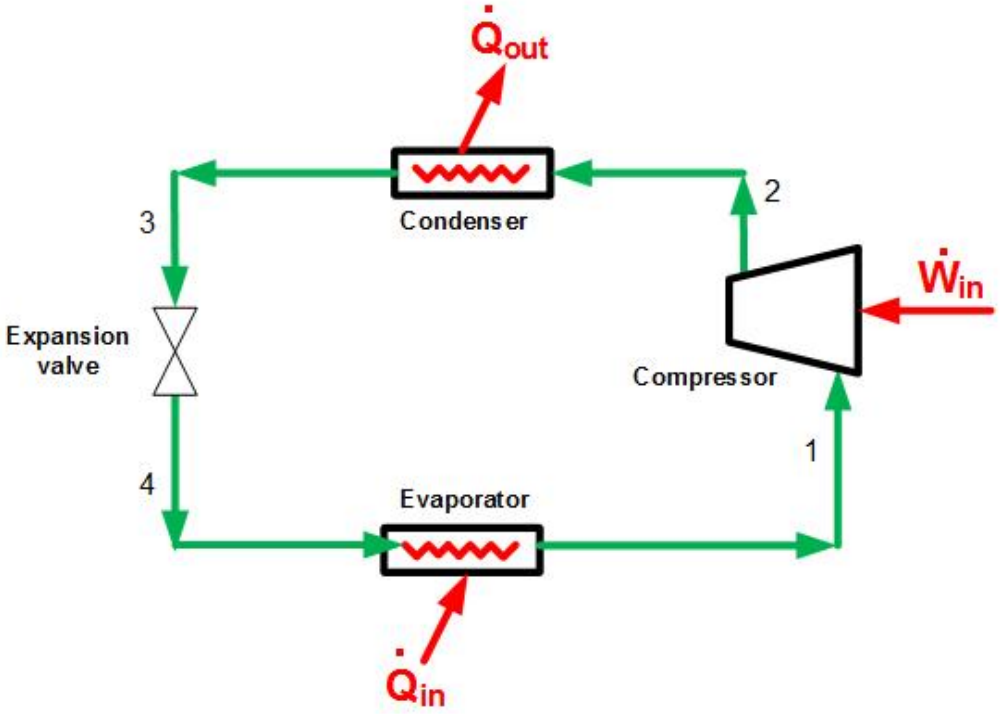

Figure 2.6 Basic vapour compression cycle

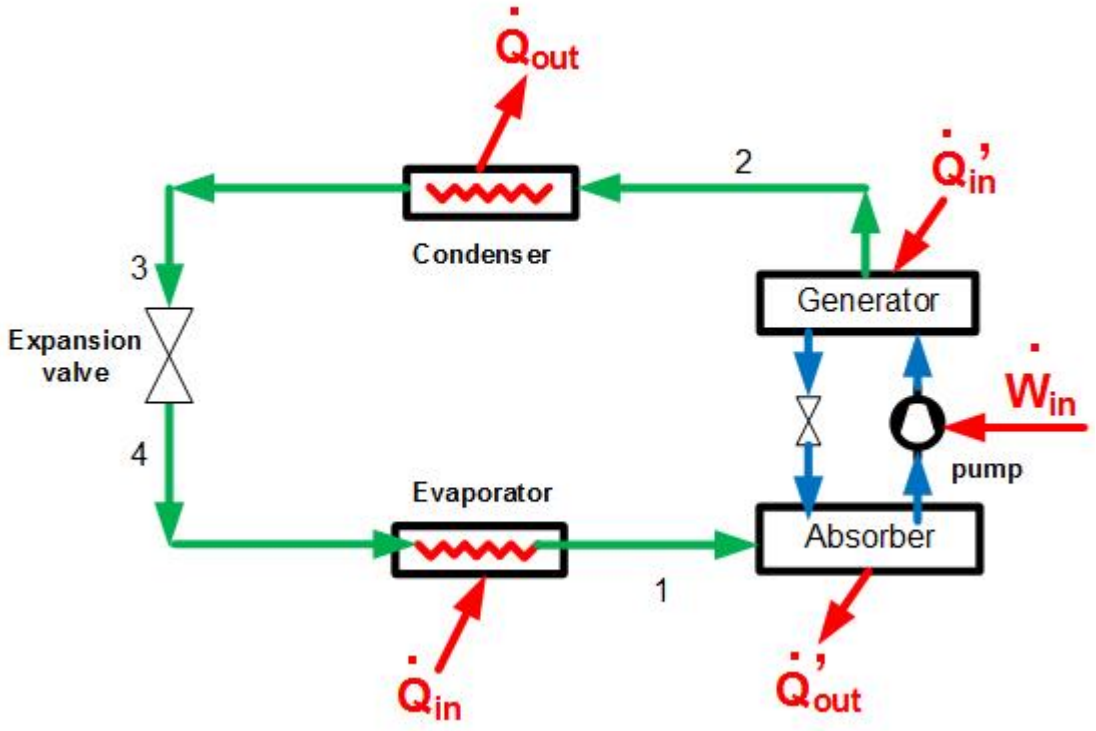

Figure 2.7 Basic absorption cooling cycle

Compared to mechanical chillers, absorption chillers have a low coefficient of performance (COP = chiller load (cooling)/heat input). Nonetheless, they can substantially reduce operating costs because they are energized by low-grade waste heat, while vapor compression chillers must be motor-or engine-driven [77].

Bereche *et al.* [78] presented a methodology to calculate the exergy of lithium bromide-water solution ($LiBr/H_2O$) widely used in absorption refrigeration systems, absorption heat pumps and absorption heat transformers. Some cases in the literature are compared with the results obtained with the methodology proposed in this study.

Marc *et al.* [79] assessed performance and controlling operating conditions of a solar driven absorption chiller using simplified numerical models. They created a steady state chiller model and developed the identification method. The correlation between the prediction and the experimental results allows the use of the model not only to design an installation but also to follow and control its performance.

Chua *et al.* [80] modelled an ammonia-water absorption chiller thermodynamically. Component models of the chiller have been assembled so as to quantify the internal entropy production and thermal conductance in a thermodynamically rigorous formalism, which is in accordance with the simultaneous heat and mass transfer processes occurring within the exchanger.

Kim and Ferreira [81] investigated theoretically a low temperature-driven absorption cycle for the development of an air-cooled LiBr-water absorption chiller to be combined with low-cost flat solar collectors, for solar air conditioning in hot and dry regions. Simulation results predicted that the chillers would deliver chilled water around 7°C with a COP of 0.37 from 90°C hot water under 35°C ambient condition.

Farshi *et al.* [82] reported exergoeconomic analyses for three classes of double effect LiBr/water absorption refrigeration systems in order to investigate the influence of various operating parameters on investment costs of the overall systems and product cost flow rates.

Adewusi and Zubair [83] analyzed single-stage and two-stage ammonia-water absorption systems based on the second law of thermodynamics. They calculated the entropy generation of each component as well as COPs at various operating conditions.

Chua *et al.* [84] developed a general thermodynamic framework for the modeling of an irreversible absorption chiller at the design point, with application to a single-stage ammonia-water absorption chiller.

Shokati *et al.* [85] compared Rankine with LiBr and ammonia-water absorption power cycles from an exergoeconomic viewpoint, using similar conditions and heat sources. Exergoeconomic analysis is performed using the specific energy costing method.

Colonna and Gabrielli [86] presented a thermodynamic system study of industrial trigeneration using ammonia-water absorption refrigeration systems. The study analyzed and compared heat recovery from the primary mover at different temperature levels.

Huicochea *et al.* [87] analyzed a trigeneration system consisting of a micro gas turbine and a double effect absorption chiller thermodynamically. The results demonstrated that this system represents an attractive technological alternative utilizing the simultaneous production of the energy from the microturbine exhaust gases for electric power generation, cooling and heating.

Absorption chillers are often used in multigeneration systems to make use of the waste heat of the power cycle for cooling purpose. Single effect and double effect are most popular in this area so a quadruple effect absorption chiller is used in System 3 to evaluate its effect on the system.

2.8 Thermal Energy Storages

Thermal energy storage (TES) is storage of thermal energy in the form of a cold, hot, or a chemical media [88]. TES is usually installed for two major reasons:

- To lower initial costs.
- To lower operating costs.

The main objective of most TES systems can be achieved in three ways as in the following examples [89]:

- The consumption of solar energy can be reduced by storing surplus thermal energy available during the day for use at night.
- The demand of purchased electrical energy can be reduced by charging a chilled water storage system during off-peak periods (at night) to reduce electrical demand that occur during high-demand periods (during the day).

- Heating, cooling, or air-conditioning applications equipment can be operated when thermal loads are low to charge the TES, and energy is withdrawn from storage to help meet the thermal loads that exceed equipment capacity to reduce equipment size.

Thermal energy storage increases the efficiency of a system as energy is saved instead of wasting it. Output of the system increases without changing the input.

Chapter 3: Description of Systems

Three different solar energy based multigeneration energy systems are analyzed in this thesis. Three novel renewable multigeneration energy systems are selected to produce electricity, heating, cooling, hot water, fresh water, and hydrogen. This chapter is categorized in three subsections to describe each system.

3.1 System 1

System 1 is a hybrid system using both solar and wind energy. It utilizes both energy sources efficiently as the extra energy is saved in the hot storage tank and hydrogen tank. During nighttime or when there is not strong enough wind, this extra energy can be used. System 1 is shown in Figure 3.1.

System 1 produces domestic heating, cooling, electricity and hydrogen for a multi-unit building. The system is designed to meet the energy needs of a multi-suite building. The configuration of the system lets the Rankine system makes optimum use of the energy coming from the solar collectors. The waste heat from the cycle is used for obtaining hot water and cooling the suites by means of the absorption chiller.

In this system, the solar energy is collected by parabolic solar collector. Working fluid is Therminol 66. Hot working fluid (35) is transferred to the hot storage tank to be used when there is not enough sun. From the storage tank it passes through to the boiler (29-30) to heat the ammonia-water mixture in the Rankine cycle (20-21). Evaporated mixture is expanded (21-22) to produce work. Waste heat from the expander is used to heat domestic water (26-27) in condenser. The pump is used to pressurize the mixture (19-20).

The mechanical energy produced is converted to electrical energy by means of a turbine and the generator.

The rest of the solar energy is first used in domestic heating (30-17). Then it is used in the generator of an absorption chiller for cooling purposes. The inlet temperature of the generator (17) should be at least 120°C in order to run the absorption cooling system. The absorption chiller uses heat instead of mechanical energy, to provide cooling.

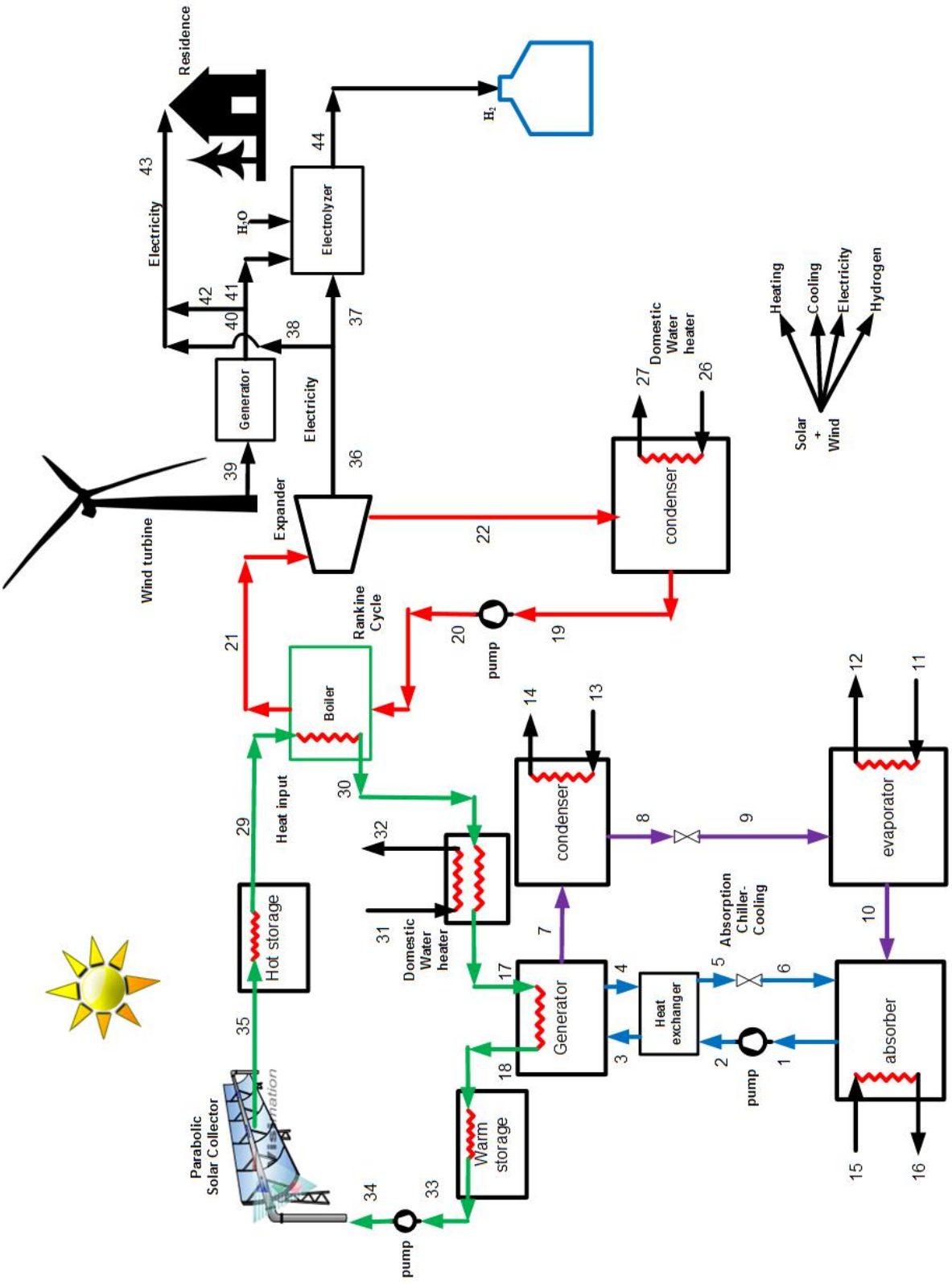

Figure 3.1 Schematic diagram of the proposed system 1

The mechanical vapor compressor is replaced by a thermal compressor that consists of an absorber, a generator, a pump, and a throttling device. Refrigerant is ammonia in the cycle (7-8-9-10). Absorbent is water in the cycle (1-2-3-4-5-6). The ammonia vapor from the evaporator (10) is absorbed by the absorber water (6-1). This solution is then pumped to the generator where the refrigerant is revaporized (3-4) using the remaining solar energy heat source. The ammonia depleted solution is then returned to the absorber via a throttling device (5-6).

The electricity produced by the ammonia-water Rankine cycle turbine can be used in residences or to run the electrolyzer to produce hydrogen when there is extra energy.

Wind turbine also produces electricity when there is enough wind. This electricity is also used in the building or in an electrolyzer to produce hydrogen if there is extra energy.

This system is an example of a hybrid, stand-alone, renewable, multigeneration system. It can be a good example for the future use. Detailed analysis of System 1 is presented by Ozlu and Dincer [90].

3.2 System 2

System 2 uses solar energy to achieve heating, desalination, electricity and hydrogen for a district or a residential building. It is shown in Figure 3.2. The system is configured firstly to make use of the heat energy in the double-effect steam Rankine and ammonia-water Rankine cycles, then waste heat is utilized in desalination and domestic hot water production. The two- stage Rankine cycles are chosen over single effect to increase efficiency and for comparison reasons. Different components such as steam cycle and desalination are used to study different combinations and find the optimum one.

Solar energy is collected by a parabolic solar collector. When there is no sunlight a thermal storage tank is used to store energy.

Hot temperature working fluid (19) goes to the hot storage tank. It then passes through a heat exchanger (20-21) to boil the water in the two stage steam Rankine cycle (2-3). The rest of the heat energy passes (21-18) through another heat exchanger to heat the domestic water (22-23).

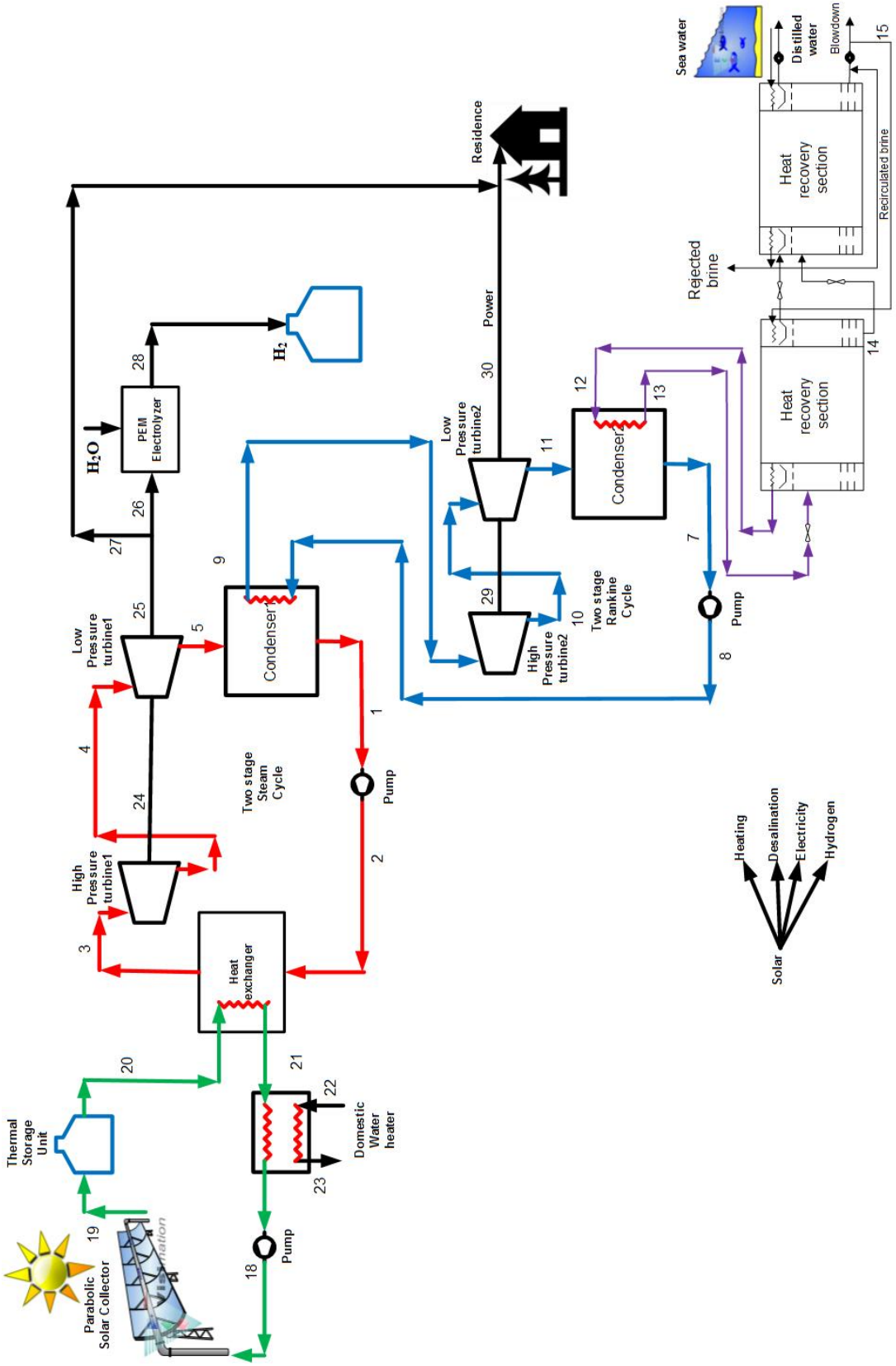

Figure 3.2 Schematic diagram of the proposed system 2

Heated steam in the heat exchanger is expanded in the high pressure turbine (3-4) to produce work. Waste heat from the turbine expands in the low pressure turbine (4-5) to produce more work. Two stages are used, to increase efficiency and use the waste heat, to produce more electricity. The steam exiting from the second turbine is then condensed (5-1) by means of the cold ammonia-water in the Rankine cycle (8-9).

Ammonia-water Rankine cycle is the same as steam Rankine cycle. The only difference is that ammonia-water is used in the cycle instead of steam. Hot mixture generates electricity in two stages, first in the high pressure turbine (9-10), then the low pressure turbine (10-11). The power produced in both turbines is used by the electrolyzer and the residents. Electrolyzer produces hydrogen from water.

Sea water is desalinated by evaporating sea water in the condenser of the ammonia-water Rankine cycle (12-13). Sea water is also used to condense the working fluid.

The difference between this system and the first system is that of achieving desalination instead of cooling. This system can be used in hot areas near the sea to have fresh water, electricity, heating, and hydrogen. System 2 is analyzed in detail by Ozlu and Dincer [91].

3.3 System 3

System 3 provides heating, cooling, electricity and hydrogen using solar energy. Solar energy is collected in the collector and stored in the thermal storage. Kalina cycle utilizes the largest portion of heat energy.

System 3 is a novel system because the use of the Kalina cycle and quadruple effect absorption chiller, have not been addressed and/or operated before in research literature. Although Kalina cycle is more effective than Rankine cycle, it has not been studied as much as Rankine cycle. The quadruple effect has a higher coefficient of performance than single effect absorption chiller. For this reason, it is preferred as the power cycle. In the first system the single effect absorption chiller is chosen. For comparison purposes, quadruple effect absorption chiller is used in System 3.

Kalina cycle produces electricity and heating using the heat energy supplied by the evaporator in the solar cycle. At state 55, ammonia-water mixture leaves the evaporator. Once the

working fluid mixture leaves the evaporator, it enters the phase separator. Working fluid is separated into two separate streams and phases in the separator. The saturated vapor goes to state 56, which is an ammonia rich mixture. The saturated vapor goes to the turbine where it is expanded isentropically to produce work. The vapor saturates at the end of the turbine. The saturated mixture is at state 60. The saturated liquid portion of the working fluid at state 57 is a weaker ammonia mixture than the saturated vapor at state 56. The hot saturated liquid passes through the regenerator where it gives up its thermal energy to the cold working fluid mixture coming from the condenser. The working fluid mixture at state 58 is cooled. It is at the maximum cycle pressure. In order to mix with the working fluid at the exit of the turbine which is at low pressure, the working fluid at state 58 has to be in a lower pressure. Throttling valve drops the pressure and brings to state 59. The two flows that are at the same pressure enter the absorber. The reunited mixture leaves the absorber at state 51. The working fluid then passes through the condenser where heat is used to heat water for the building and the working fluid is brought back to a saturated liquid. The saturated liquid leaves the condenser at state 52. A pump compresses the working fluid mixture to the maximum pressure of the cycle to state 53. The cold working fluid transfers some of the thermal energy to the saturated liquid portion of the working fluid. Even colder working fluid mixture is preheated in the evaporator, and leaves at state 54. The preheated working fluid mixture then enters the evaporator to start the process over again [69].

Excess heat is used in the quadruple effect absorption chiller to produce cooling. Heated ammonia-water mixture in the cycle cools the environment in four steps to maximize efficiency. Heat is used in the absorption chiller, instead of mechanical energy in the conventional systems, to provide cooling. The mechanical vapor compressor is replaced by a thermal compressor that consists of an absorber, a generator, a pump, and a throttling device. The ammonia-water vapor from the evaporator is absorbed by a solution mixture in the absorber. This solution is then pumped to the generator where the ammonia water mixture is revaporized using a branch from the solar collector. The ammonia-water-depleted solution is then returned to the absorber via a throttling device. To maximize efficiency, four generators and four heat exchangers are used instead of one.

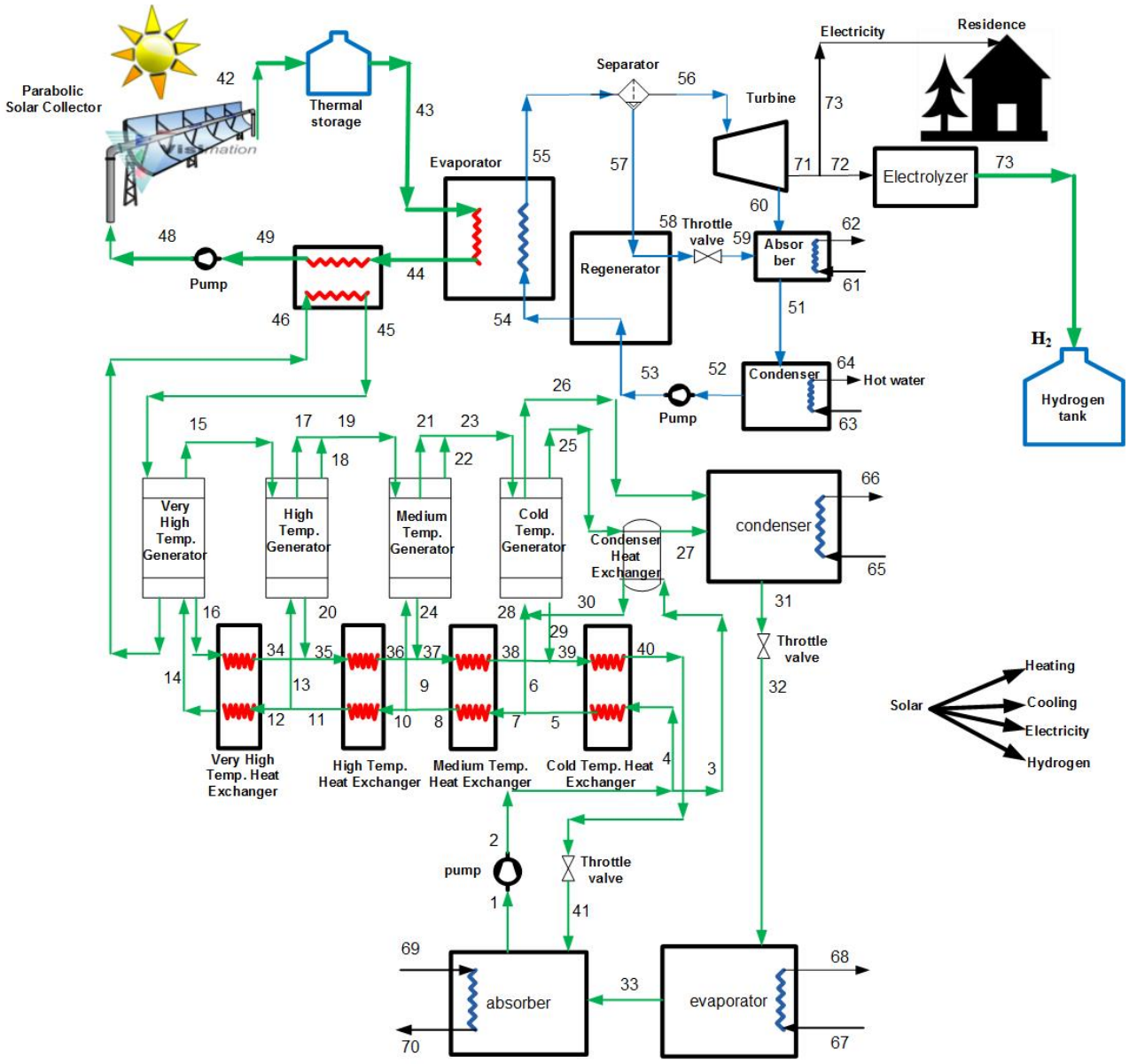

Figure 3.3 Schematic diagram of the proposed system 3

One branch of hot water is first passed through the absorption chiller, where it releases heat to the ammonia–water mixture. The process is triggered by providing heat to the very high temperature generator (VHTG) using excessive heat coming from the evaporator. In the VHTG a strong solution coming from the absorber at state 14 is heated to leave the VHTG as a weak solution at state 16 and an ammonia–water vapor with high concentration at state 15. Heat is transferred from the weak solution coming from the VHTG at state 16 in the very high temperature heat exchanger (VHHX). Then it mixes with a weak solution from the high temperature generator

(HTG) at state 20 to leave as a weak solution at state 35. This weak solution from state 35 releases heat in the medium temperature heat exchanger (MTHX) and is mixed the with weak solution leaving the medium temperature generator (MTG) at state 24, leading to a weak solution at state 37. This weak solution at state 37 is mixed with the weak solution from state 29 after giving out heat to the MTHX. This leads to a weak solution at state 39. This mixed weak solution then enters the cold temperature heat exchanger (CTHX). It warms up the strong solution coming from the pump at state 4. After releasing heat, the weak solution at state 40 enters the throttle valve where both pressure and temperature drop. Then the solution goes to the absorber at state 41. The refrigerant vapor leaving the VHTG at state 15 then ends up in the HTG where it warms up the strong solution coming from the HTHX at state 13. Then it exits as ammonia–water vapor at states 17 and 18. These two streams mix and exit at state 19, to enter the MTG where it warms up the strong solution coming from the CTHX at state 9. Then it exits as ammonia–water vapor at states 21 and 22. These two ammonia–water vapor flows are then combined to exit at state 23. The ammonia–water vapor at state 23 enters the low temperature generator (LTG) and warms up the strong solution coming from state 28. Then it exits as ammonia–water vapor at states 25 and 26. State 26 goes directly into the condenser, while state 25 is directed to the condenser heat exchanger (CHX). By this way it releases heat to part of the liquid that is fed backward by the pump at state 3. This fluid gains heat and exits the CHX at state 30. The ammonia–water vapor leaving the CHX at state 27 enters the condenser where it gives out heat and then exits the condenser at state 31. This stream then goes to the expansion valve and exits at state 32 to enter the evaporator. In the evaporator, heat is being absorbed by the system and the heated mixture exits at state 33 to enter the absorber. In the absorber two incoming fluids combine together and release heat to exit at state 1 in liquid form and enter the pump. The cooling of the building is achieved by passing air through the evaporator of the absorption chiller.

The mechanical energy in the turbine is converted to electricity by a generator. Electricity is then supplied to the electrolyzer to produce hydrogen from water. Electricity is also used in the residential building. More detailed analysis of System 3 is performed by Ozlu and Dincer [92].

Chapter 4: Model Development and Analyses

4.1 Introduction

This chapter outlines the model development and analyses carried out in this thesis. General formulas for thermodynamical, exergoeconomical and exergoenvironmental analyses are introduced. Then optimization approach is explained. It is shown how electrical and heat loads are calculated. Then finally the analyses of each component in the system are performed thermodynamically, exergoeconomically and exergoenvironmentally.

4.2 Thermodynamic Analyses

In order to analyze a control volume, four things need to be considered; mass balance, energy balance, entropy balance and exergy balance. By writing these equations for each system and subsystem, equations can be solved correctly.

4.2.1 Mass Balance Equation

According to conservation of mass principle, the mass flow rate of the entering flow equals to the mass flow rate of the exiting flow the control volume [14] as shown in the equation below:

According to conservation of mass principle, mass entering the control volume equals to mass exiting the control volume [14] as shown in the equation below:

$$\dot{m}_{in} = \dot{m}_{out} \tag{4.1}$$

where $\dot{m}_{in}$ and $\dot{m}_{out}$ are the mass flow rate of inlet and outlet.

4.2.2 Energy Balance Equation

According to First Law of Thermodynamics energy is conserved. If this principle is applied to a steady flow system and a control volume, the following equation is obtained [14]:

$$\dot{Q}_{in} + \dot{W}_{in} + \sum_{in} \dot{m}(h + \frac{V^2}{2} + gz) = \dot{Q}_{out} + \dot{W}_{out} + \sum_{out} \dot{m}(h + \frac{V^2}{2} + gz) \tag{4.2}$$

where $\dot{Q}$ is heat transfer rate, $\dot{W}$ is work rate, h is specific enthalpy, $\dot{m}$ is velocity, g is gravitational acceleration, z is the elevation.

4.2.3 Entropy Balance Equation

There is an increase in the sum of the entropies of the participating systems according to the Second Law of Thermodynamics. Entropy balance equation applied to a control volume can be expressed as [14]:

$$\dot{S}_{gen} = \sum \dot{m}_{out} s_{out} - \sum \dot{m}_{in} s_{in} - \sum \frac{\dot{Q}_k}{T_k} \quad (4.3)$$

where *out* denotes outlet, *in* denotes inlet, $\dot{Q}$ is heat transfer rate, s is the entropy. Positive direction of heat transfer is to the system.

4.2.4 Exergy Balance Equation

When an exergy analysis is performed, the thermodynamic imperfections can be quantified as exergy destructions, which represent losses in energy quality or usefulness [12]. The exergy of a substance is often in 4 different forms: physical, chemical, kinetic and potential energy. Last 2 forms are assumed as negligible as elevation changes are small and speeds are low. Chemical energy is not considered as well as solar energy is used as a source.

According to the second law of thermodynamics, an exergy balance equation can be written as

$$\dot{E}x_Q + \sum_{in} \dot{m}_{in}\, ex_{in} = \sum_{out} \dot{m}_{out}\, ex_{out} + \dot{E}x_W + \dot{E}x_D \quad (4.4)$$

where subscripts *in* and *out* denote the control volume inlet and outlet flow respectively and $\dot{E}x_D$ is the exergy destruction rate. Other terms can be explained as:

$\dot{E}x_W$ is the exergy transfer associated with mechanical work is equal to the mechanical work as shown below:

$$\dot{E}x_W = \dot{W} \quad (4.5)$$

$\dot{E}x_Q$ is the exergy transfer associated with heat transfer and it depends on the temperature at which it occurs in relation to the temperature of the environment [12]. The equation of $\dot{E}x_Q$ is shown below:

$$\dot{E}x_Q = (1 - \frac{T_0}{T_i})\dot{Q}_i \quad (4.6)$$

where T_0 is the ambient temperature, T_i is the temperature of the heat transferred to the boundary of the control volume and $\dot{Q}_i$ is the heat transfer to the control volume.

4.3 Exergoeconomic Analysis

Thermoeconomics is an area of engineering in which the thermodynamics are combined with economics to provide energy system designers with information not available through conventional energy analysis and economic evaluation. However, these are important to the design and operation of a cost effective system. Since in thermoeconomic analysis, exergy is used instead of energy as thermodynamic criteria, the term exergoeconomics is also used to describe the process.

For a system flow cost rate $\dot{C}$ (\$/h) can be defined as

$$\dot{C} = d\dot{E}x \tag{4.7}$$

where d is the cost per exergy in \$/kWh and $\dot{E}x$ is the associated exergy transfer rate.

Exergy cost rates associated with matter, electricity and heat flows may be written respectively as

$$\dot{C}_{matter} = (d\dot{E}x)_{matter} \tag{4.8}$$

$$\dot{C}_{electricity} = (d\dot{E}x)_{electricity} = (d\dot{E})_{electricity} \tag{4.9}$$

$$\dot{C}_{heat} = (d\dot{E}x)_{heat} = d\dot{Q}(1 - \frac{T_0}{T}) \tag{4.10}$$

For a system that has inlet stream i and exit stream e, the cost balance is:

$$\sum_k \dot{C}_{i,k} + Z = \sum_j \dot{C}_{e,j} \tag{4.11}$$

where Z is expenses of investment, operating, and maintenance, k is the index for inlet streams and j is the index for exit streams.

The value of Z can be defined as [93]:

$$Z = \frac{(\beta+\gamma)C_o}{\tau} \tag{4.12}$$

where β is the capital recovery factor, γ is the operating and maintenance costs excluding fuel, C_o is the investment cost of the component and τ is the annual system operation time at nominal capacity.

The total cost to produce the exiting streams (electricity, hydrogen, oxygen, heating load, cooling load) is equal to the entering stream (solar heat) plus the capital and other costs. The following cost rate balance can be expressed for the cycle:

$$\dot{C}_{electricity} + \dot{C}_{H_2} + \dot{C}_{O_2} + \dot{C}_{heating\ load} + \dot{C}_{cooling\ load} + \dot{C}_{losses} = \dot{C}_{solar\ heat} + Z \qquad (4.13)$$

4.4 Exergoenvironmental Analysis

Air polluting emissions such as nitrogen oxides (NO_x), carbon dioxide (CO_2), sulfur dioxide (SO_2), methane (CH_4), and mercury (Hg) compounds associated with generating electricity, heat and hydrogen from solar technologies are negligible because no fuels are combusted.

As there is no pollution caused by these systems, air emissions from fossil fuel fired power plants with an equivalent power output can be calculated and reduced emissions can be determined [94].

According to United States Environmental Protection Agency, average emissions emitted by power plants with respect to the fuel are shown in Table 4.1. As natural gas is widely used in North America, calculations are based on the usage of natural gas.

Table 4.1 Average emissions from US power plants

	CO_2 (kg/MWh)	**SO_2 (kg/MWh)**	**NO_x (kg/MWh)**
Natural Gas	515	0.04	0.77
Coal	1020	6	3
Oil	758	5	2

Source: [95]

Environmental analysis is made based on the emissions produced using fossil fuels to achieve the same results. As SO_2 and NO_x are very low compared to CO_2, they are not considered in the calculations.

4.5 Optimization Study

Optimization is maximizing or minimizing an objective function playing with the independent variables considering the constraints and the boundaries. In this section, the main parameters of optimization such as objective function, decision variables, bounds and guess values will be introduced.

4.5.1 Objective Function

Objective function is the variable to be minimized or maximized depending on the targets of the decision maker.

In multigeneration systems the objective function can be as follows:

- Efficiency (energy, exergy etc.)
- Cost (investment, annualized costs, cost of exergy destruction etc.)
- Emitted pollutants (CO_2, SO_2, NO_x etc.)

If more than one objective is chosen, it is called multi-objective optimization [12].

4.5.2 Decision Variables

Decision variables are the variables that affect the objective function. It is necessary to select as many independent variables as there are degrees of freedom. However only the most important variables with a major effect should be chosen. Examples for the decision variables are solar radiation, ambient temperature, number of solar units, condenser outlet temperature, pump pressure ratio etc.

4.5.3 Bounds

Each independent variable requires lower and upper bounds. These bounds are specified for the following properties:

- Dimensions or weight of the system
- Highest temperature that fluids and the components are used having regard to safety
- Highest pressure allowed by the fluids and the components
- Maximum flow rate of the working fluids

- Minimum temperature that the components or working fluids can operate

4.5.4 Guess Value(s)

Choosing the correct guess value(s) will improve the likelihood of finding an optimum. Incorrect selection may result in it taking too long or even be impossible, for the program to converge into a solution.

4.5.5 Local vs Global Optimization

Local and global optimization are two kinds of application. A local minimum of a function is a point where the function value is smaller than or equal to the value at nearby points, but possibly greater than at a distant point. A global minimum is a point where the function value is smaller than or equal to the value at all other feasible points. The practical application of local and global minimum is shown in Figure 4.1. Local and global maximum can be explained the same manner.

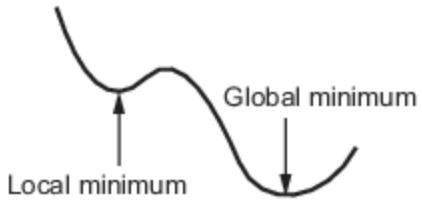

Figure 4.1 Local and global minimum values

In this study, local minimum is found based on the use of the variable-metric method, which is a property of EES Min/Max Optimization.

4.6 Estimation of Heating, Cooling, Electricity Loads

When designing multigeneration systems, it is important to determine the target of the output. The systems designed in this thesis are for a Toronto multi-unit residential building. The building characteristics considered are in Table 4.2.

Table 4.2 Building characteristics of units considered

Average number of storeys per building	13
Average number of suites per building	188
Average date of construction	1984
Average gross floor area per building(m^2)	18,400
Average attributed suite area (m^2)	104

Source: [94]

The average energy intensities per suite and per building are shown in Table 4.3. Energy intensity is a building's annual energy consumption per unit of gross floor area. The table shows the annual energy needed to heat a suite in Toronto in equivalent kWh. Natural gas consumption in cubic meters is used to find the energy intensity. The conversion from cubic meters of natural gas supplied to equivalent kilowatt-hours of energy was based on a factor of 37.08 MJ/m^3 or 10.3 kWh/m^3 [96].

Table 4.3 Annual natural gas intensity of a suite in Toronto

	Annual Value Per m^2 ($ekWh/m^2$)	**Annual Value Per Suite (ekWh)**
Natural gas energy intensity	295	25,100

Source: [96]

According to Binkley [96], the average end-use distribution for Toronto buildings is 38% electricity, 37% space heating (30% electricity and 70% natural gas), and 25% domestic hot water. The annual energy intensity is based on the total annual energy consumed from both electric and natural gas sources divided by the building's gross floor area. The ratio of electricity is 38% and natural gas is 62%.

In order to calculate the percentage of electricity for cooling, historical data related to degree days for Toronto was obtained from Toronto Hydro [97].

The average annual degree days for heating for Toronto between 2001 and 2013 were 3638, whereas average annual degree days for cooling was 380. As a result the cooling load is 10% of heating load. By sharing the energy intensity to loads based on the percentages, the loads in equivalent annual kWh in Table 4.4 are found.

Table 4.4 Design loads of the systems

Load	**Annual Value Per m^2 (ekWh/m^2)**	**Annual Value Per Suite (ekWh)**
Electricity (Cooling + the rest)	112 (11 + 101)	9538 (929 + 8609)
Space heating	109	9287
Domestic hot water	74	6275

4.7 Analyses of System 1

After introducing the thermodynamic, economic and environmental methods of solving the problem, equations can be written for each component in System 1 to analyze it. The three subsections in this section are thermodynamic, exergy and exergoeconomic analyses.

4.7.1 Thermodynamic Analysis

Thermodynamic analysis consists of the equations needed to lay out each component. In order to solve the unknown parameters of the system, each component should be solved on a one by one basis, before proceeding to the next one in order to arrive at a solution.

- **Parabolic Solar Collector**

A parabolic collector can accept both beam and diffuse radiation because of its large acceptance angle. Actual useful energy gain in the collector is expressed as [98]:

$$Q_u = E_R A_u [S - \frac{A_{re}}{A_o} U_L (T_{34} - T_0)] \quad (4.14)$$

where A_u is the unshaded area of the concentrator aperture (m^2), A_{re} is the area of the receiver (m^2), S is the absorbed solar radiation per unit of aperture area (W/m^2) and can be found from:

$$S = I_{ap} \tau \rho \alpha \quad (4.15)$$

where I_{ap} is the effective incident radiation measured on the plane of the aperture (W/m^2), τ is the effect of angle of incidence, ρ is the specular reflectance of the concentrator and α is the absorptivity.

$$A_u = (w - D) l \quad (4.16)$$

where w is the width of the receiver (m), D is the absorber envelope outer diameter (m), l is the concentrator length (m).

$$A_{re} = \pi D_0 l \tag{4.17}$$

where D_0 is the absorber outside diameter (m).

E_R is the heat removal factor and can be found from the following equation:

$$E_R = \frac{\dot{m}c_{pr}}{A_r U_L}\left[1 - \exp\left(\frac{A_{re}U_L F'}{\dot{m}C_p}\right)\right] \tag{4.18}$$

where $\dot{m}$ is the mass flow rate of the heating fluid (kg/s), c_{pr} is the specific heat of the heating fluid (kJ/kgK), U_L is the overall heat transfer coefficient (W/m^{2}K).

F' can be found from the following equation:

$$F' = \frac{\frac{1}{U_L}}{\frac{1}{U_L} + \frac{D_o}{H_{te}D_i} + \left(\frac{D_o}{2k} ln \frac{D_o}{D_i}\right)} \tag{4.19}$$

where H_{te} is the heat transfer coefficient inside the tube (W/m^{2}K), D_i is the absorber inside diameter (m), k is the conductivity of the absorber tube material (W/mK).

With the assistance of the equations introduced in this section, a general model for the collector optical and thermal performance can be constructed.

- **Hot Storage**

If an insulation of thickness ξ (m) and thermal conductivity k (W/mK) is used, the coefficient of heat transfer U (W/m^{2}K) between the working fluid and air is given by:

$$\frac{1}{U} = \frac{1}{h} + \frac{\xi}{k} \tag{4.20}$$

where h is the coefficient of heat transfer from working fluid to air (W/m^{2}K).

Corresponding hot storage heat loss $\dot{Q}_{hs}$ (W/m^2) per unit area of the surface of the tank is given by:

$$\dot{Q}_{hs} = U(T_{35} - T_0) \tag{4.21}$$

where T_{35} is the temperature of the fluid entering the hot thermal storage (K) and T_0 is the atmospheric temperature.

Note that the recommended type of insulation is 20 cm mineral wool insulation [39].

Warm storage heat loss can be found by inserting T_{18} instead of T_{35} if all the parameters are the same.

where T_{18} is the temperature of the fluid entering the cold thermal storage (K).

- **Domestic Water Heater**

The hot gases from the ammonia-water Rankine cycle boiler enter the water heater to warm domestic hot water to 60°C. The water enters this heater at atmospheric pressure and ambient temperature. The energy balance for this component is given as follows:

$$\dot{m}_{sc}(h_{30} - h_{17}) = \dot{m}_w(h_{32} - h_{31}) \quad (4.22)$$

- **Absorption Chiller Generator**

The rate of heat to the generator of an absorption system is provided using solar energy and calculated using the following equation:

$$\dot{Q}_{gen} = \dot{m}_{sc}(h_{17} - h_{18}) \quad (4.23)$$

where $\dot{m}_{sc}$ is the mass flow rate of the working fluid in the solar cycle (kg/s).

In order to obtain the outlet conditions of the generator, the following equation is used:

$$\dot{m}_3 h_3 + \dot{Q}_{gen} = \dot{m}_4 h_4 + \dot{m}_7 h_7 \quad (4.24)$$

The exergy destruction in generator is defined as:

$$\dot{E}x_{d,gen} = \dot{E}x_3 + \dot{E}x_{gen} - \dot{E}x_4 - \dot{E}x_7 \quad (4.25)$$

where

$$\dot{E}x_{gen} = (1 - \frac{T_O}{T_{gen}})\dot{Q}_{gen} \quad (4.26)$$

$$\dot{E}x_3 = \dot{m}_3((h_3 - h_0) - T_0(s_3 - s_0)) \quad (4.27)$$

And the same relation is employed for other states.

- **Absorption Chiller Heat exchanger**

The mass balance equations for heat exchanger are given below:

$$\dot{m}_2 = \dot{m}_3 \quad (4.28)$$

$$\dot{m}_4 = \dot{m}_5 \quad (4.29)$$

The energy balance equation for heat exchanges is given below:

$$\dot{m}_2(h_3 - h_2) = \dot{m}_4(h_4 - h_5) \quad (4.30)$$

The exergy balance equation for heat exchanges is given below:

$$\dot{m}_4\left(\dot{E}x_4 - \dot{E}x_5\right) = \dot{m}_2\left(\dot{E}x_3 - \dot{E}x_2\right) + Ex_{d,3} \quad (4.31)$$

- **Absorption Chiller Condenser**

The mass balance equation for the condenser is given below:

$$\dot{m}_7 = \dot{m}_8 \quad (4.32)$$

The energy balance equation for the condenser is given below:

$$\dot{m}_8 h_8 + \dot{Q}_{con} = \dot{m}_7 h_7 \quad (4.33)$$

The exergy balance equation for the condenser is given below:

$$\dot{m}_7\left(\dot{E}x_7 - \dot{E}x_8\right) = \left(1 - \frac{T_O}{T_{con}}\right)\dot{Q}_{con} + Ex_{d,con} \quad (4.34)$$

- **Absorption Chiller Evaporator**

The equation for mass balances for the evaporator is given as follows:

$$\dot{m}_9 = \dot{m}_{10} \quad (4.35)$$

The equation for energy balance for the evaporator can be written as follows:

$$\dot{m}_9 h_9 + \dot{Q}_{eva} = \dot{m}_{10} h_{10} \quad (4.36)$$

The exergy balance equation for the evaporator is expressed as follows:

$$\dot{m}_{10}\left(\dot{E}x_{10} - \dot{E}x_9\right) + \left(1 - \frac{T_O}{T_{eva}}\right)\dot{Q}_{eva} = Ex_{d,eva} \quad (4.37)$$

- **Absorption Chiller Absorber**

The mass balance equations for the absorption chiller absorber are given as follows:

$$\dot{m}_1 x_1 = \dot{m}_6 x_6 + \dot{m}_{10} x_{10} \quad (4.38)$$

$$\dot{m}_1 = \dot{m}_6 + \dot{m}_{10} \quad (4.39)$$

Energy balance equation used to calculate the heat rejected from the absorber is as follows:

$$\dot{m}_6 h_6 + \dot{m}_{10} h_{10} = \dot{m}_1 h_1 + \dot{Q}_{abs} \quad (4.40)$$

The exergy balance equation for the absorber is given as follows:

$$\dot{m}_6 \dot{Ex}_6 + \dot{m}_{10} \dot{Ex}_{10} = \dot{m}_1 \dot{Ex}_1 + \left(1 - \frac{T_O}{T_{abs}}\right) \dot{Q}_{abs} + Ex_{d,abs} \quad (4.41)$$

- **Absorption Chiller Pump**

The work done by the pump is calculated using the equation given below:

$$\dot{W}_p = \dot{m}_1 (h_2 - h_1) \quad (4.42)$$

$$\dot{m}_1 = \dot{m}_2 \quad (4.43)$$

The energetic COP is found using the following equation:

$$COP_{en} = \frac{\dot{Q}_{eva}}{\dot{Q}_{gen} + \dot{W}_p} \quad (4.44)$$

The exergetic COP can be expressed as follows:

$$COP_{ex} = \frac{\dot{Ex}_{eva}}{\dot{Ex}_{gen} + \dot{W}_p} \quad (4.45)$$

- **Ammonia-water Rankine Cycle**

The power that can be obtained from the cycle is defined as

$$\dot{W}_{t,rc} = \dot{m}_{rc} (h_{21} - h_{22}) \quad (4.46)$$

The enthalpy of state 22 is calculated using isentropic efficiency of the turbine as follows:

$$\eta_t = \frac{h_{21} - h_{22}}{h_{21} - h_{22,s}} \quad (4.47)$$

where $\eta_t = 70\%$

The power consumed by pump is expressed as

$$\dot{W}_{p,rc} = \dot{m}_{rc} (h_{20} - h_{19}) \quad (4.48)$$

The actual net power obtained from the cycle is expressed as

$$\dot{W}_{net,rc} = \dot{W}_{t,rc} - \dot{W}_{p,rc} - \dot{W}_{parasitic} \quad (4.49)$$

In order to have a more realistic model, the parasitic losses are considered to account for different losses occurring in the system. The percentage of parasitic losses is assumed to be 20% and calculated as

$$\dot{W}_{parasitic,rc} = 0.2\ (\dot{W}_{t,rc} - \dot{W}_{p,rc}) \quad (4.50)$$

The rate of heat rejected by the condenser is defined as

$$\dot{Q}_{con,rc} = \dot{m}_{rc}\ (h_{22} - h_{19}) \quad (4.51)$$

The exergy rate carried by condenser heat is calculated as

$$\dot{E}x_{con,rc} = (1 - \frac{T_o}{T_{con}})\dot{Q}_{con,rc} \quad (4.52)$$

The energy efficiency of ammonia-water Rankine cycle is defined as:

$$\eta_{en} = \frac{\dot{W}_{net,rc}}{\dot{Q}_{boiler,rc}} \quad (4.53)$$

The exergy efficiency of ammonia-water Rankine cycle can be expressed as follows:

$$\eta_{ex} = \frac{\dot{W}_{net,rc}}{\dot{E}x_{boiler,rc}} \quad (4.54)$$

- **Wind Turbine**

Average power obtained from the wind turbine is expressed as follows [98]:

$$\dot{p}_{wt} = \frac{1}{2}\rho_{air} A_{wt} C_t V^3 \quad (4.55)$$

where ρ_{air} is the air density (kg/m^3), A_{wt} is the wind turbine area (m^2), C_t is the turbine power coefficient, V is the average velocity of the wind (m^2/s).

Area of the wind turbine can be found from the following equation:

$$A_{wt} = \pi \frac{D^2}{4} \quad (4.56)$$

where D is wind turbine diameter.

The exergy efficiency of the wind turbine is:

$$\eta_{ex} = \frac{\dot{W}_{wt}}{\dot{E}x_{wt}} \tag{4.57}$$

where $\dot{E}x_{wt}$ is the exergy of the wind turbine and calculated as::

$$\dot{E}x_{wt} = \frac{1}{2}\rho_{air} A_{wt} V^3 \tag{4.58}$$

The exergy destruction in the wind turbine is:

$$\dot{E}x_{d,wt} = (\frac{1}{C_p} - 1)\dot{p}_{wt} \tag{4.59}$$

- **Electrolyzer**

The mass flow rate of the hydrogen produced from the electrolyzer is:

$$\dot{m}_{h2} = \eta_{elec} \frac{\dot{W}_{elec}}{HHV_{h2}} \tag{4.60}$$

where η_{elec} is the efficiency of the electrolyzer, $\dot{W}_{elec}$ is the power input to the electrolyzer (W), HHV_{h2} is the higher heating value of hydrogen (142.19×10^6 J/kg)

The exergy balance of the electrolyzer is given as follows:

$$\dot{E}x_{h2} = \dot{m}_{h2}(ex_{ph} + ex_{ch})_{h2} \tag{4.61}$$

where $\dot{m}_{h2}$ the mass flow rate of the hydrogen (kg/s), ex_{ph} is the specific physical exergy of the hydrogen, ex_{ch} is the specific chemical exergy of the hydrogen.

$$ex_{ch} = \frac{253{,}153}{MM_{h2}} \tag{4.62}$$

where MM_{h2} is the molar mass of h_2 (kg/kmol)

$$ex_{ph} = h_{h2} - h_0 - T_o(s_{h2} - s_0) \tag{4.63}$$

Power available from the hydrogen obtained can be expressed as follows:

$\dot{p}_{h2} = 33{,}400\ \dot{m}_{h2}$ (kW)

where 33,400 kWh is equivalent in energy to one kilogram of hydrogen gas.

The energy efficiency of the electrolyzer is calculated by

$$\eta_{elec} = \frac{\dot{E}n_{elec,out,H2}}{\dot{E}n_{elec,in}} \tag{4.64}$$

4.7.2 Exergy Analysis

Exergy destruction in each component of System 1, energy and exergy efficiency equations will be introduced here for exergy analysis.

- **Exergy Balance Equations**

The exergy destructions for basic components in System 1 are listed in Table 4.5. The expressions are based on state points shown in Figure 3.1. Exergy of each state point can be calculated using EES software based on state pressure and temperature.

- **Energy Efficiency**

Energy efficiency is defined as the ratio of useful energy produced to the input energy supplied to the system. In System 1 energy efficiencies of ammonia-water Rankine cycle can be calculated by the following formula:

$$\eta_{en,rc} = \frac{\dot{W}_{exp} - \dot{W}_{p,rc}}{\dot{Q}_{boiler}} \tag{4.65}$$

System efficiency equation can be expressed as follows:

$$\eta_{en,system} = \frac{\dot{W}_{exp} + \dot{W}_{wind} - \dot{W}_{p,solar} - \dot{W}_{p,rc}}{\dot{Q}_{solar} + \dot{W}_{wind}} \tag{4.66}$$

Also energy coefficient of performance for the absorption chiller can be calculated as follows:

$$COP_{en,chiller} = \frac{\dot{Q}_{eva}}{\dot{Q}_{gen} + \dot{W}_{p}} \tag{4.67}$$

- **Exergy Efficiency**

The exergy efficiency is the product exergy output divided by the exergy input. Solar system exergy efficiency formula can be written as follows:

$$\eta_{ex,sc} = \frac{Q_{boiler}\left(1 - \frac{T_0}{T_{boiler}}\right) + Q_{gen}\left(1 - \frac{T_0}{T_{gen}}\right) + Q_{dwh}\left(1 - \frac{T_0}{T_{dwh}}\right)}{\dot{Q}_{solar}\left(1 - \frac{T_0}{T_{sun}}\right)} \tag{4.68}$$

Table 4.5 Exergy destruction rates of components in System 1

Component	**Exergy destruction rate expression**
Parabolic solar collector	$\dot{E}x_{d,sc} = \dot{Q}_{solar}(1 - \frac{T_0}{T_{sun}}) + \dot{E}x_{34} - \dot{E}x_{35}$
Hot storage	$\dot{E}x_{d,hot\ ts} = \dot{E}x_{35} - \dot{E}x_{29} - \dot{E}x_Q$
Warm storage	$\dot{E}x_{d,warm\ ts} = \dot{E}x_{18} - \dot{E}x_{33} - \dot{E}x_Q$
Domestic water heater	$\dot{E}x_{d,dwh} = \dot{E}x_{30} - \dot{E}x_{17} + \dot{E}x_{31} - \dot{E}x_{32}$
Solar cycle	$\dot{E}x_{d,sc} = \dot{Q}_{solar}\left(1 - \frac{T_0}{T_{sun}}\right) - \dot{Q}_{dwh}\left(1 - \frac{T_0}{T_{dwh}}\right) - \dot{Q}_{boiler}\left(1 - \frac{T_0}{T_{boiler}}\right) - \dot{Q}_{gen}\left(1 - \frac{T_0}{T_{gen}}\right) - \dot{Q}_{hs}\left(1 - \frac{T_0}{T_{hs}}\right) - \dot{Q}_{cs}\left(1 - \frac{T_0}{T_{cs}}\right) - \dot{W}_{p,solar}$
Absorption generator	$\dot{E}x_{d,gen} = \dot{E}x_3 - \dot{E}x_4 - \dot{E}x_7 + \dot{E}x_{17} - \dot{E}x_{18}$
Absorption condenser	$\dot{E}x_{d,con} = \dot{E}x_7 - \dot{E}x_8 + \dot{E}x_{13} - \dot{E}x_{14}$
Absorption expansion valve	$\dot{E}x_{d,valve} = \dot{E}x_8 - \dot{E}x_9$
Absorption evaporator	$\dot{E}x_{d,eva} = \dot{E}x_9 - \dot{E}x_{10} + \dot{E}x_{11} - \dot{E}x_{12}$
Absorption absorber	$\dot{E}x_{d,abs} = \dot{E}x_{10} + \dot{E}x_6 - \dot{E}x_1 + \dot{E}x_{15} - \dot{E}x_{16}$
Absorption pump	$\dot{E}x_{d,p} = \dot{E}x_1 - \dot{E}x_2 + \dot{W}_{p,abs}$
Absorption throttling valve	$\dot{E}x_{d,throttle} = \dot{E}x_5 - \dot{E}x_6$
Absorption heat exchanger	$\dot{E}x_{d,hx} = \dot{E}x_2 - \dot{E}x_3 + \dot{E}x_4 - \dot{E}x_5$
Absorption cycle	$\dot{E}x_{d,abs} = \dot{Q}_{gen}\left(1 - \frac{T_0}{T_{gen}}\right) - \dot{Q}_{eva}\left(1 - \frac{T_0}{T_{eva}}\right) - \dot{W}_{p,abs}$
Boiler	$\dot{E}x_{d,boiler} = \dot{E}x_{20} - \dot{E}x_{21} + \dot{E}x_{29} - \dot{E}x_{30}$
Ammonia-water Rankine pump	$\dot{E}x_{d,p\ rc} = \dot{E}x_{19} - \dot{E}x_{20} + \dot{W}_{p,rc}$
Ammonia-water Rankine condenser	$\dot{E}x_{d,rc\ con} = \dot{E}x_{22} - \dot{E}x_{19} + \dot{E}x_{26} - \dot{E}x_{27}$
Expander	$\dot{E}x_{d,exp} = \dot{E}x_{21} - \dot{E}x_{22}$
Ammonia-water Rankine cycle	$\dot{E}x_{d,rc} = \dot{Q}_{boiler}\left(1 - \frac{T_0}{T_{boiler}}\right) - \dot{Q}_{con}\left(1 - \frac{T_0}{T_{con}}\right) + \dot{W}_{exp} - \dot{W}_{p,rc}$
Wind turbine	$\dot{E}x_{d,wt} = \left(\frac{1}{C_{p,wt}} - 1\right).\dot{p}_{wt}$

The exergy efficiency of the Rankine cycle can be expressed as follows:

$$\eta_{ex,rc} = \frac{W_{exp} - W_{p,rc} + Q_{con}(1 - \frac{T_0}{T_{con}})}{Q_{boiler}} \quad (4.69)$$

The system exergy efficiency is defined as follows:

$$\eta_{ex,system} = \frac{\dot{W}_{exp}+\dot{Q}_{con}\left(1-\frac{T_0}{T_{con}}\right)+\dot{Q}_{eva}\left(1-\frac{T_0}{T_{eva}}\right)+\dot{Q}_{dwh}\left(1-\frac{T_0}{T_{dwh}}\right)+\dot{p}_{wt}-\dot{W}_{p,sc}-\dot{W}_{p,rc}}{\dot{Q}_{solar}\left(1-\frac{T_0}{T_{sun}}\right)+\frac{\rho_{air}A_{wt}V_{wind}{}^3}{2}} \quad (4.70)$$

The exergetic coefficient of performance for the absorption chiller can be calculated as follows:

$$COP_{ex,chiller} = \frac{\dot{Q}_{eva}(1-\frac{T_0}{T_{eva}})}{\dot{Q}_{gen}(1-\frac{T_0}{T_{gen}})+\dot{W}_p} \quad (4.71)$$

4.7.3 Exergoeconomic Analysis

The cost function of each component in System 1 is given and explained in this section. Cost of each component is a function of parameters defining the system.

- **Parabolic Solar Collector**

Purchase cost of parabolic solar collector is a function of collector width and length and can be expressed as [100]:

$$Z_{sc}(\$) = 310WL \quad (4.72)$$

- **Thermal Storage**

Purchase cost of thermal storage is a function of heat stored. It can be expressed as [8]:

$$Z_{ts}(\$) = 27\dot{Q} \quad (4.73)$$

- **Domestic Water Heater**

Purchase cost of the domestic water heater considered in this system can be expressed as follows [100]:

$$Z_{dwh}(\$) = 0.3V_{dwh} \quad (4.74)$$

Here, V_{dwh} is the hot water production in m^3.

- **Absorption Chiller**

Although purchase cost of absorption chiller is a function of design parameters, it can be approximated by a function of cooling load [101].

$$Z_{chiller}(\$) = 1144.3(\dot{Q}_{eva})^{0.67} \quad (4.75)$$

where $\dot{Q}_{eva}$ is the cooling load of the absorption chiller in kW.

- **Boiler**

As a heat exchanger, purchase cost of the boiler can be calculated with the following equation [8]:

$$Z_{boiler}(\$) = 130(\frac{A_{boiler}}{0.093})^{0.83} \quad (4.76)$$

where A_{boiler} can be found from the following equations:

$$A_{boiler} = \frac{\dot{Q}}{U_{boiler}\Delta T_{ln}} \quad (4.77)$$

Here U_{boiler} is overall heat transfer coefficient for boiler with the value of 2 kW/m^{2}K and ΔT_{ln} is the logarithmic temperature difference and can be expressed as:

$$\Delta T_{ln} = \frac{\Delta T_A - \Delta T_B}{\ln(\frac{\Delta T_A}{\Delta T_B})} \quad (4.78)$$

where ΔT_A is the temperature difference between the two streams at end A, and ΔT_B is the temperature difference between the two streams at end B.

$$\Delta T_{ln} = \frac{(T_{29} - T_{21}) - (T_{30} - T_{20})}{\ln(\frac{T_{29} - T_{21}}{T_{30} - T_{20}})} \quad (4.79)$$

- **Condenser**

To calculate the purchase cost of condenser the following expression can be used [8]:

$$Z_{con}\ (\$) = 280.74\,\frac{\dot{Q}_{con}}{K\Delta T_{ln}} + 746\dot{m}_{rc} \quad (4.80)$$

$$K = 2200\ \frac{W}{m^2K}$$

Here, $\dot{m}_{rc}$ is the Rankine cycle mass flow rate, ΔT_{ln} is the logarithmic temperature difference and *k* is the purchase cost constant. ΔT_{ln} can be expressed as:

$$\Delta T_{ln} = \frac{(T_{22} - T_{27}) - (T_{19} - T_{26})}{\ln(\frac{T_{22} - T_{27}}{T_{19} - T_{26}})} \quad (4.81)$$

- **Pump**

The purchase cost of pump is defined as follows [8]:

$$Z_p(\$) = 705.48\left(\dot{W}_P\right)^{0.71}\left(1 + \frac{0.2}{1-\eta_p}\right) \quad (4.82)$$

where $\dot{W}_P$ is the pump power and η_p is the pump efficiency.

- **Expander**

The purchase cost of the expander can be defined as a function of expander inlet temperature, expander isentropic efficiency and expander work [102]:

$$Z_{exp} = 3880.5(\dot{W}_{exp})^{0.7}\left[1 + \left(\frac{0.05}{1-\eta_{exp}}\right)^3\right]\{1 - \exp\left(\frac{T_{21}-866K}{10.42K}\right)\} \quad (4.83)$$

- **Electrolyzer**

The purchase cost of the electrolyzer is a function of the inlet electricity to split water which can be expressed as [44]:

$$Z_{elec}(\$) = 1000\dot{W}_{elec} \quad (4.84)$$

- **Wind Turbine**

The purchase cost of wind turbine is a function of turbine power and expressed as [100]:

$$Z_{wt} = 5000\dot{W}_{wt} \quad (4.85)$$

4.8 Analyses of System 2

Thermodynamic, exergy and exergoeconomic analyses for System 2 is the main focus in this section.

4.8.1 Thermodynamic Analysis

Thermodynamic equations for each component in the system are covered in this subsection. State points that are shown in Figure 3.2 are used in the equations.

- **Parabolic Solar Collector**

Because if its preferred temperature range, the same collector as in System 1 is used. Identical absorber areas are considered for System 1 and System 2. The same equations in section

4.7.1 can be used. The only difference is the collector inlet temperature. T_{18} should be used instead of T_{34}.

- **Hot Water Storage**

Hot Water Storage is the same as in System 1. Hot storage heat loss can be found by inserting T_{19} instead of T_{35} in equation 4.21 if all the parameters are the same.

- **Domestic Water Heater**

The hot fluid coming from the heat exchanger enters the heat exchanger to warm domestic hot water to 60°C. Water enters this heater at atmospheric pressure and ambient temperature. The energy balance for this component is given as follows:

$$\dot{m}_{sc}(h_{21} - h_{18}) = \dot{m}_{dwh}(h_{23} - h_{22}) \quad (4.86)$$

- **Two Stage Steam Rankine Cycle**

The power that can be obtained from the high pressure turbine of two-stage steam Rankine cycle is defined as

$$\dot{W}_{st,hp} = \dot{m}_{st}(h_3 - h_4) \quad (4.87)$$

Here, the power obtained from the low pressure turbine is:

$$\dot{W}_{st,lp} = \dot{m}_{st}(h_4 - h_5) \quad (4.88)$$

The enthalpies of states 4 and 5 are calculated using the following equations:

$$\eta_{t,hp} = \frac{h_3 - h_4}{h_3 - h_{4,s}} \quad (4.89)$$

and

$$\eta_{t,lp} = \frac{h_4 - h_5}{h_4 - h_{5,s}} \quad (4.90)$$

The power consumed by pump is expressed as

$$\dot{W}_{p,st} = \dot{m}_{st}(h_2 - h_1) \quad (4.91)$$

The actual net power that can be obtained from a two-stage steam Rankine cycle is expressed as

$$\dot{W}_{net\ st} = \dot{W}_{t,st} - \dot{W}_{p,st} - \dot{W}_{parasitic\ st} \quad (4.92)$$

In order to have a more realistic model, the parasitic losses are considered to account for different losses occurring in the system. The percentage of parasitic losses is assumed to be 20% and calculated as

$$\dot{W}_{parasitic\ st} = 0.2\ (\dot{W}_{turb,st} - \dot{W}_{p\ st}) \quad (4.93)$$

The rate of heat rejected by the condenser is defined as

$$\dot{Q}_{con,st} = \dot{m}_{st}\ (h_5 - h_1) \quad (4.94)$$

The exergy rate carried by condenser heat is calculated as

$$\dot{E}x_{con,st} = (1 - \frac{T_o}{T_{con}})\dot{Q}_{con,st} \quad (4.95)$$

The energy efficiency of steam Rankine cycle are defined as follows:

$$\eta_{en} = \frac{\dot{W}_{net,st}}{\dot{Q}_{he}} \quad (4.96)$$

The exergy efficiency of steam Rankine cycle can be expressed as follows:

$$\eta_{ex} = \frac{\dot{W}_{net,st} + \dot{E}x_{con,st}}{\dot{E}x_{he}} \times 100 \quad (4.97)$$

- **Two Stage Ammonia-Water Rankine Cycle**

The power that can be obtained from the cycle is defined as

$$\dot{W}_{t,rc} = \dot{m}_{rc}(h_9 - h_{11}) \quad (4.98)$$

The enthalpies of states 10 and 11 are calculated using isentropic efficiency of the turbine as follows:

$$\eta_{t,hp} = \frac{h_9 - h_{10}}{h_9 - h_{10,s}} \quad (4.99)$$

and

$$\eta_{t,lp} = \frac{h_{10} - h_{11}}{h_{10} - h_{11,s}} \quad (4.100)$$

The power consumed by pump is expressed as

$$\dot{W}_{p,rc} = \dot{m}_{rc} (h_8 - h_7) \quad (4.101)$$

The actual net power obtained from the ammonia-water Rankine cycle is expressed as

$$\dot{W}_{net,rc} = \dot{W}_{t,rc} - \dot{W}_{p,rc} - \dot{W}_{parasitic} \quad (4.102)$$

In order to have a more realistic model, the parasitic losses are considered to account for different losses occurring in the system. The percentage of parasitic losses is assumed to be 20% and calculated as

$$\dot{W}_{parasitic,rc} = 0.2 (\dot{W}_{t,rc} - \dot{W}_{p,rc}) \quad (4.103)$$

The rate of heat rejected by the condenser is defined as

$$\dot{Q}_{con,rc} = \dot{m}_{rc} (h_{11} - h_7) \quad (4.104)$$

The exergy rate carried by condenser heat is calculated as

$$\dot{E}x_{con,rc} = (1 - \frac{T_o}{T_{con}})\dot{Q}_{con,rc} \quad (4.105)$$

The energy efficiency of ammonia-water Rankine cycle is defined as follows:

$$\eta_{en} = \frac{\dot{W}_{net,rc}}{\dot{Q}_{con,sc}} \quad (4.106)$$

The exergy efficiency of ammonia-water Rankine cycle can be given as follows:

$$\eta_{ex} = \frac{\dot{W}_{net,rc} + \dot{E}x_{con,rc}}{\dot{E}x_{con,sc}} \quad (4.107)$$

- **Electrolyzer**

The total net power supplied to the electrolyzer is calculated as

$$\dot{W}_{net} = \dot{W}_{net,st} + \dot{W}_{net,rc} \quad (4.108)$$

The rate of hydrogen produced by electrolyzer is found using:

$$\eta_{elec} = \frac{\dot{m}_{H_2} LHV}{\dot{W}_{net}} \quad (4.109)$$

- **Desalination**

Desalination used in System 2 is a multi-stage-flash (MSF) type desalination. The equations in this section are taken from [104].

The MSF process is composed of a series of elements, called stages. In each stage, condensing steam is used to pre-heat the seawater feed. By fractioning the overall temperature differential between the warm source and seawater into a large number of stages, the system approaches ideal total latent heat recovery. Current commercial installations are designed with 10–30 stages [98].

Initially the number of stages is designed as 15 stages. This parameter can be changed during calculations

The ratio of feed water to distillate water is given by [104]:

$$\frac{\dot{m}_f}{\dot{m}_{dt}} = \frac{L_v}{c\Delta f} + \frac{N-1}{2N} \tag{4.110}$$

where $\dot{m}_f$ is the mass flow rate of feed (kg/h), $\dot{m}_{dt}$ is the mass flow rate of distillate (kg/h), L_v is the average latent heat of vaporization (kJ/kg), N is the total number if stages or effects, c is the mean specific heat under constant pressure for all liquid streams (kJ/kgK), Δf is the flashing temperature range (K).

Flashing temperature range can be calculated from the following equation:

$$\Delta f = T_{tb} - T_{bN} = (T_{b1} - T_{bN})\frac{N}{N-1} \tag{4.111}$$

where T_{tb} is the top brine temperature (K), T_{bN} is the temperature of brine in the last effect (K), T_{b1} is the temperature of brine in first effect (K).

Total thermal load per unit product obtained by approximating (N-1)/N=1 is given by [104]:

$$\frac{\Sigma Q}{\dot{m}_{dt}} = \frac{\dot{m}_{rb}}{\dot{m}_{dt}} c(T_{tb} - T_o) = L_v \frac{T_h - T_0}{\Delta F} \tag{4.112}$$

where $\dot{m}_{rb}$ is the mass flow rate of the recirculated brine (kg/s).

4.8.2 Exergy Analysis

Exergy analysis of System 2 will be carried out in this section by giving the exergy destruction equations of each component, energy and exergy efficiencies.

- **Exergy Balance Equations**

The exergy destructions for main components in System 2 are listed in Table 4.6. The equations are given in properties with state point subscripts shown in Figure 3.2.

- **Energy Efficiency**

The energy efficiency is defined as the ratio of useful energy produced to the input energy supplied to the system. In System 2, the energy efficiency of steam Rankine cycle can be calculated by the following formula:

$$\eta_{en,st} = \frac{\dot{W}_{hpt,st}+\dot{W}_{lpt,st}-\dot{W}_{p,st}}{\dot{Q}_{he}} \tag{4.113}$$

The energy efficiency of ammonia-water Rankine cycle is given as follows:

$$\eta_{en,rc} = \frac{\dot{W}_{hpt,rc}+\dot{W}_{lpt,rc}-\dot{W}_{p,rc}}{\dot{Q}_{con,st}} \tag{4.114}$$

The system energy efficiency equation is written as follows:

$$\eta_{en,system} = \frac{\dot{W}_{hpt,st}+\dot{W}_{lpt,st}+\dot{W}_{hpt,rc}+\dot{W}_{lpt,rc}-\dot{W}_{p,sc}-\dot{W}_{p,st}-\dot{W}_{p,rc}}{\dot{Q}_{solar}} \tag{4.115}$$

- **Exergy Efficiency**

The exergy efficiency is the product exergy output divided by the exergy input. Solar cycle exergy efficiency formula can be written as follows:

$$\eta_{ex,sc} = \frac{\dot{Q}_{he}\left(1-\frac{T_0}{T_{he}}\right)+\dot{Q}_{dwh}\left(1-\frac{T_0}{T_{dwh}}\right)-\dot{W}_{p,sc}}{\dot{Q}_{solar}(1-\frac{T_0}{T_{sun}})} \tag{4.116}$$

The exergy efficiency of the steam Rankine cycle can be expressed as follows:

$$\eta_{ex,st} = \frac{\dot{W}_{hpt,st}+\dot{W}_{lpt,st}+\dot{Q}_{con,st}(1-\frac{T_0}{T_{con,st}})-\dot{W}_{p,st}}{\dot{Q}_{he}(1-\frac{T_0}{T_{he}})} \quad (4.117)$$

The exergy efficiency of the ammonia-water Rankine cycle can be formulated as follows:

$$\eta_{ex,rc} = \frac{\dot{W}_{hpt,rc}+\dot{W}_{lpt,rc}+\dot{Q}_{con,rc}(1-\frac{T_0}{T_{con,rc}})-\dot{W}_{p,rc}}{\dot{Q}_{con,st}(1-\frac{T_0}{T_{con,st}})} \quad (4.118)$$

Table 4.6 Exergy destruction rates of components in System 2

Component	**Exergy destruction rate expression**
Parabolic solar collector	$\dot{E}x_{d,sc} = \dot{Q}_{solar}(1-\frac{T_0}{T_{sun}}) + \dot{E}x_{18} - \dot{E}x_{19}$
Thermal storage	$\dot{E}x_{d,s} = \dot{E}x_{19} - \dot{E}x_{20} - \dot{E}x_{Q,loss}$
Domestic water heater	$\dot{E}x_{d,dwh} = \dot{E}x_{21} - \dot{E}x_{18} + \dot{E}x_{22} - \dot{E}x_{23}$
Heat exchanger	$\dot{E}x_{d,he} = \dot{E}x_{20} - \dot{E}x_{21} + \dot{E}x_{2} - \dot{E}x_{3}$
Solar cycle	$\dot{E}x_{d,sc} = \dot{Q}_{solar}\left(1-\frac{T_0}{T_{sun}}\right) - \dot{Q}_{dwh}\left(1-\frac{T_0}{T_{dwh}}\right) - \dot{Q}_{ts}\left(1-\frac{T_0}{T_{ts}}\right) - \dot{Q}_{he}\left(1-\frac{T_0}{T_{he}}\right) - \dot{W}_{p,sc}$
Steam Rankine cycle high pressure turbine	$\dot{E}x_{d,hpt,st} = \dot{E}x_{3} - \dot{E}x_{4}$
Steam Rankine cycle low pressure turbine	$\dot{E}x_{d,lpt,st} = \dot{E}x_{4} - \dot{E}x_{5}$
Steam Rankine cycle condenser	$\dot{E}x_{d,con,st} = \dot{E}x_{5} - \dot{E}x_{1} + \dot{E}x_{8} - \dot{E}x_{9}$
Steam Rankine cycle pump	$\dot{E}x_{d,p,st} = \dot{E}x_{1} - \dot{E}x_{2} + \dot{W}_{p,st}$
Steam Rankine cycle	$\dot{E}x_{d,st} = \dot{Q}_{he}\left(1-\frac{T_0}{T_{he}}\right) - \dot{Q}_{con}\left(1-\frac{T_0}{T_{con}}\right) + \dot{W}_{hpt,st} + \dot{W}_{lpt,st} - \dot{W}_{p,st}$
Ammonia-water Rankine cycle high pressure turbine	$\dot{E}x_{d,hpt,rc} = \dot{E}x_{9} - \dot{E}x_{10}$
Ammonia-water Rankine cycle low pressure turbine	$\dot{E}x_{d,hpt,rc} = \dot{E}x_{10} - \dot{E}x_{11}$
Ammonia-water Rankine cycle condenser	$\dot{E}x_{d,con,rc} = \dot{E}x_{11} - \dot{E}x_{7} + \dot{E}x_{12} - \dot{E}x_{13}$
Ammonia-water Rankine cycle pump	$\dot{E}x_{d,p,st} = \dot{E}x_{7} - \dot{E}x_{8} + \dot{W}_{p,rc}$
Ammonia-water Rankine cycle	$\dot{E}x_{d,rc} = \dot{Q}_{con,st}\left(1-\frac{T_0}{T_{con,st}}\right) - \dot{Q}_{con,rc}\left(1-\frac{T_0}{T_{con,rc}}\right) + \dot{W}_{hpt,rc} + \dot{W}_{lpt,rc} - \dot{W}_{p,rc}$

The system exergy efficiency is defined as follows:

$$\eta_{ex,system} = \frac{\dot{W}_{hpt,st}+\dot{W}_{lpt,st}+\dot{W}_{hpt,rc}+\dot{W}_{lpt,rc}+\dot{Q}_{con,rc}\left(1-\frac{T_0}{T_{con,rc}}\right)+\dot{Q}_{dwh}\left(1-\frac{T_0}{T_{dwh}}\right)-\dot{W}_{p,sc}-\dot{W}_{p,st}-\dot{W}_{p,rc}}{\dot{Q}_{solar}\left(1-\frac{T_0}{T_{sun}}\right)} \quad (4.119)$$

4.8.3 Exergoeconomic Analysis

Equations relating to the purchase cost of each component are explained in this section. Each cost is given as a function of the parameters related to the component.

- **Parabolic Solar Collector**

Purchase cost of parabolic solar collector is a function of collector width and length and can be expressed as [100]:

$$Z_{sc}(\$) = 310WL \quad (4.120)$$

- **Thermal Storage**

The purchase cost of thermal storage is a function of heat stored. It can be expressed as [8]:

$$Z_s(\$) = 27\dot{Q}_s \quad (4.121)$$

- **Domestic Water Heater**

The purchase cost of the domestic water heater considered in this system can be expressed as follows [100]:

$$Z_{dwh}(\$) = 0.3V_{dwh} \quad (4.122)$$

where V_{dwh} is the hot water production in m^3.

- **Heat Exchanger**

The purchase cost of the heat exchanger can be calculated with the following equation [8]:

$$Z_{he}(\$) = 130\left(\frac{A_{he}}{0.093}\right)^{0.83} \quad (4.123)$$

where A_{he} can be found from the following equation:

$$A_{he} = \frac{\dot{Q}}{U_{he}\Delta T_{ln}} \quad (4.124)$$

Here, U_{he} is overall heat transfer coefficient for heat exchanger with the value of 2 kW/m^{2}K and ΔT_{ln} is the logarithmic temperature difference

$$\Delta T_{ln} = \frac{\Delta T_A - \Delta T_B}{\ln(\frac{\Delta T_A}{\Delta T_B})} \quad (4.125)$$

where ΔT_A is the temperature difference between the two streams at end A, and $\Delta T_B$is the temperature difference between the two streams at end B.

$$\Delta T_{ln} = \frac{(T_{20} - T_3) - (T_{21} - T_2)}{\ln(\frac{T_{20} - T_3}{T_{21} - T_2})} \quad (4.126)$$

- **Condenser**

To calculate the purchase cost of condenser the following expression can be used [8]:

$$Z_{con}\ (\$) = 280.74 \frac{\dot{Q}_{con}}{K \Delta T_{ln}} + 746 \dot{m}_{rc} \quad (4.127)$$

and

$$K = 2200\ W/m^2K \quad (4.128)$$

Here, $\dot{m}_{rc}$ is the ammonia-water Rankine cycle mass flow rate, ΔT_{ln} is the logarithmic temperature difference and *k* is the condenser purchase cost constant and can be expressed as

$$\Delta T_{ln} = \frac{(T_5 - T_9) - (T_1 - T_8)}{\ln(\frac{T_5 - T_9}{T_1 - T_8})} \quad (4.129)$$

- **Pumps**

The purchase cost of pump is defined as follows [8]:

$$Z_p(\$) = 705.48\left(\dot{W}_P\right)^{0.71}(1 + \frac{0.2}{1 - \eta_p}) \quad (4.130)$$

where $\dot{W}_P$ is the pump power and η_p is the pump efficiency

- **Turbines**

The purchase cost of the turbines can be defined as a function of turbine inlet temperature, turbine isentropic efficiency and turbine work [102]:

For the high-pressure turbine in steam Rankine cycle:

$$Z_{hpt,st} = 3880.5(\dot{W}_{hpt,st})^{0.7}\left[1 + \left(\frac{0.05}{1 - \eta_{hpt,st}}\right)^3\right]\{1 - \exp\left(\frac{T_3 - 866K}{10.42K}\right)\} \quad (4.131)$$

For the low-pressure turbine in steam Rankine cycle:

$$Z_{lpt,st} = 3880.5(\dot{W}_{lpt,st})^{0.7}\left[1+\left(\frac{0.05}{1-\eta_{lpt,st}}\right)^{3}\right]\{1-\exp\left(\frac{T_4-866K}{10.42K}\right)\} \quad (4.132)$$

For the high-pressure turbine in ammonia-water Rankine cycle:

$$Z_{hpt,rc} = 3880.5(\dot{W}_{hpt,rc})^{0.7}\left[1+\left(\frac{0.05}{1-\eta_{hpt,rc}}\right)^{3}\right]\{1-\exp\left(\frac{T_9-866K}{10.42K}\right)\} \quad (4.133)$$

For the low-pressure turbine in ammonia-water Rankine cycle:

$$Z_{lpt,rc} = 3880.5(\dot{W}_{lpt,rc})^{0.7}\left[1+\left(\frac{0.05}{1-\eta_{lpt,rc}}\right)^{3}\right]\{1-\exp\left(\frac{T_{10}-866K}{10.42K}\right)\} \quad (4.134)$$

- **Electrolyzer**

The purchase cost of the electrolyzer is a function of the inlet electricity to split water which can be expressed as [8]:

$$Z_{elec}(\$) = 1000\dot{W}_{elec} \quad (4.135)$$

- **Desalination Unit**

The purchase cost of desalination unit can be expressed as a function of $\dot{m}_f$, mass flow rate of feed (kg/h) [100]:

$$Z_{desalination} = 24\dot{m}_f \quad (4.136)$$

4.9 Analyses of System 3

In this section thermodynamic, exergy and exergoeconomic analysis equations will be introduced. By using these equations, complete analyses of System 3 can be carried out.

4.9.1 Thermodynamic Analysis

In this subsection thermodynamic equations of each component will be given. These equations are used in analyzing the system.

- **Solar System**

Same system is used as in System 3 because if its preferred temperature range. Identical absorber areas are considered for System 1 and System 3. The same equations in section 4.7.1 can be used. T_{48} should be used instead of T_{34} as the collector inlet temperature.

- **Absorption Chiller Very High Temperature Generator (VHTG)**

The rate of heat to the VHTG of an absorption system is provided using solar energy and calculated using the following equation:

$$\dot{Q}_{VHTG} = \dot{Q}_{solar} \tag{4.137}$$

The mass balance equations for the ammonia-water mixture of VHTG are given as follows:

$$\dot{m}_{14}x_{14} = \dot{m}_{15}x_{15} + \dot{m}_{16}x_{16} \tag{4.138}$$

$$\dot{m}_{14} = \dot{m}_{15} + \dot{m}_{16} \tag{4.139}$$

In order to obtain the outlet conditions of the VHTG, the following equation is used:

$$\dot{m}_{14}h_{14} + \dot{Q}_{VHTG} = \dot{m}_{15}h_{15} + \dot{m}_{16}h_{16} \tag{4.140}$$

The exergy destruction in VHTG can be expressed as follows:

$$\dot{Ex}_{d,HTG} = \dot{Ex}_{14} + \dot{Ex}_{VHTG} - \dot{Ex}_{15} - \dot{Ex}_{16} \tag{4.141}$$

where

$$\dot{Ex}_{VHTG} = (1 - \frac{T_O}{T_{VHTG}})\dot{Q}_{VHTG} \tag{4.142}$$

$$\dot{Ex}_{15} = \dot{m}_{15}((h_{15} - h_0) - T_0(s_{15} - s_0)) \tag{4.143}$$

And the same relation is employed for other states.

- **Absorption Chiller Very High Temperature Heat Exchanger (VHHX)**

The energy balance equations for VHHX are given below:

$$\dot{m}_{12}h_{12} + \dot{Q}_{HHX} = \dot{m}_{14}h_{14} \tag{4.144}$$

$$\dot{m}_{16}h_{16} = \dot{Q}_{HHX} + \dot{m}_{34}h_{34} \quad (4.145)$$

- **Absorption Chiller Condenser**

The mass balance equation for the condenser is given below:

$$\dot{m}_{31} = \dot{m}_{26} + \dot{m}_{27} \quad (4.146)$$

The energy balance equation for the condenser can be expressed as follows:

$$\dot{m}_{31}h_{31} + \dot{Q}_{con} = \dot{m}_{26}h_{26} + \dot{m}_{27}h_{27} \quad (4.147)$$

- **Absorption Chiller Evaporator**

The equation for mass balance of evaporator is given as

$$\dot{m}_{32} = \dot{m}_{33} \quad (4.148)$$

The equation for energy balance of evaporator can be written as follows:

$$\dot{m}_{32}h_{32} + \dot{Q}_{eva} = \dot{m}_{33}h_{33} \quad (4.149)$$

- **Absorption Chiller Absorber**

The energy balance equation used to calculate the heat rejected from the absorber is written as

$$\dot{m}_{33}h_{33} + \dot{m}_{41}h_{41} = \dot{m}_{1}h_{1} + \dot{Q}_{con} \quad (4.150)$$

- **Absorption Chiller Pump**

The work done by the pump is calculated using the equation given below:

$$\dot{W}_p = \dot{m}_1(h_2 - h_1) \quad (4.151)$$

- **Kalina Cycle Separator**

The mass balance equation is:

$$\dot{m}_{55} = \dot{m}_{57} + \dot{m}_{56} \quad (4.152)$$

The ammonia mass balance equation is:

$$\dot{m}_{55}x_{55} = \dot{m}_{57}x_{57} + \dot{m}_{56}x_{56} \quad (4.153)$$

The mass flow rate of saturated vapor separated by the separator is:

$$\dot{m}_{57} = \dot{m}_{56}\frac{(x_{56}-x_{55})}{(x_{55}-x_{57})} \quad (4.154)$$

- **Kalina Cycle Turbine**

The isentropic efficiency of the turbine can be expressed as:

$$\eta_t = \frac{h_{56}-h_{60}}{h_{56}-h_{60s}} \quad (4.155)$$

The power output of ammonia-water turbine is given by:

$$\dot{W}_t = \dot{m}_{56}(h_{56} - h_{60}) \quad (4.156)$$

- **Kalina Cycle Absorber**

In the absorber, the mass balances balance equation can be written as follows:

$$\dot{m}_{59} + \dot{m}_{60} + \dot{m}_{61} = \dot{m}_{51} + \dot{m}_{62} \quad (4.157)$$

The exergy balance equation of the absorber can be given as

$$\dot{m}_{59}x_{59} + \dot{m}_{60}x_{60} + \dot{m}_{61}x_{61} = \dot{m}_{51}x_{51} + \dot{m}_{62}x_{62} \quad (4.158)$$

- **Kalina Cycle Pump**

The isentropic efficiency in the pump is:

$$\eta_p = \frac{h_{53s}-h_{52}}{h_{53}-h_{52}} \quad (4.159)$$

The work input by the pump is:

$$\dot{W}_p = \dot{m}_{52}(h_{53} - h_{52}) \quad (4.160)$$

- **Kalina Cycle Regenerator**

The energy balance equation in the distiller is:

$$\dot{m}_{57}(h_{58} - h_{57}) = \dot{m}_{53}(h_{54} - h_{53}) \quad (4.161)$$

- **Kalina Cycle Evaporator**

The energy balance equation in the evaporator is:

$$\dot{m}_{54}(h_{55} - h_{54}) = \dot{m}_{43}(h_{44} - h_{43}) \quad (4.162)$$

4.9.2 Exergy Analysis

In this section, System 3 exergy balance equations for each component, energy efficiency and exergy efficiency are introduced.

- **Exergy Balance Equations**

The exergy destruction levels for main components in System 3 are listed in Table 4.7. The state point numbers shown in Figure 3.3 are used accordingly.

Table 4.7 Exergy destruction rates of components in System 3

Component	**Exergy destruction rate expression**
Parabolic solar collector	$\dot{E}x_{d,sc} = \dot{Q}_{solar}(1 - \frac{T_0}{T_{sun}}) + \dot{E}x_{48} - \dot{E}x_{42}$
Thermal storage	$\dot{E}x_{d,s} = \dot{E}x_{42} - \dot{E}x_{43} - \dot{E}x_{Q,loss}$
Evaporator	$\dot{E}x_{d,eva} = \dot{E}x_{43} - \dot{E}x_{44} + \dot{E}x_{54} - \dot{E}x_{55}$
Solar cycle heat exchanger	$\dot{E}x_{d,solar\ he} = \dot{E}x_{44} - \dot{E}x_{49} + \dot{E}x_{46} - \dot{E}x_{45}$
Solar cycle	$\dot{E}x_{d,sc} = \dot{Q}_{solar}\left(1 - \frac{T_0}{T_{sun}}\right) - \dot{Q}_{eva}\left(1 - \frac{T_0}{T_{eva}}\right) - \dot{Q}_{htg}\left(1 - \frac{T_0}{T_{htg}}\right) - \dot{W}_{p,sc}$
Absorption cycle very high temperature generator	$\dot{E}x_{d,vhtg} = \dot{E}x_{14} - \dot{E}x_{15} - \dot{E}x_{16} + \dot{E}x_{45} - \dot{E}x_{46}$
Absorption cycle high temperature generator	$\dot{E}x_{d,htg} = \dot{E}x_{13} - \dot{E}x_{20} - \dot{E}x_{15} + \dot{E}x_{17} - \dot{E}x_{18}$
Absorption cycle medium temperature generator	$\dot{E}x_{d,mtg} = \dot{E}x_{9} - \dot{E}x_{24} + \dot{E}x_{19} - \dot{E}x_{21} - \dot{E}x_{22}$
Absorption cycle very low temperature generator	$\dot{E}x_{d,vltg} = \dot{E}x_{28} - \dot{E}x_{29} + \dot{E}x_{23} - \dot{E}x_{25} - \dot{E}x_{26}$
Absorption cycle very high temperature heat exchanger	$\dot{E}x_{d,vhhx} = \dot{E}x_{16} - \dot{E}x_{34} + \dot{E}x_{12} - \dot{E}x_{14}$

Absorption cycle high temperature heat exchanger	$\dot{E}x_{d,hhx} = \dot{E}x_{35} - \dot{E}x_{36} + \dot{E}x_{10} - \dot{E}x_{11}$
Absorption cycle medium temperature heat exchanger	$\dot{E}x_{d,lhx} = \dot{E}x_{37} - \dot{E}x_{38} + \dot{E}x_{7} - \dot{E}x_{8}$
Absorption cycle very cold temperature heat exchanger	$\dot{E}x_{d,vlhx} = \dot{E}x_{4} - \dot{E}x_{5} + \dot{E}x_{39} - \dot{E}x_{40}$
Absorption cycle condenser heat exchanger	$\dot{E}x_{d,chx} = \dot{E}x_{25} - \dot{E}x_{27} + \dot{E}x_{3} - \dot{E}x_{30}$
Absorption cycle pump	$\dot{E}x_{d,abs\,p} = \dot{E}x_{1} - \dot{E}x_{2} + \dot{W}_{p,abs}$
Absorption cycle absorber	$\dot{E}x_{d,abs} = \dot{E}x_{33} + \dot{E}x_{41} - \dot{E}x_{1} - \dot{Q}_{abs}\left(1 - \frac{T_0}{T_{abs}}\right)$
Absorption cycle throttle valve 1	$\dot{E}x_{d,th\,valve1} = \dot{E}x_{31} - \dot{E}x_{32}$
Absorption cycle evaporator	$\dot{E}x_{d,eva} = \dot{E}x_{32} - \dot{E}x_{33} + \dot{Q}_{eva}\left(1 - \frac{T_0}{T_{eva}}\right)$
Absorption cycle throttle valve 2	$\dot{E}x_{d,th\,valve2} = \dot{E}x_{40} - \dot{E}x_{41}$
Absorption cycle condenser	$\dot{E}x_{d,con} = \dot{E}x_{26} + \dot{E}x_{27} - \dot{E}x_{31} - \dot{Q}_{con}\left(1 - \frac{T_0}{T_{con}}\right)$
Absorption cycle	$\dot{E}x_{d,abs} = \dot{Q}_{vhtg}\left(1 - \frac{T_0}{T_{vhtg}}\right) - \dot{Q}_{eva}\left(1 - \frac{T_0}{T_{eva}}\right) - \dot{W}_{p,abs}$
Kalina cycle separator	$\dot{E}x_{d,separator} = \dot{E}x_{55} - \dot{E}x_{56} - \dot{E}x_{57}$
Kalina cycle turbine	$\dot{E}x_{d,t\,kc} = \dot{E}x_{56} - \dot{E}x_{60} - \dot{W}_{t,kc}$
Kalina cycle absorber	$\dot{E}x_{d,abs,kc} = \dot{E}x_{59} + \dot{E}x_{60} - \dot{E}x_{51} + \dot{Q}_{abs}\left(1 - \frac{T_0}{T_{abs}}\right)$
Kalina cycle pump	$\dot{E}x_{d,p,kc} = \dot{E}x_{52} - \dot{E}x_{53} + \dot{W}_{p,kc}$
Kalina cycle throttle valve	$\dot{E}x_{d,throttle\,kc} = \dot{E}x_{58} - \dot{E}x_{59}$
Kalina cycle condenser	$\dot{E}x_{d,con\,kc} = \dot{E}x_{51} - \dot{E}x_{52} - \dot{Q}_{con}\left(1 - \frac{T_0}{T_{con}}\right)$
Kalina cycle	$\dot{E}x_{d,kc} = \dot{Q}_{eva}\left(1 - \frac{T_0}{T_{eva}}\right) + \dot{W}_{t} - \dot{W}_{p,kc}$
System 3	$\dot{E}x_{d,system\,3} = \dot{Q}_{solar}\left(1 - \frac{T_0}{T_{sun}}\right) - \dot{Q}_{eva}\left(1 - \frac{T_0}{T_{eva}}\right) + \dot{W}_{t} - \dot{W}_{p,kc} - \dot{W}_{p,abs} - \dot{W}_{p,sc}$

- **Energy Efficiency**

The energy efficiency is defined as the ratio of useful energy produced to the input energy supplied to the system. In System 3, energy efficiency of the Kalina cycle can be calculated by the following formula:

$$\eta_{en,kc} = \frac{\dot{W}_t - \dot{W}_{p,kc}}{\dot{Q}_{eva}} \quad (4.163)$$

The system energy efficiency can be expressed as follows:

$$\eta_{en,system} = \frac{\dot{W}_t - \dot{W}_{p,sc} - \dot{W}_{p,abs} - \dot{W}_{p,kc}}{\dot{Q}_{solar}} \quad (4.164)$$

The energetic coefficient of performance for the quadruple effect absorption chiller can be calculated as:

$$COP_{en,chiller} = \frac{\dot{Q}_{eva}}{\dot{Q}_{vhtg} + \dot{W}_p} \quad (4.165)$$

- **Exergy Efficiency**

The exergy efficiency is the product exergy output divided by the exergy input. The exergy efficiency of the solar cycle is given as follows:

$$\eta_{ex,sc} = \frac{\dot{Q}_{vhtg}\left(1 - \frac{T_0}{T_{vhtg}}\right) + \dot{Q}_{eva}\left(1 - \frac{T_0}{T_{eva}}\right)}{\dot{Q}_{solar}\left(1 - \frac{T_0}{T_{sun}}\right)} \quad (4.166)$$

Kalina cycle exergy efficiency can be expressed as follows:

$$\eta_{ex,kc} = \frac{\dot{W}_t - \dot{W}_{p,kc} + + \dot{Q}_{con,kc}\left(1 - \frac{T_0}{T_{con,kc}}\right)}{\dot{Q}_{eva}\left(1 - \frac{T_0}{T_{eva}}\right)} \quad (4.167)$$

System 3 exergy efficiency equation is written as follows:

$$\eta_{ex,system} = \frac{\dot{W}_t + \dot{Q}_{eva,abs}\left(1 - \frac{T_0}{T_{eva,abs}}\right) + \dot{Q}_{con,kc}\left(1 - \frac{T_0}{T_{con,kc}}\right) - \dot{W}_{p,sc} - \dot{W}_{p,abs} - \dot{W}_{p,kc}}{\dot{Q}_{solar}\left(1 - \frac{T_0}{T_{sun}}\right)} \quad (4.168)$$

The exergetic coefficient of performance for the absorption chiller can be calculated as

$$COP_{ex,chiller} = \frac{\dot{Q}_{eva}\left(1 - \frac{T_0}{T_{eva}}\right)}{\dot{Q}_{vhtg}\left(1 - \frac{T_0}{T_{vhtg}}\right) + \dot{W}_p} \quad (4.169)$$

4.9.3 Exergoeconomic Analysis

In this subsection, exergoeconomic analyses equations of each component in System 3 is given and explained.

- **Parabolic Solar Collector**

The purchase cost of parabolic solar collector is a function of collector width and length and can be expressed as [100]:

$$Z_{sc}(\$) = 310WL \tag{4.170}$$

- **Thermal Storage**

The purchase cost of thermal storage is a function of heat stored. It can be expressed as [8]:

$$Z_s(\$) = 27\dot{Q}_s \tag{4.171}$$

- **Absorption Chiller**

Although purchase cost of absorption chiller is a function of design parameters, it can be approximated by a function of cooling load [101]:

$$Z_{chiller}(\$) = 1144.3(\dot{Q}_{eva})^{0.67} \tag{4.172}$$

where $\dot{Q}_{eva}$ is the cooling load of the absorption chiller in kW.

- **Kalina Cycle Regenerator**

As a heat exchanger, purchase cost of the regenerator can be calculated with the following equation [8]:

$$Z_{regenerator}(\$) = 130(\frac{A_{regenerator}}{0.093})^{0.83} \tag{4.173}$$

where $A_{regenerator}$ can be found from the following equation:

$$A_{regenerator} = \frac{\dot{Q}}{U_{regenerator}\Delta T_{ln}} \tag{4.174}$$

Here $U_{regenerator}$ is overall heat transfer coefficient for regenerator with the value of 2 kW/m^{2}K. ΔT_{ln} is the logarithmic temperature difference and can be defined as:

$$\Delta T_{ln} = \frac{\Delta T_A - \Delta T_B}{\ln(\frac{\Delta T_A}{\Delta T_B})} \tag{4.175}$$

where ΔT_A is the temperature difference between the two streams at end A, and ΔT_B is the temperature difference between the two streams at end B. ΔT_{ln} is defined as follows:

$$\Delta T_{ln} = \frac{(T_{54} - T_{57}) - (T_{53} - T_{58})}{\ln(\frac{T_{54} - T_{57}}{T_{53} - T_{58}})} \tag{4.176}$$

- **Kalina Cycle Turbine**

The purchase cost of the turbine can be defined as a function of turbine inlet temperature, turbine isentropic efficiency and turbine work [102]:

$$Z_t = 3880.5(\dot{W}_t)^{0.7}\left[1+\left(\frac{0.05}{1-\eta_t}\right)^3\right]\{1-\exp\left(\frac{T_{21}-866K}{10.42K}\right)\} \quad (4.177)$$

- **Kalina Cycle Condenser**

To calculate the purchase cost of condenser the following expression can be used [8]:

$$Z_{con}\ (\$) = 280.74\frac{\dot{Q}_{con}}{K\Delta T_{ln}} + 746\dot{m}_{kc} \quad (4.178)$$

and

$$K = 2200\ \frac{W}{m^2K}$$

Here, $\dot{m}_{kc}$ is the Kalina cycle mass flow rate, ΔT_{ln} is the logarithmic temperature difference and *k* is the condenser purchase cost constant. ΔT_{ln} is defined as follows:

$$\Delta T_{ln} = \frac{(T_{51}-T_{64})-(T_{52}-T_{63})}{\ln(\frac{T_{51}-T_{64}}{T_{52}-T_{63}})} \quad (4.179)$$

- **Kalina Cycle Pump**

The purchase cost of pump is defined as follows [8]:

$$Z_p(\$) = 705.48\left(\dot{W}_P\right)^{0.71}(1+\frac{0.2}{1-\eta_p}) \quad (4.180)$$

where $\dot{W}_P$ is the pump power and η_p is the pump efficiency.

- **Electrolyzer**

The purchase cost of the electrolyzer is a function of the inlet electricity to split water which can be expressed as [8]:

$$Z_{elec}(\$) = 1000\dot{W}_{elec} \quad (4.181)$$

Chapter 5: Results and Discussion

5.1 System 1

In this section System 1 results are presented and analyzed. This is done by explaining the methods, assumptions and input data, laying out comparison graphs and optimizing the system parameters.

5.1.1 Assumptions and Data Considered

The thermodynamic and cost analyses are based on some assumptions and input data. The assumptions made for all the systems are given as follows:

- The heat losses from the system boundaries are negligible.
- Possible sources of data noise, e.g. sudden changes in solar irradiance and electric power demand, are not considered in the analyses (i.e. average hourly values are used).
- Solar collector operates during the day and stores heat in the thermal storage units, then uses this energy during the night.
- The turbines operate with 70% efficiency [8].
- The pumps operate with 85% efficiency [8].
- The electrolyzer operates with 60% efficiency [8].
- There are no pressure changes except through flow restrictors and pump.
- The systems operate in steady state.

The assumptions made for System 1 are listed as follows:

- The wind turbine operates with 59% efficiency (Betz limit) [98].
- The wind turbine operates with the average Toronto wind speed.
- States at points 1, 4, 8 are saturated liquid.
- State at point 10 is saturated vapor.

Table 5.1 shows input parameters for modeling System 1. These parameters have to be set at commencement in order to perform the other calculations.

Table 5.1 Input parameters used to model System 1

Collector	
Width	2 m
Length	2 m
Absorber diameter	25 mm
Transparent envelope outer diameter	40 mm
Tube material	Stainless steel
Receiver efficiency	75% [91]
Solar system working fluid	Therminol 66
Thermal storage	
Insulation thickness	30 cm
Insulation material	Polyurethane [39]
Total surface area	6 m^2
Rankine cycle	
Working fluid	Ammonia-water
Wind turbine	
Diameter	34 m
Average wind speed	4.2 m/s
Power coefficient	60 % [98]
Absorption chiller	
Evaporator temperature	7°C
Condenser temperature	35°C
Absorber temperature	40°C
Generator temperature	80°C

In the modeling of the systems, the EES program is used. EES is a general equation-solving program that can numerically solve thousands of coupled non-linear algebraic and differential equations. The program can also be used to solve differential and integral equations, evaluate optimization, convert units, check unit consistency, and generate publication-quality plots. A major feature of EES program is the high accuracy thermodynamic and transport property database that is provided for hundreds of substances, in a manner that allows it to be used with the equation solving capability [103]. The program was developed by Prof. Sanford A. Klein from Department of Mechanical Engineering University of Wisconsin-Madison for F-Chart Software in 1992. V9.698 (2014) version of the program has been used is used as that is the program currently provided to UOIT students.

The EES program uses numerical integration to determine the value of an integral or to solve differential equations. The "Equation-based integral function" can use either a fixed user-supplied step or an automatic step, adjusted to meet pre-determined accuracy criteria. If a fixed step is used, "Richardson Extrapolation" can be used to improve the numerical estimate [103].

5.1.2 Results of System 1

The results obtained from System 1 are tabulated in Table 5.2. These outputs are subject to change depending on the parameter that is under consideration. For maximum efficiency, efficiency may increase, while other parameters would drop. This is discussed in optimization section.

Table 5.2 Parameter values resulting from energy and exergy analyses of System 1

$\dot{Q}_{heating}$ (kW)	298.5
$\dot{Q}_{cooling,absorption}$ (kW)	28
Maximum $\dot{W}_{turbine}$ (kW)	48
Maximum η_{multi} (%)	43
Maximum ψ_{multi} (%)	65
ψ_{wind} (%)	35
$\dot{m}_{H_2}$ (kg/h)	1.96
$\dot{m}_{dwh}$(kg/s)	0.26
Absorption chiller COP_{en}	0.80
Absorption chiller COP_{ex}	0.31
CO_2 emissions reduced (tons/year)	1613
Total exergy destruction rate (kW)	485

The exergy destruction for the main components of System 1 are shown in Figure 5.1. The last column shows the total exergy destruction in System 1.

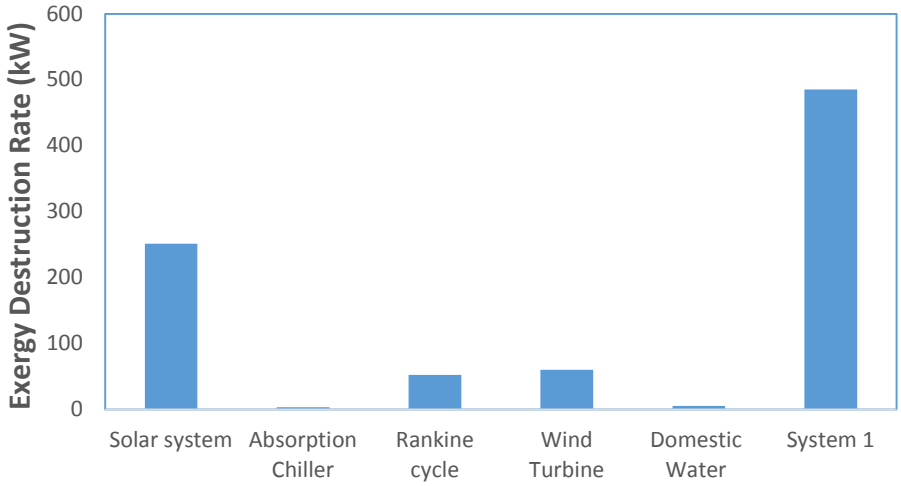

Figure 5.1 Exergy destructions in System 1

Highest exergy destruction occurs in the solar system, while the lowest is in the absorption chiller. This means that due to irreversibilities, 251 kW of energy is lost in the wind turbine and

485 kW is lost in the system. An exergy destruction graph is a useful to tool to focus on the sources of irreversibilities.

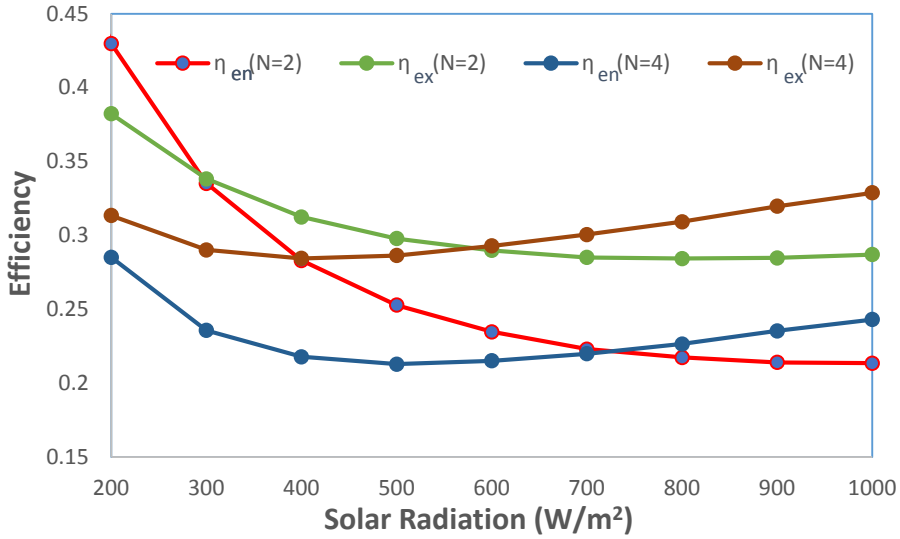

Figure 5.2 Solar radiation vs. system energy and exergy efficiencies

Figure 5.2 shows the effect of solar radiation on a number of solar units and corresponding the efficiency levels. When there are 2 solar units installed, both system energy and exergy efficiencies drop radically, they stabilize after around 800 W/m^2. The reason for this is that solar radiation increases but the output does not increase at the same rate as the solar radiation. When there are 4 solar units installed, both energy and exergy efficiencies are lower compared to 2 solar units for low solar radiation. Efficiencies for 4 units are greater than that for 2 units after 600 and 700 W/m^2 for exergy and energy efficiencies respectively. The reason for this phenomena is that when there are 4 solar units installed, for higher solar radiation the increase in output is much higher than 2 solar units compared to the increase in solar heat input. The curve trends show that a minimum peak is reached for every configuration. According to energy efficiency definition, the ratio of the system output (work done in the turbines) over solar power input is the minimum at these points. For the exergy efficiency curves, the exergy output of the system (work done in the turbines plus heat output from Rankine cycle condenser, absorption chiller evaporator and domestic hot water heat output) over solar power input exergy value is minimized at these peak points.

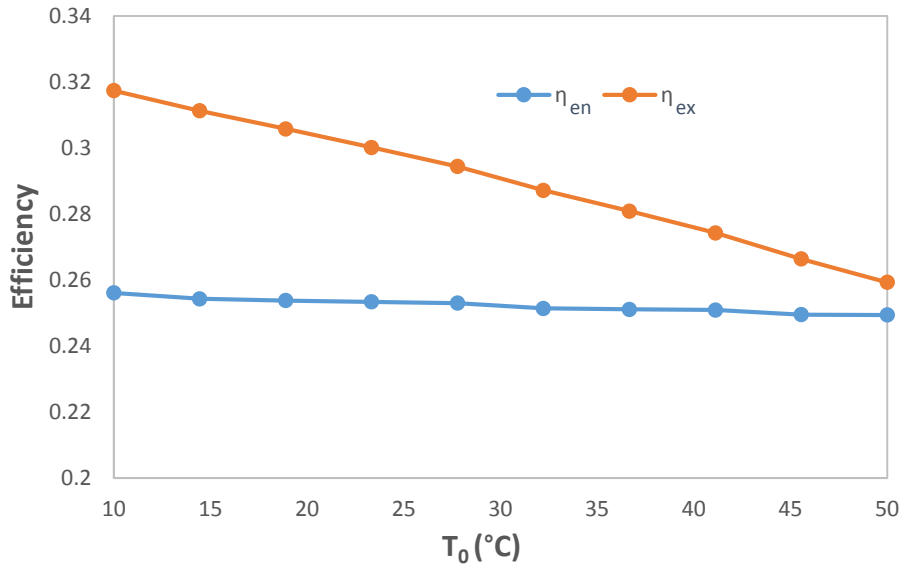

Figure 5.3 System energy and exergy efficiencies vs. ambient temperature

The variation of ambient temperature (T_0) affects system energy and exergy efficiencies indirectly in Figure 5.3. Energy efficiency drops because the increase in the output is lower than the increase in solar energy. Exergy efficiency drops at a faster rate because it is more affected by the increase in ambient temperature. As reference temperature increases, the temperature difference of the process temperature drops. If the process temperature does not increase at the same rate as the reference temperature, the exergy value drops.

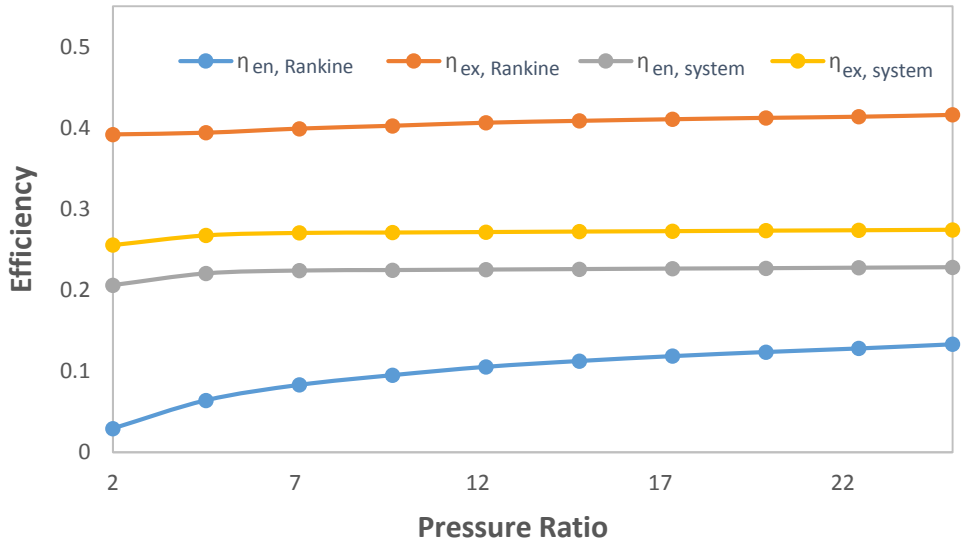

Figure 5.4 System and Rankine cycle efficiencies vs. Rankine cycle pump pressure ratio

As it is shown in Figure 5.4, the pressure ratio of the Rankine cycle pump affects the Rankine cycle and system efficiencies. System efficiencies increase at the same rate with increasing pressure ratio. However, Rankine cycle exergy efficiency increases at a faster rate, while energy efficiency increases at an even faster rate, then stabilizes at a value of 10% after a pressure ratio of 20. The reason for the fast rate of increase in the Rankine cycle energy efficiency at low pressure ratios is that by increasing pressure ratio, the increase in output drops and stabilizes. The reason for the slower rate of increase in exergy efficiency is because heat output from the Rankine cycle drops. However, as the work output increase surpasses heat output increase, the efficiency increases.

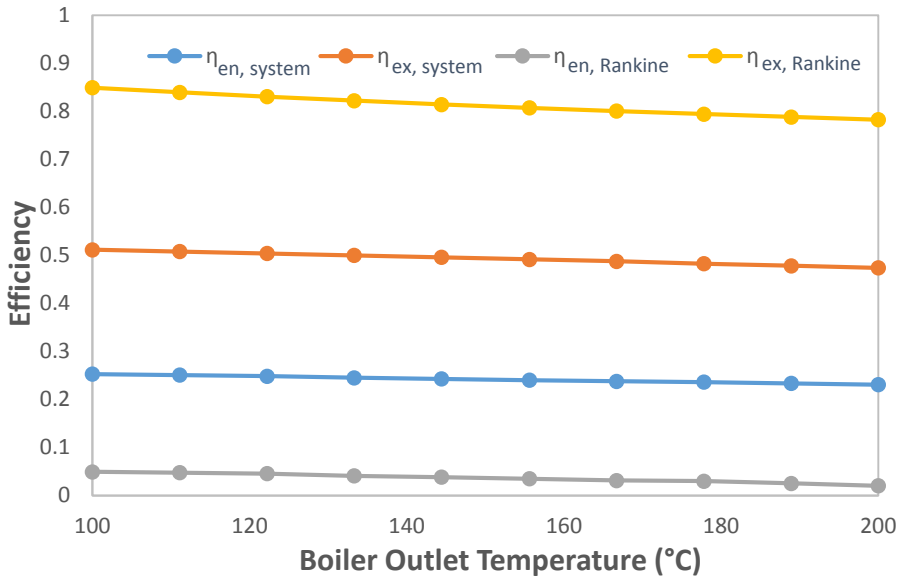

Figure 5.5 System and Rankine cycle efficiencies vs. boiler outlet temperature

According to Figure 5.5, by increasing boiler outlet temperature all the efficiencies drop. The drop is more significant in Rankine cycle exergy efficiency, then in system exergy efficiency. System energy and exergy efficiencies are affected negatively because heat output from the Rankine system drops. Although heat output to the domestic water heater increases, this increase is not enough to increase the efficiency. The reason for the drop in Rankine cycle efficiencies is due to the decrease in work and heat outputs from the Rankine system.

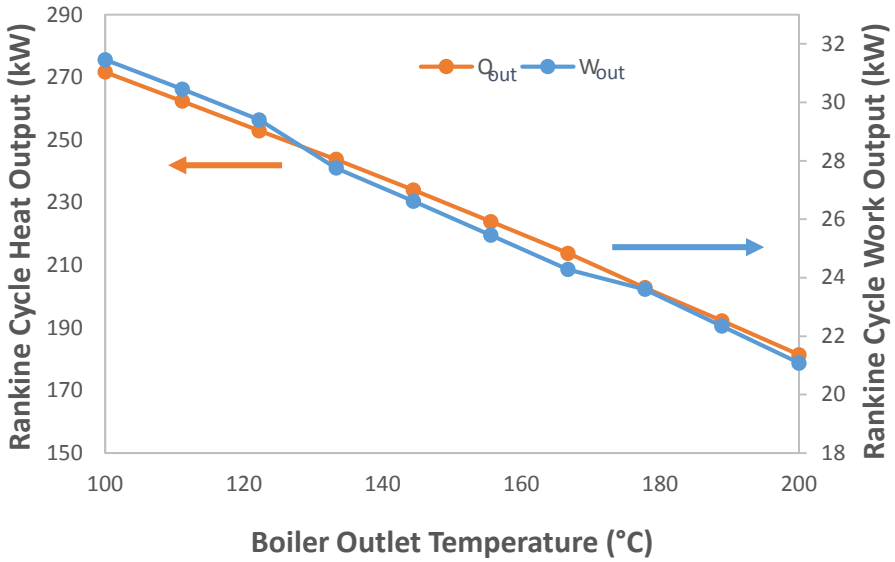

Figure 5.6 Rankine cycle heat and work outputs vs. boiler outlet temperature

Both work output and heat output from the Rankine cycle are negatively affected by an increase in boiler outlet temperature as seen in Figure 5.6. When the boiler outlet temperature increases, less heat is transferred to the Rankine cycle, hence reducing the heat and work outputs from the system. The reason for the irregularity in work output graph is because the number of data is not sufficient to make the curve smooth. If larger number of data are taken to plot the graph, it would be a smooth curve.

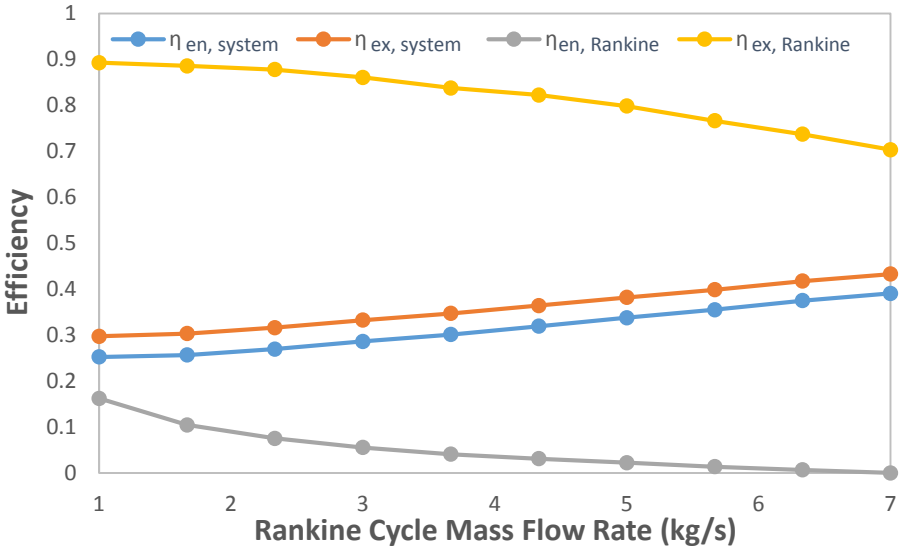

Figure 5.7 System and Rankine cycle efficiencies vs. Rankine cycle mass flow rate

Figure 5.7 shows that when the mass flow rate of the Rankine cycle is increased, the energy and exergy efficiency of Rankine cycle drops, while system energy and exergy efficiencies increase. The rate of increase is the same in system efficiencies, while rate of drop is higher in Rankine cycle exergy efficiency than energy efficiency. The reason for the drop in Rankine cycle efficiencies is pump work input increases when the mass flow rate increases. The pump has to work harder to pump high mass flow rate fluid. The increase in work output is not as high as work input as a result Rankine cycle energy and exergy efficiencies drop.

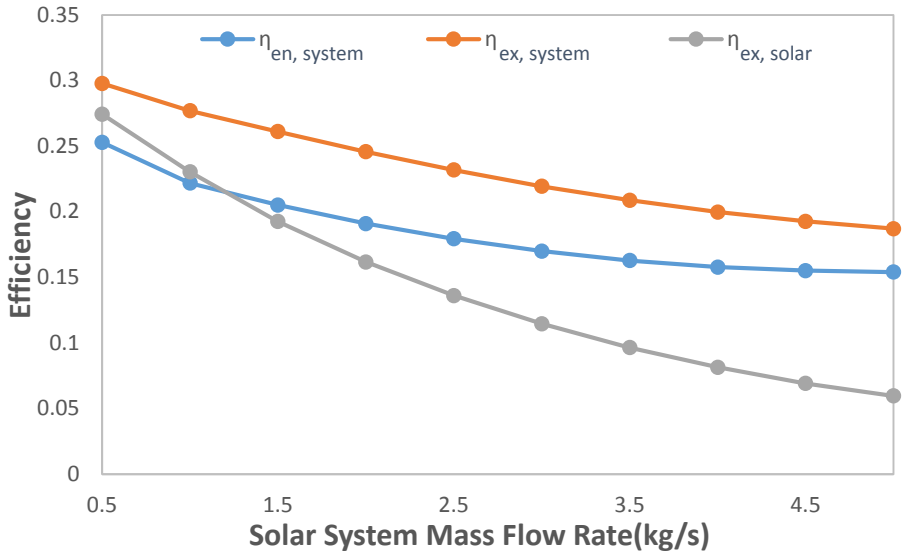

Figure 5.8 System and solar system efficiencies vs. solar system mass flow rate

In Figure 5.8 the system and solar system energy and exergy efficiencies versus solar system mass flow rate are analyzed. All the efficiencies drop with an increasing mass flow rate of the solar system. The most significant drop is in solar system and system exergy efficiencies, followed by solar system energy efficiency. All the graphs are parabolic with the rate of drop decreasing. Efficiencies decrease because the pump in the solar system has to work much harder to pump working fluid. As a result, work input in the system increases but the output heat and work do not increase at the same rate as the work input. The reason that solar system exergy efficiency drops faster than system efficiencies is that solar system exergy increases at a much higher rate than the system efficiency parameters.

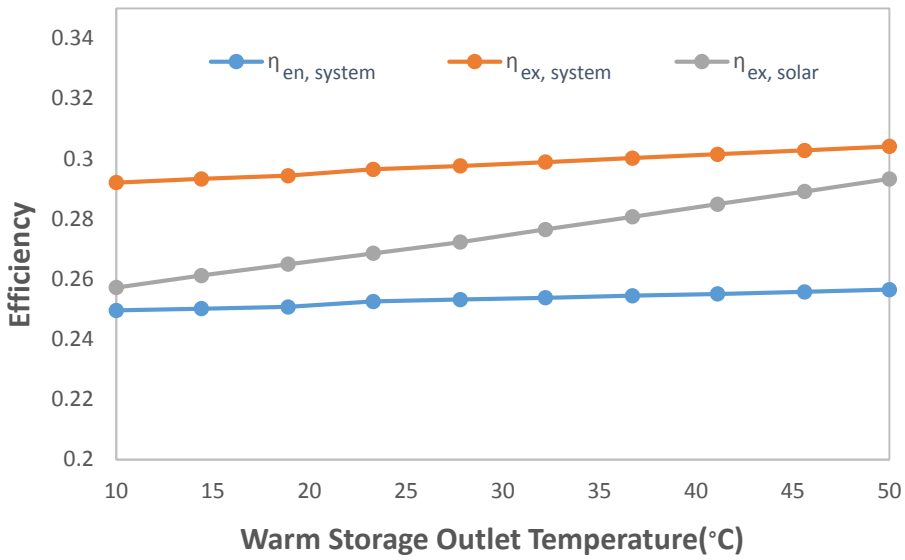

Figure 5.9 System and solar cycle efficiencies vs. warm storage outlet temperature

Warm storage outlet temperature affects the efficiencies. All the efficiencies increase with increasing outlet temperature as shown in Figure 5.9. The effect is more significant in the solar system exergy efficiency. The rate of increase of solar system efficiency is much higher than system efficiencies because the heat input to the Rankine cycle increases at a high rate (which is an output for the solar cycle). The rate of increase is the same in system efficiencies. System efficiencies increase because of the increase of work and heat output from Rankine cycle.

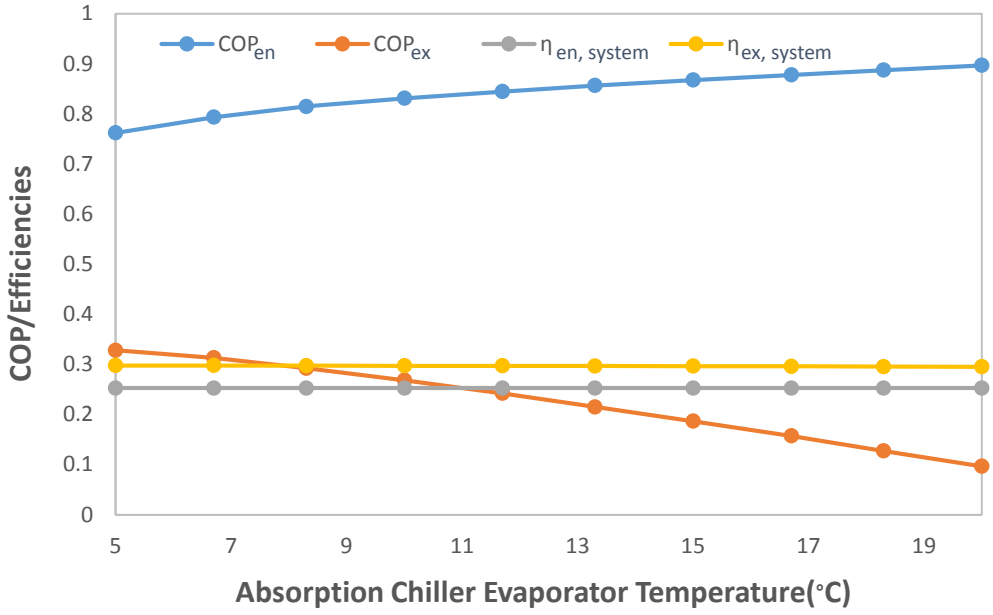

Figure 5.10 Absorption chiller COPs and system efficiencies vs. absorption chiller evaporator temperature

Figure 5.10 shows that the energy coefficient of performance (COP) of absorption chiller increases with increasing evaporator temperature, while exergy COP drops. Energy COP straight-lines after 18°C. System energy efficiency stays constant, while system exergy efficiency decreases slightly. The reason for the increase of energy COP is due to the increase in evaporator heat input with increasing evaporator temperature. Exergy COP decreases because evaporator temperature is an effective factor for exergy COP calculation. Numerator is $\dot{Q}_{eva}(1-\frac{T_0}{T_{eva}})$ for COP exergy calculation. Because of the increase in evaporator temperature, heat output from the evaporator increases, and exergy COP decreases.

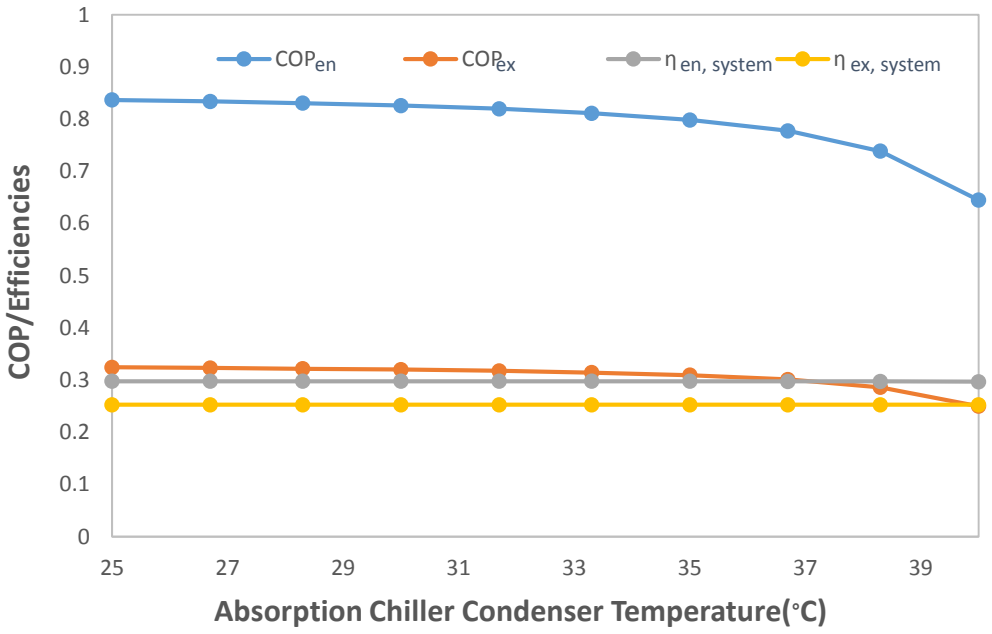

Figure 5.11 Absorption chiller COPs and system efficiencies vs. absorption chiller condenser temperature

All the COPs and efficiencies drop with increasing absorption chiller condenser temperature as Figure 5.11 shows. The drop is more significant for the COPs, while efficiencies are almost constant, slightly dropping. The highest drop is in the energy COP. Because of the output of the absorption chiller, evaporator heat drops at a faster rate. The drop for the exergy COP is slower that energy COP because during the calculation of exergy COP, evaporator heat is multiplied by a factor which reduces the decrease rate.

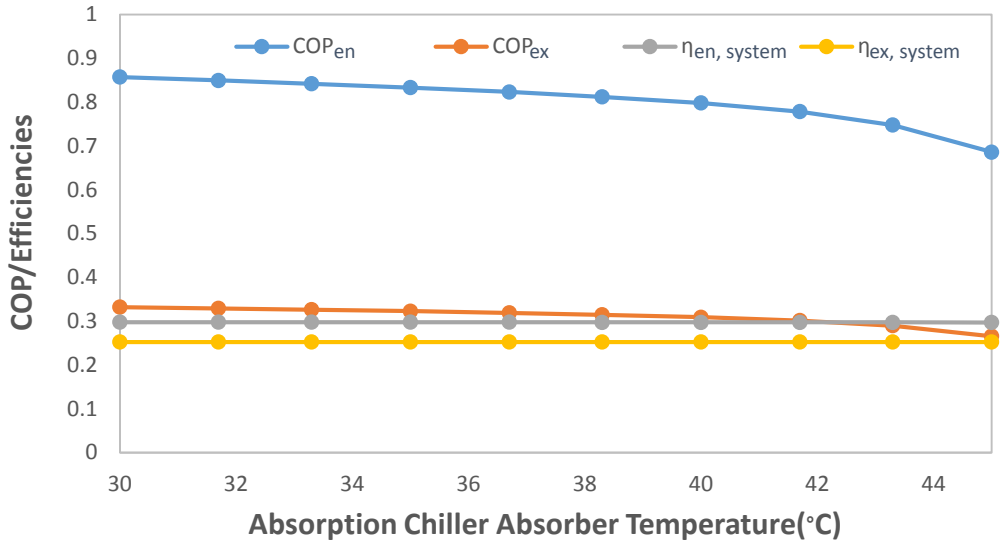

Figure 5.12 Absorption chiller COPs and system efficiencies vs absorption chiller absorber temperature

All the COPs and efficiencies drop by increasing absorption chiller absorber temperature in Figure 5.12. The graphs are exactly the same as absorption chiller condenser temperature graphs with a shift of 5°C. The drop is more significant for the COPs, while efficiencies are almost constant, slightly dropping. The highest drop is in the energy COP because output of the absorption chiller, evaporator heat drops at a faster rate. The drop for the exergy COP is slower than energy COP because during the calculation of exergy COP, evaporator heat is multiplied by a factor which reduces the drop rate.

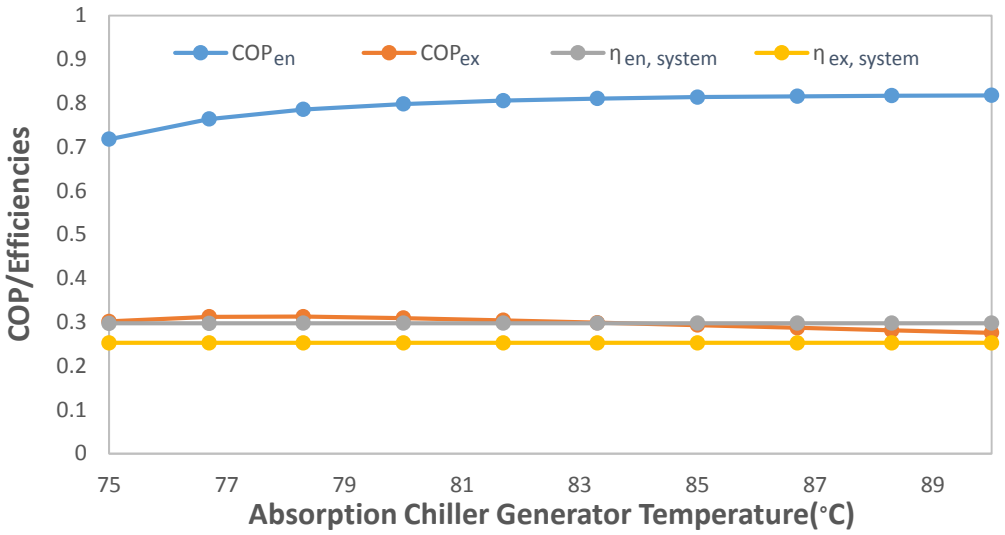

Figure 5.13 Absorption chiller COPs and system efficiencies vs absorption chiller generator temperature

As it is shown in Figure 5.13, all the parameters except energy COP increase with the increasing absorption chiller generator temperature. The changes are not very significant for efficiencies, while COPs change more significantly. Energy COP increases because evaporator heat input increases. Exergy COP drops because as generator temperature increases, the denominator also increases, thereby decreasing the fraction.

5.1.3 Optimization

In this section significant output parameters are tested for optimization by finding the appropriate values of the input parameters. Four functions are optimized; power output, system efficiency and CO_2 reduction are maximized, and cost is minimized. In order to perform optimization, independent variables affecting the target function are selected, and then minimum and maximum bounds are determined. Optimization is achieved by utilizing the EES Min/Max property, using the Conjugate Directions method. To find the optimum value of the target function all the variables are tested one by one within the boundary range to find the optimum value of the target function.

- **Power Output Maximization**

First function to be maximized is the power output from the Rankine cycle. As discussed in section 4.5.3, system bounds should be specified. The independent variables and minimum, maximum values for each variable are given in Table 5.3.

After running the maximization property of EES, the results in "Opt W_{out}" column of Table 5.3 is achieved. The results show that 330 equations are solved by 199 iterations in 10.9 seconds. Maximum number of iterations is set initially to have the opportunity to abort the optimization if an optimum value is not found in a specific time. For a solar system flow rate of 2 kg/s, Rankine cycle pressure ratio of 100 and ambient temperature of 323 K (50°C) the power output is maximized at 47.75 kW.

Ambient temperature (T_0) and solar radiation (G) are not adjustable but the optimum value of it is calculated as a reference to the designers or builders. Thus, optimum climate for the system can be determined from the results.

Table 5.3 Independent variables of System 1 for power output maximization

Variable	Min	Max	Opt W_{out}
Solar radiation (*G*), W/m^2	0	100	660
Ambient temperature (T_0),°C	10	50	50
Rankine cycle pressure ratio (*PR*)	5	150	100
Solar cycle mass flow rate ($\dot{m}_{oil}$), kg/s	0.5	5	2
Boiler exit temperature (T_{30}),°C	100	150	100

The study show that as the number of variables is increased, the optimization takes longer and more iterations have to be done but better results can be achieved.

- **Efficiency Maximization**

In order to increase efficiency, five independent variables are chosen. These are; solar radiation, solar cycle mass flow rate, ambient temperature, Rankine cycle pressure ratio and boiler exit temperature. These variables are input values of the model created in EES. Minimum and maximum values of these variables can be seen in Table 5.4.

Table 5.4 Independent variables of System 1 for efficiency maximization

Variable	Min	Max	Opt η_{en}	Opt η_{ex}
Solar radiation (*G*), W/m^2	0	1000	100	660
Solar cycle mass flow rate ($\dot{m}_{oil}$), kg/s	0.5	5	1.989	1.989
Ambient temperature (T_0),°C	10	35	10	10
Rankine cycle pressure ratio (*PR*)	1	100	20	1
Boiler exit temperature (T_{30}), °C	100	150	100	100
Maximum Efficiency			43.2 %	65 %

The value of the variables to reach maximum efficiency in System 1 are in the "Opt η_{en}" column in Table 5.4. In order to check maximum exergy efficiency of System 1, another run is performed. The optimum variables are shown in "Opt η_{ex}" column.

- **Cost Minimization**

If the goal of the optimization is to minimize the cost, the results in Table 5.5 are achieved. The variables affecting the cost are; solar radiation, solar cycle mass flow rate, ambient temperature, Rankine cycle pressure ratio and boiler exit temperature. The minimum and

maximum of these variables are shown in the "Min" and "Max" columns of Table 5.5. The optimum values of the variables are listed in the "Opt. Cost" column. It is found that if solar radiation is minimum at 100 W/m^2, solar cycle mass flow rate is maximum at 5 kg/s, ambient temperature is minimum at 10°C, Rankine cycle pressure ratio is minimum at 2, and boiler exit temperature is at 134°C, then total cost of $236,024 is achieved. Note that in the above scenario the outputs of the system are minimized.

Table 5.5 Independent variables of System 1 for cost minimization

Variable	**Min**	**Max**	**Opt. Cost**
Solar radiation (G), W/m^2	0	1000	100
Solar cycle mass flow rate ($\dot{m}_{oil}$), kg/s	0.5	5	5
Ambient temperature (T_0),°C	10	50	10
Rankine cycle pressure ratio (PR)	2	100	2
Boiler exit temperature (T_{30}), °C	100	150	134
Minimum Cost			$236,024

- **Maximization of CO_2 Reduction**

As the system is totally renewable, there are no polluting gas emissions and therefore it cannot be minimized. An assessment of the CO_2 reduced through this system is done as part of the environmental analysis. For this analysis, the CO_2 emission of an equivalent system working with fossil fuels is calculated. The results in Table 5.6 show that if the solar radiation is 738 W/m2, solar cycle mass flow rate is 5 kg/s, ambient temperature is 50°C, Rankine cycle pressure ratio is 90, boiler exit temperature is 100°C, then 5079 tons of CO_2 is reduced. Note that these values maximize the output of the system, hence CO_2 reduced is maximized.

Table 5.6 Independent variables of System 1 for CO_2 reduction maximization

Variable	**Min**	**Max**	**Opt. CO_2**
Solar radiation (G), W/m^2	0	1000	738
Solar cycle mass flow rate ($\dot{m}_{oil}$), kg/s	0.5	5	5
Ambient temperature (T_0),°C	10	50	50
Rankine cycle pressure ratio (PR)	2	100	90
Boiler exit temperature (T_{30}), °C	100	150	100
Maximum CO_2 reduction (tons/year)			5079

5.1.4 Sensitivity Analysis

In this section, the effects of the independent variables on the optimization targets are discussed. System work output, efficiency, cost and CO_2 reduction optimization are performed up to this point. However, it is important to understand which variable affects the optimization targets and in what direction.

- **Solar Radiation**

The effect of solar radiation on the optimization targets is analyzed in this section. The resulting chart is shown in Figure 5.14. Solar radiation range is between 0 and 1000 W/m^2. The vertical axis on the left (primary axis) shows the cost as a factor of $10,000 and the system efficiency, while the secondary vertical axis on the right shows CO_2 reduction in tons/year.

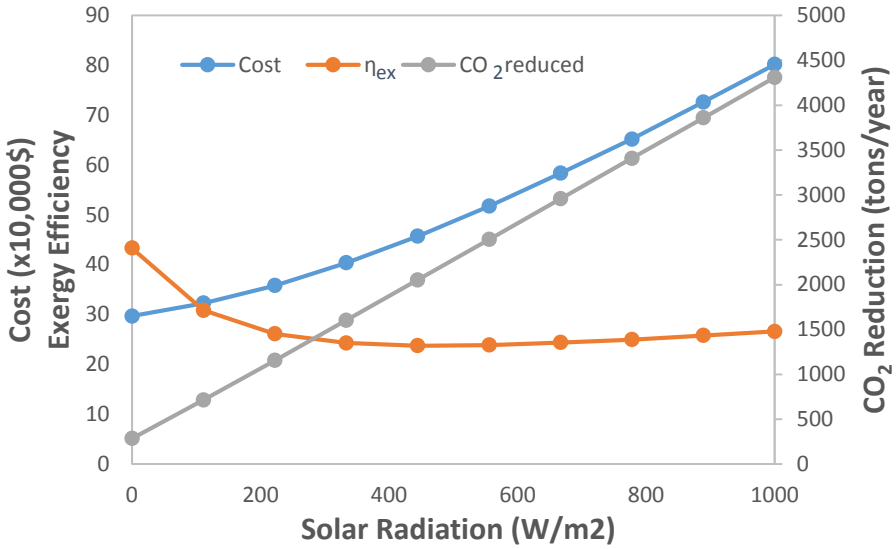

Figure 5.14 Effect of solar radiation on optimization targets

By increasing solar radiation the total cost and CO_2 reductions are increased. Costs increase as the system outputs increase hence system component sizes increase. CO_2 reduction increases because the system outputs increase. In a similar system working with fossil fuels, CO_2 emissions increase with increasing system outputs. The exergy efficiency drops by increasing solar radiation, reaches a peak at around 500 W/m^2, and then starts increasing. The outcome from solar radiation is smaller than the system input increase up to 500 W/m^2 therefore the exergy efficiency drops.

- **Ambient Temperature**

The effect of ambient temperature is analyzed in this section and the result is shown in Figure 5.15. Ambient temperature range is between 10°C and 50°C. The primary vertical axis on the left shows the cost of the system in $10,000s and the system efficiency, while the secondary vertical axis on the right shows CO_2 reduction in tons/year.

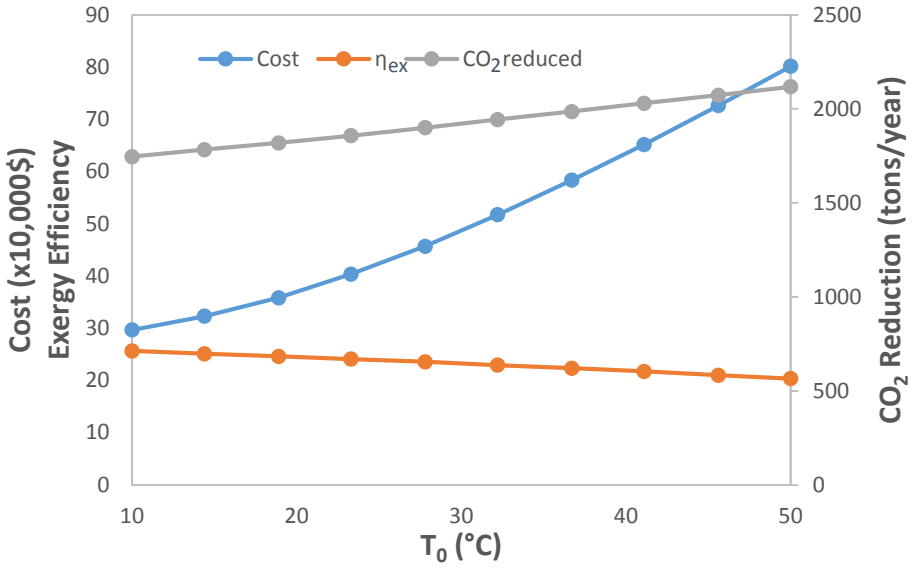

Figure 5.15 Effect of ambient temperature on optimization targets

Increasing ambient temperature increases reduction of CO_2 and cost of system 1. CO_2 reduction increases as a straight line, while CO_2 curve is parabolic. An increase in ambient temperature increases the system output hence an increase in CO_2 reduction. As the size of the system components require upgrading, the costs of the systems will vary. Increasing ambient temperature decreases the exergy efficiency of the system. An increase in the ambient temperature affects the system output to a greater extent than it affects the system input. As a result efficiency drops.

- **Solar System Mass Flow Rate**

The effect of solar system mass flow rate on cost, CO_2 reduction and system exergy efficiency is discussed in this section. The results are shown in Figure 5.16. For physical limits the solar cycle mass flow rate boundaries are determined as 0.5 and 5 kg/s. The primary vertical axis on the left shows the costs and efficiency values of the system, while secondary vertical axis on the right shows the CO_2 reduction.

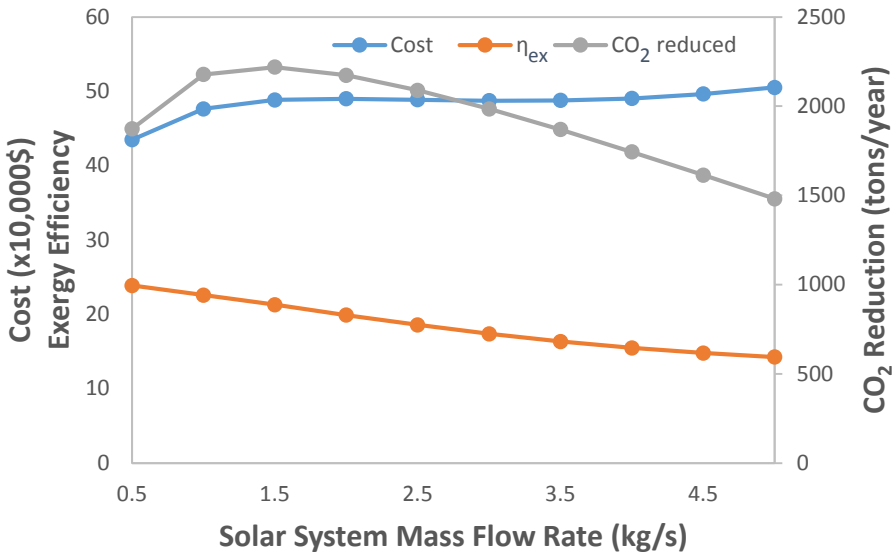

Figure 5.16 Effect of solar cycle mass flow rate on optimization targets

Solar cycle mass flow rate increase elevates the cost. In order to increase flow rate, a higher capacity pump and other components are needed hence the cost increases. Increasing solar cycle mass flow rate diminishes exergy efficiency. The rate in the exergy output doesn't match the rate of increase in the exergy input so the efficiency drops. CO_2 reduction increases initially, then after reaching a peak at 1.5 kg/s, it starts dropping. Effectively, the system output energy increases initially, then drops. Note that cost increase rate slows down until the CO_2 reduction peak point which is 1.5 kg/s, then remains constant.

- **Rankine Cycle Pressure Ratio**

The Rankine cycle pressure ratio is an input parameter that has an effect on the system output. Its effect on the optimization targets is shown in Figure 5.17. The Rankine cycle pressure ratio changes between 10 and 150. All three curves are shown on the same graph to find the optimum pressure ratio. Primary vertical axis shows cost and exergy efficiency, while secondary axis on the right shows CO_2 reduction.

The amount of CO_2 reduction increases with increasing pressure ratio. When the pressure ratio increases, turbine output increases in the Rankine cycle, hence the output and CO_2 reduction increases. Exergy efficiency also increases with increasing pressure ratio. Again the increase in pressure ratio elevates turbine output and exergy efficiency increases. The cost of the system increases initially, however after a pressure ratio of 50 is achieved, the increase is minimal. This shows that increasing the pressure ratio above 50 has very little effect on the system cost.

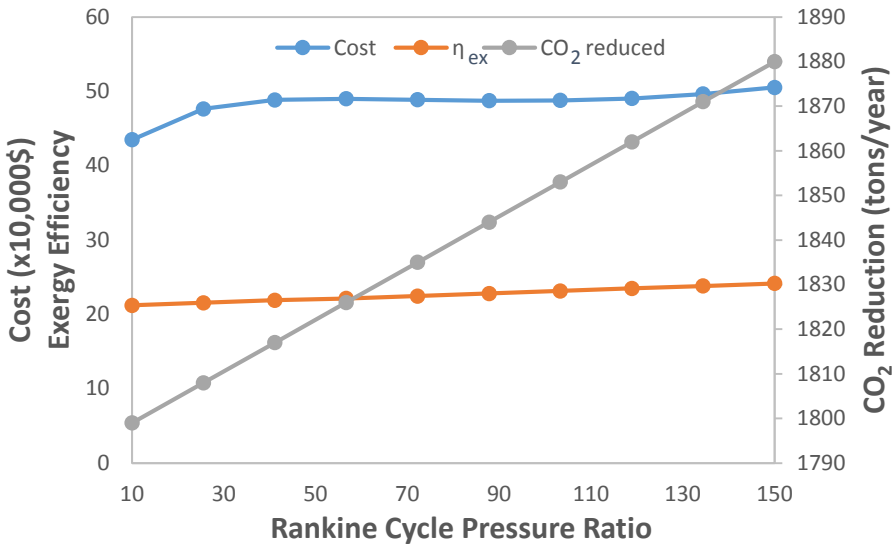

Figure 5.17 Effect of Rankine cycle pressure ratio on optimization targets

- **Boiler Exit Temperature**

Boiler exit temperature (T30) is an independent variable that affects the system outputs. Its effect on cost of the system, CO_2 reduction and exergy efficiency are shown in Figure 5.18. The boiler exit temperature effect is observed between 100°C and 150°C. The cost and exergy efficiency values are shown on the left vertical axis and the value of the CO_2 reduction is shown in the right vertical axis.

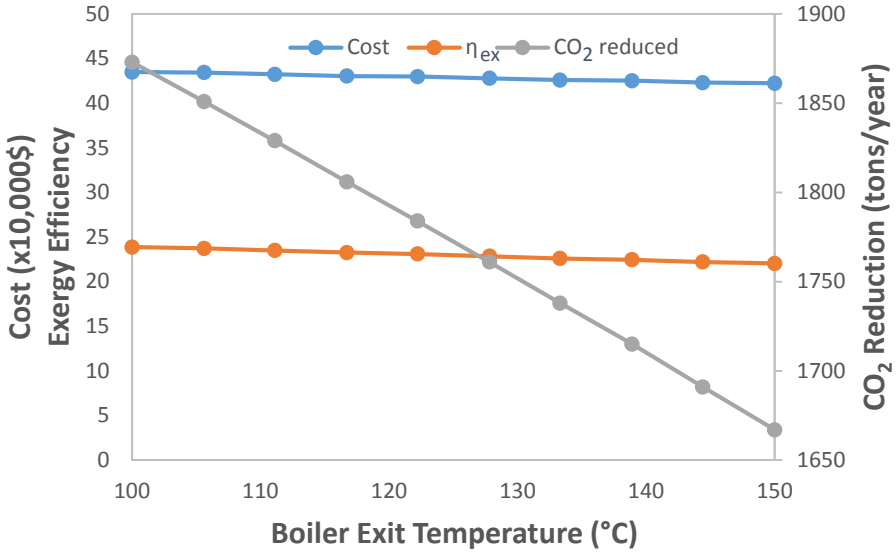

Figure 5.18 Effect of boiler exit temperature on optimization targets

All of the optimization target parameters drop with increasing boiler exit temperature. As the boiler exit temperature increases, CO_2 reductions drops. The reason for this change is that when boiler exit temperature increases, less energy is transferred to the power cycle, hence system output drops. A similar effect is observed for the cost and exergy efficiency of the system. To achieve less output, less investment is required. In addition, exergy efficiency drops when turbine output drops.

5.2 System 2

System 2 results are analyzed in this section. Firstly, all assumptions and data considered are introduced. The results are shown graphically and they are discussed. Finally optimization is carried out for the important system outputs.

5.2.1 Assumptions and Data Considered

The assumptions for all the systems are explained in section 5.1.1. The thermodynamic and cost analyses are based these assumptions. Additional assumptions for System 2 are as follows:

- States at points 1 and 7 are saturated liquid.
- State at points 3 and 10 are saturated vapor.

Table 5.7 shows input parameters used to model System 2. These are the values commonly used in the similar systems or set by the designer as a common sense.

5.2.2 Results of System 2

The results obtained from the model of System 2 in EES can be summarized in Table 5.8. Input parameters in Table 5.8 are used to obtain these results. These results can be optimized for a specific parameter. For example if maximum efficiency is the target, other results would change accordingly.

Table 5.7 Input parameters used to model System 2

Collector	
Width	2 m
Length	2 m
Absorber diameter	25 mm
Transparent envelope outer diameter	40 mm
Tube material	Stainless steel
Receiver efficiency	75% [96]
Solar system working fluid	Therminol 66
Thermal storage	
Insulation thickness	30 cm
Insulation material	Polyurethane [39]
Total surface area	6 m^2
Rankine cycle	
Working fluid	Steam/Ammonia-water
Desalination	
Number of stages	15
Salinity of the sea water	35 g/kg
Sea water temperature	18°C

Exergy destruction rates for main components of System 2 are shown in Figure 5.19. Each component is considered as a control volume and exergy input and outputs from this control volume are calculated to find exergy destruction.

Table 5.8 Parameter values resulting from energy and exergy analyses of System 2

$\dot{m}_f$ (kg/s)	0.90
$\dot{Q}_{heating}$ (kW)	68
Maximum $\dot{W}_{turbine}$ (kW)	116
Maximum η_{multi} (%)	36
Maximum ψ_{multi} (%)	44
$\dot{m}_{H_2}$ (kg/h)	0.63
$\dot{m}_{dwh}$(kg/s)	0.34
CO_2 emissions reduced (tons/year)	476
Total exergy destruction rate (kW)	1982

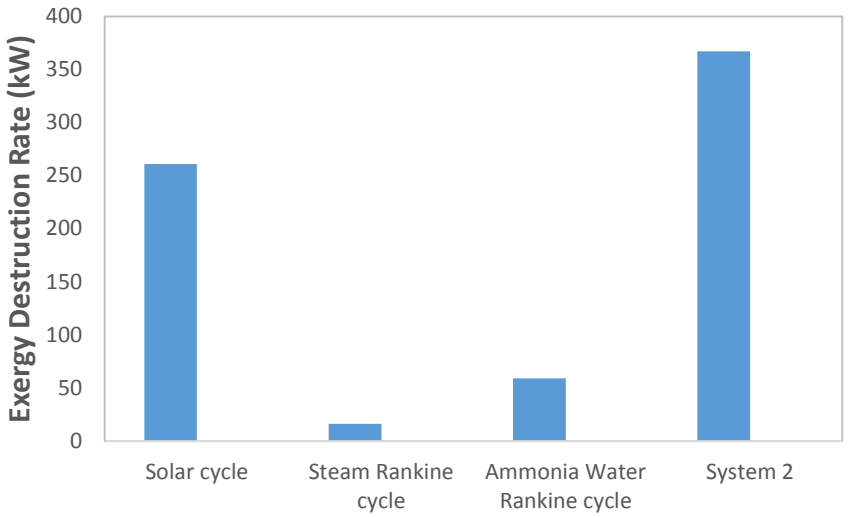

Figure 5.19 Exergy destruction rates in System 2

The highest destruction in System 2 is in the solar cycle. Then comes the ammonia-water Rankine and the steam Rankine cycles respectively. The exergy destruction in System 2 is also shown in the last column. The results show that maximum irreversibilities occur in the solar cycle and the least in steam Rankine cycle. The comparison of exergy destruction is a way to compare irreversibilities in different parts of the system.

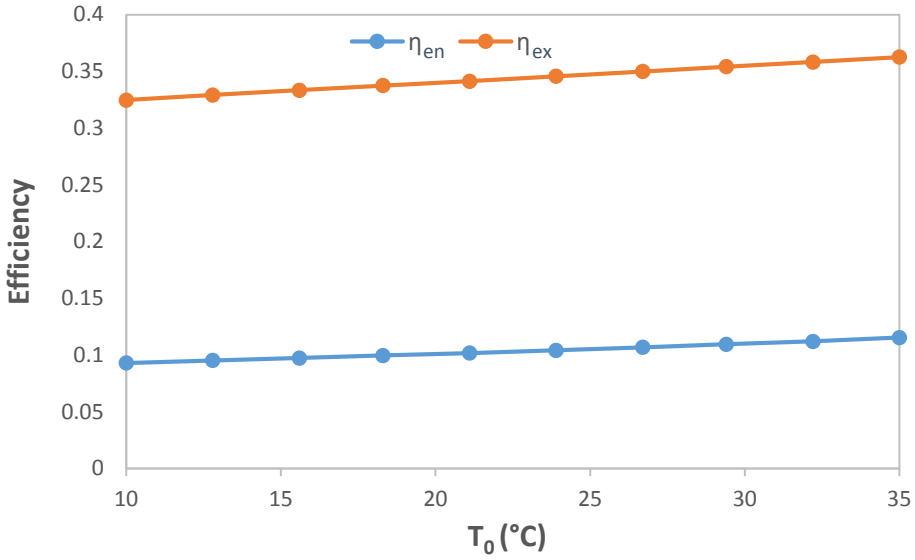

Figure 5.20 System energy and exergy efficiencies vs. ambient temperature

Both system energy and exergy efficiencies increase with increasing ambient temperature as shown in Figure 5.20. The rate of increase is the same for both graphs. The efficiencies increase because the increase in the system outputs (as a result of ambient temperature) is more noticeable than the increase of the system inputs.

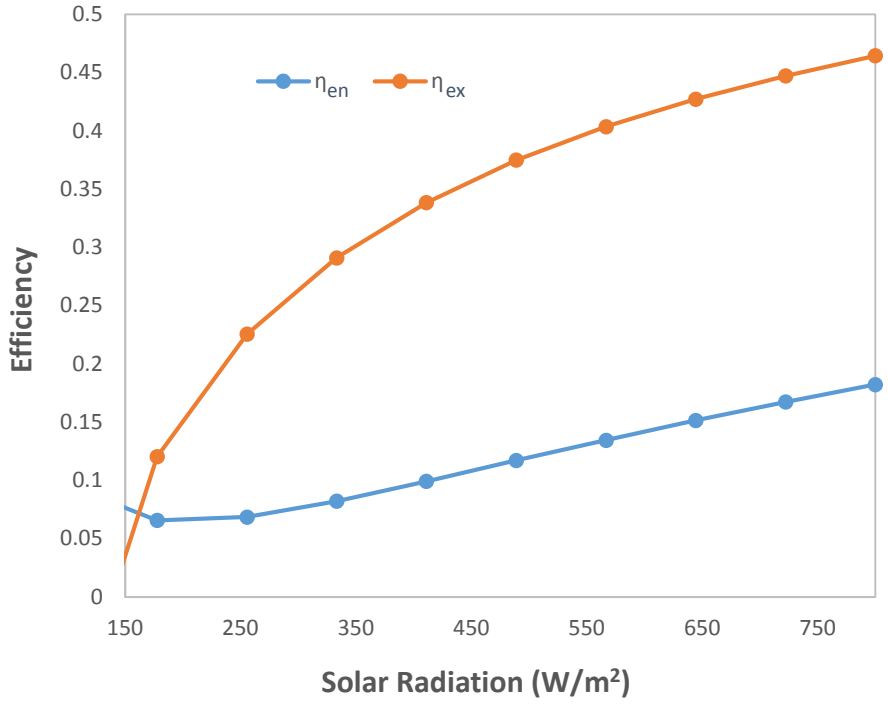

Figure 5.21 System energy and exergy efficiencies vs. solar radiation

Solar radiation is directly proportional to system energy and exergy efficiencies as Figure 5.21 shows. Both curves are parabolic, the energy efficiency curve pointing up and the exergy efficiency curve pointing down. The reason that the rate of increase of energy efficiency is more than the rate of increase of exergy efficiency is because the exergy increase of the system (by the increase in solar radiation) is much more than the increase in the system exergy outputs. For system energy outputs, the rate of increase dominates as solar radiation increases.

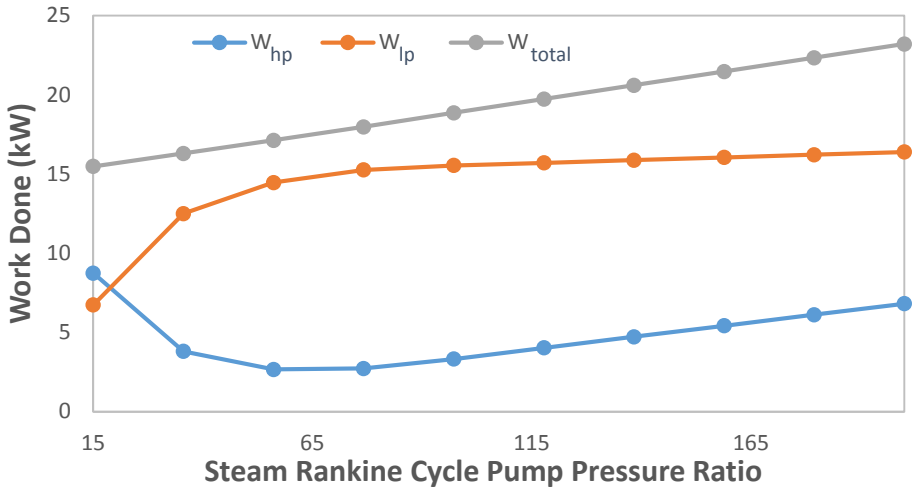

Figure 5.22 Work done by steam Rankine cycle turbines vs. steam Rankine cycle pump pressure ratio

It can be interpreted from Figure 5.22 that work done increases with the increasing pump pressure ratio for the low pressure turbine of steam Rankine cycle. The high pressure turbine curve is parabolic. It reaches a minimum at around 55. Note that the pressure ratio indicated here is the ratio of the highest pressure in the steam Rankine cycle to the lowest pressure. There is also a medium pressure between high and low pressure turbines. Here it can be seen that, after a pressure ratio of approximately 20, the work output from the low pressure turbine is higher than the output of high pressure turbine. This can be changed by changing the medium pressure. As expected, the total power output is steadily increased by increasing the pump pressure ratio, however the ratio of the output from the low pressure turbine to high pressure turbine changes.

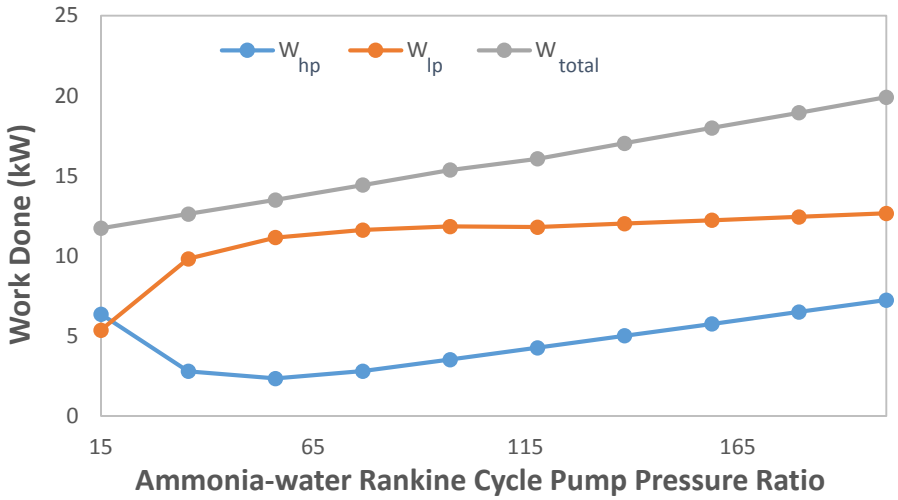

Figure 5.23 Work done by ammonia-water Rankine cycle turbines vs. cycle pump pressure ratio

As can be seen in Figure 5.23, it is very similar to steam Rankine cycle pump pressure ratio vs. work done graph (Figure 5.22). The only difference between them is a shift in the vertical axis. Work done increases with the increasing pump pressure ratio for low pressure turbine of ammonia-water Rankine cycle. High pressure turbine curve is parabolic, reaches a minimum at around 55, then the increase is almost in a straight line. Low pressure turbine has a higher work output than high pressure turbine because of medium pressure. By changing medium pressure, graphs can be shifted up or down. The total work output from both of them will be the same value. The graph also shows that with a low pump pressure ratio, a high pressure turbine has a higher turbine output than a low pressure turbine. For high pressure ratios, it is vice versa. The combined power obtained from both turbines increases based on the pump pressure ratio. The higher the pressure ratio the higher the output, but due to cost factors it is not possible to increase it indefinitely. Optimization is achieved as explained in sections 5.2.3 and 5.2.4.

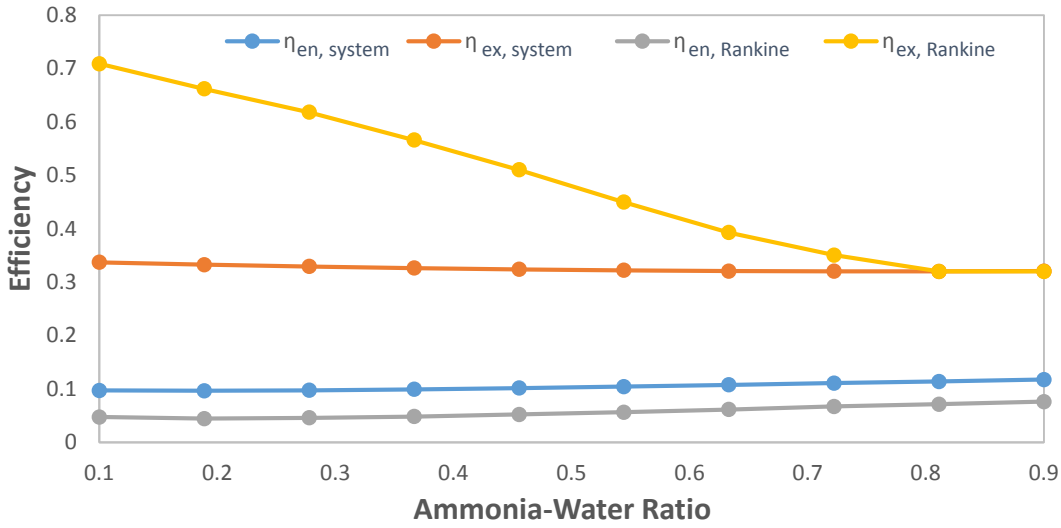

Figure 5.24 System and ammonia-water Rankine cycle efficiencies vs ammonia-water ratio

Ammonia – water ratio in the Rankine cycle is a significant property. Increasing ammonia concentration increases energy efficiencies of both system and the ammonia-water Rankine cycle as shown in Figure 5.24. The rate of increase is a little bit higher in energy efficiency of the ammonia-water Rankine system. Exergy efficiency of Rankine cycle constantly drops until it reaches 0.8, at which point it stays constant. System exergy efficiency also drops until 0.8 then starts increasing. The reason for this drop is the sharp drop of the condenser temperature due to increasing the ammonia-water ratio. This drop slows down after an ammonia-water ratio of 0.8.

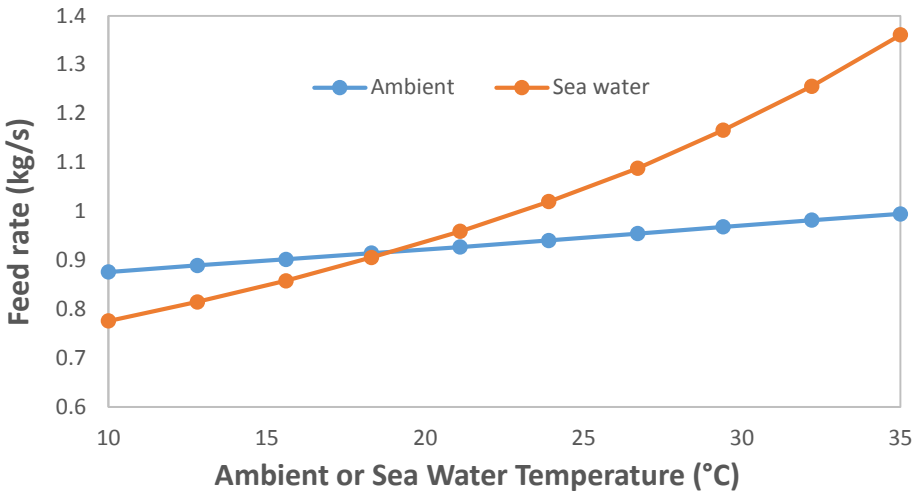

Figure 5.25 Mass flow rate of distilled water vs. ambient and sea water temperature

The mass flow rates of distilled water increase with increasing ambient and sea water temperatures as shown in Figure 5.25. As ambient temperature increases, feed rate increases at a constant rate. The feed rate increases because higher ambient temperature means higher heat input to the desalination system. High sea water temperature makes the sea water boil easily hence eases distilling fresh water. Rate of increase in the feed rate of distilled water is fast and parabolic.

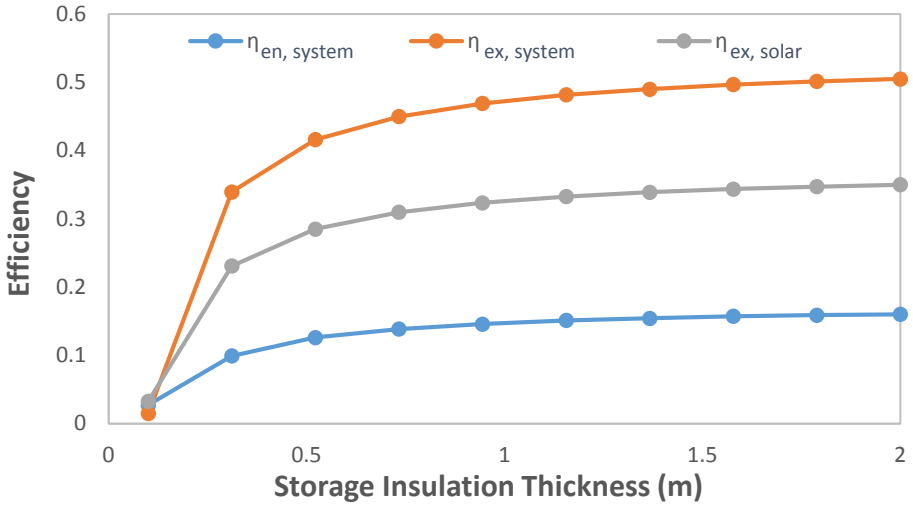

Figure 5.26 Energy/exergy efficiencies of overall system and solar system vs. thermal storage insulation thickness

Figure 5.26 clearly shows that thermal storage insulation thickness has an effect on the efficiencies until approximately 0.5 m. After this thickness, the efficiencies are almost flat-lined,

making it not particularly feasible to increase the insulation thickness. The rate of increase in the system energy, system exergy and solar system exergy efficiencies are the same.

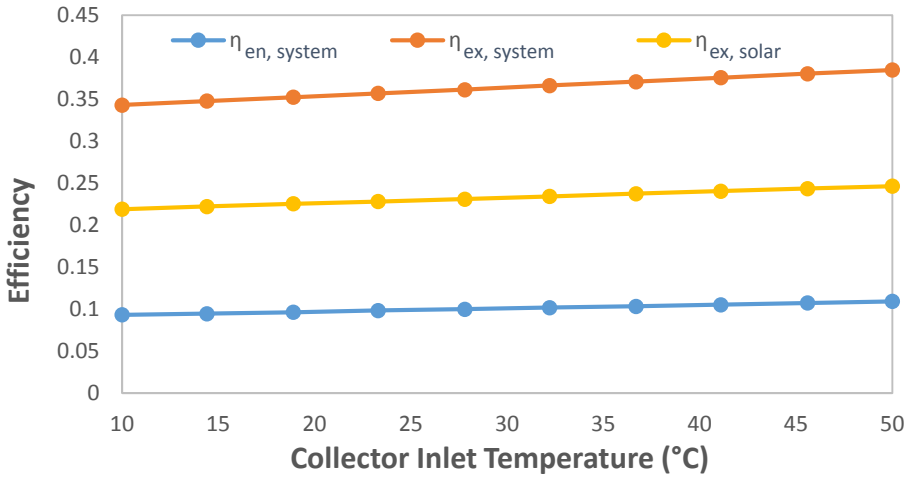

Figure 5.27 System, solar system energy and exergy efficiencies vs. collector inlet temperature

Increasing the collector inlet temperature has a positive effect on system energy, system exergy and solar system exergy efficiencies positively as shown in Figure 5.27. All the efficiencies increase with increasing collector inlet temperature. The rate of increase in the exergy efficiency of the system is slightly higher than the rate of increase of the other efficiencies. An efficiency increase by increasing collector inlet temperature shows that the effect on the system outputs is higher than the effect on the system inputs.

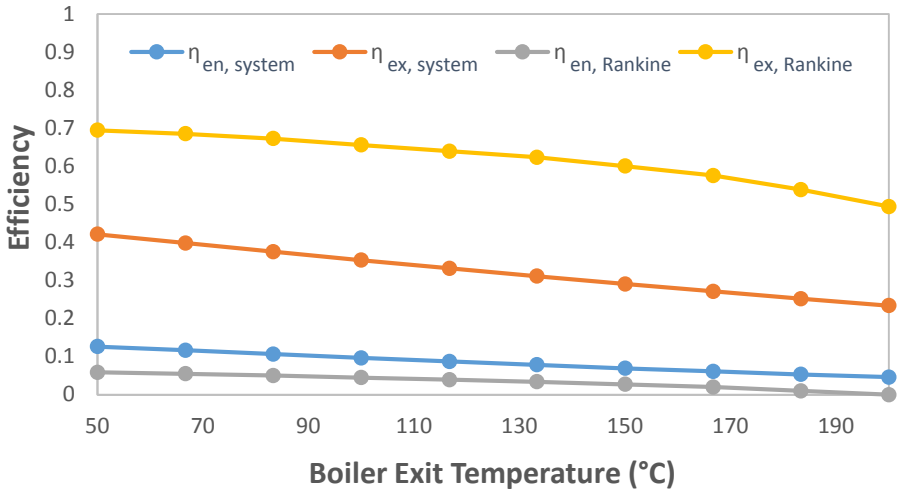

Figure 5.28 System, solar system energy and exergy efficiencies vs. boiler exit temperature

As it is shown in Figure 5.28 all the efficiencies drop by increasing the boiler exit temperature. The drop is most significant for exergy efficiencies. Ammonia-water Rankine system exergy efficiency drops steadily and at approximately 170°C, the rate of drop increases. The reason for these drops is that when the boiler exit temperature increases, less heat is transferred to the Rankine cycles hence the work outputs drop.

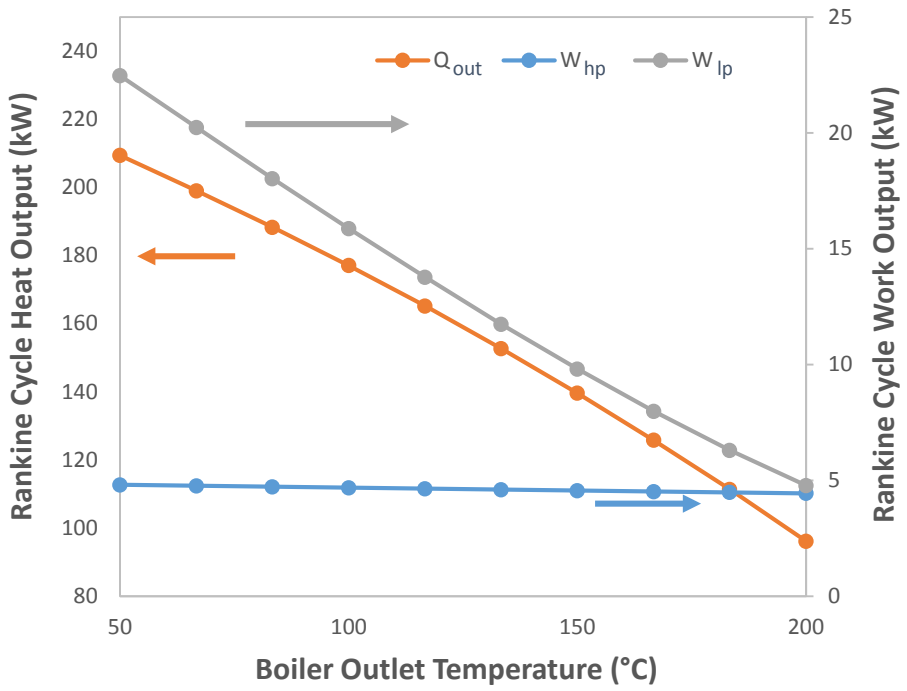

Figure 5.29 Steam Rankine cycle heat and work outputs vs. boiler outlet temperature

The work and heat outputs from Steam Rankine cycle all drop with increasing boiler outlet temperature as shown in Figure 5.29. The drop is significant for heat output and low pressure turbine work output. High pressure turbine work output remains almost constant. The reason for the drop of the outputs is because when boiler outlet temperature is higher, less energy is transferred to the steam Rankine cycle, hence output drops. The high-pressure turbine output is not affected by boiler outlet temperature change because, although the energy entering the cycle drops, there is enough to be processed in the high pressure turbine, but the remainder is not enough to achieve the same output from the low pressure turbine. This drop can be seen in a low pressure turbine but not in the high pressure turbine.

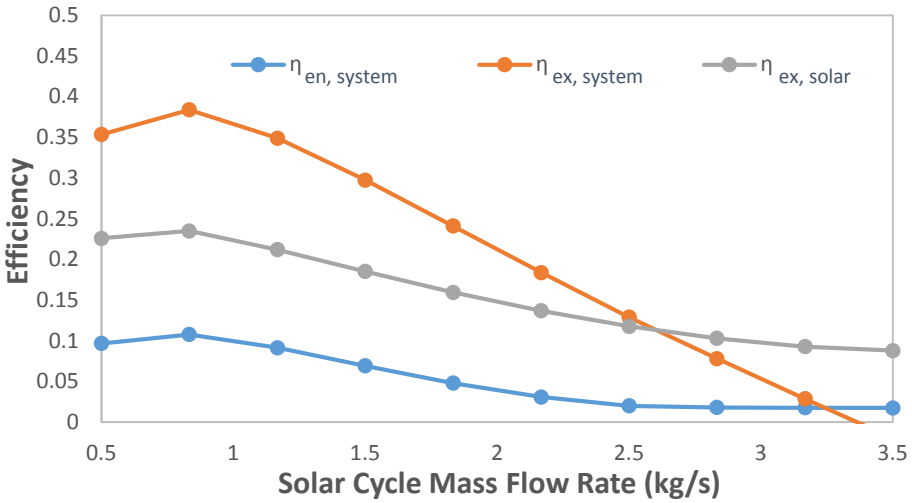

Figure 5.30 System, solar system energy and exergy efficiencies vs. solar cycle mass flow rate

It is clear in Figure 5.30 that all the efficiencies initially increase with the solar cycle mass flow rate, they then reach to a peak and starts dropping. System exergy efficiency increases and drop at a faster rate, while system energy and solar system exergy efficiencies change slowly and at the same rate. The reason for this phenomena is that the heat output from the solar system increases and starts dropping after reaching a peak at around 0.7 kg/s, respectively. From an efficiency point of view, it is not feasible to increase the solar cycle mass flow rate more than 0.7 kg/s.

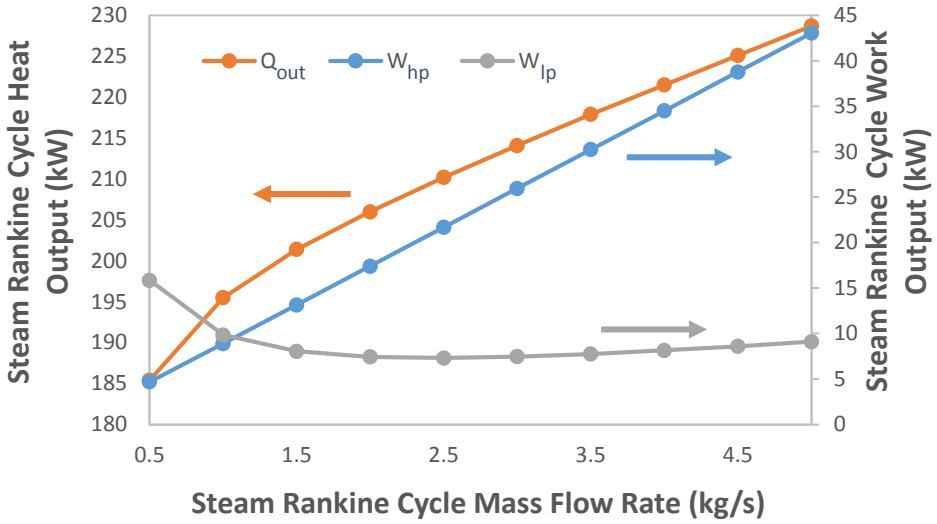

Figure 5.31 Steam Rankine cycle heat and work outputs vs. steam Rankine cycle mass flow rate

The effect of steam Rankine cycle mass flow rate is evaluated in Figure 5.31. Increasing mass flow rate of steam Rankine cycle increases heat output and high pressure turbine work output. High pressure turbine graph is straight, while heat output graph is parabolic downwards. Low pressure turbine output drops and reaches a low peak at around 2.5 kg/s and then increases after that. It can be seen that although the mass flow rate of steam Rankine cycle increases, there is a drop in low pressure turbine output. This can be explained by the increase in the high pressure turbine output. Almost all of the increase is reflected by the high pressure turbine and the low pressure turbine is affected negatively.

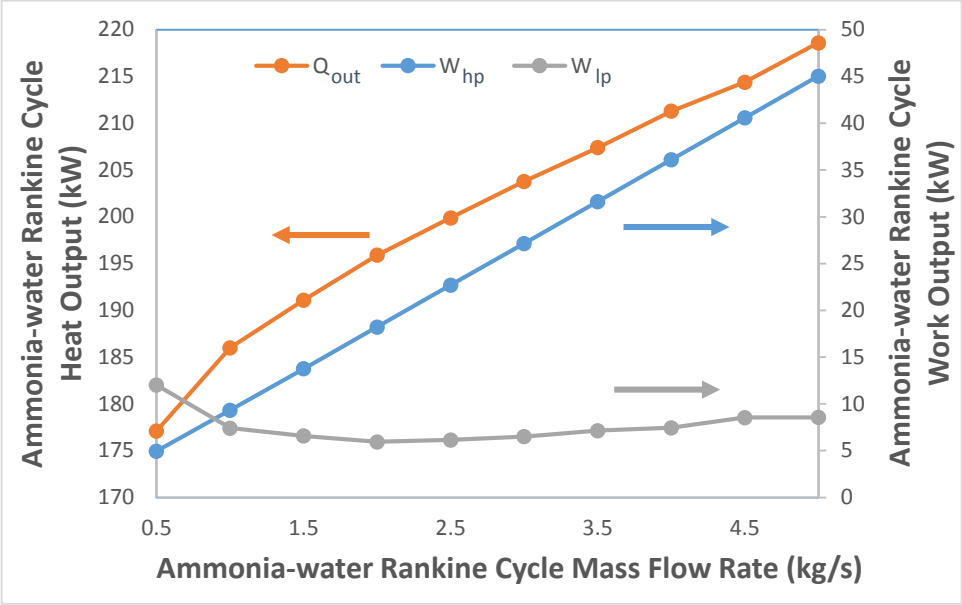

Figure 5.32 Ammonia-water Rankine cycle heat and work outputs vs. cycle mass flow rate

Ammonia-water Rankine cycle mass flow rate versus heat and work output graph (Figure 5.32) is almost the same as Steam Rankine cycle mass flow rate versus heat and output work graph (Figure 5.31). Increasing the mass flow rate of Rankine cycle increases heat output and high pressure turbine work output. High pressure turbine graph is straight, while heat output graph is parabolic downwards. Low pressure turbine output drops and reaches a low peak at around 2.5 kg/s and then increases after that. Low pressure turbine output drops with an increased mass flow rate. This is due to the fact that the increase effects primarily the high pressure turbine and the ammonia-water mixture coming out of the high pressure turbine has a lower energy than

previously. Obviously, the combined output from high and low pressure turbines increase with increasing ammonia-water Rankine cycle mass flow rate.

5.2.3 Optimization

Optimization of System 2 is performed in EES Maximization-Minimization tool as discussed earlier. For the purposes of optimizing parameters, all independent variables that have an effect on the results are chosen first, then their minimum, maximum bounds and guess values are determined and the minimum or maximum value is reached.

- **Power Output Maximization**

In the determination of maximum power output, the following variables are important; solar radiation, ambient temperature, ammonia-water Rankine cycle pressure ratio, steam Rankine cycle pressure ratio, solar cycle mass flow rate, ammonia-water Rankine cycle mass flow rate and steam Rankine cycle mass flow rate. In order to achieve optimum results, more parameters are chosen with a consequent increase in time consumed.

Table 5.9 Independent variables of System 2 for power output maximization

Variable	**Min**	**Max**	**Opt**
Solar radiation (G), W/m^2	0	1000	600
Ambient temperature (T_0),°C	10	35	17
Ammonia-water Rankine cycle pressure ratio (PR)	20	150	150
Steam Rankine cycle pressure ratio (PRR)	20	150	150
Solar cycle mass flow rate ($\dot{m}_{oil}$), kg/s	0.5	5	1.23
Ammonia-water Rankine cycle mass flow rate ($\dot{m}_r$), kg/s	0.5	5	0.50
Steam Rankine cycle mass flow rate ($\dot{m}_{st}$), kg/s	0.5	5	0.90
Maximum power output, kW			116

When the model is operated to achieve the maximum power output, a maximum of 116 kW output can be reached. The input parameters are set to the values in the “Opt” column of Table 5.9. A total number of 74 iterations are done in 4.9 seconds to find the solution.

- **Efficiency Maximization**

The operation to achieve maximum efficiency is performed by choosing the same variables as in the previous (Maximum Power Output Optimization) section. The boundaries and guess values are chosen in a similar manner.

When the optimization tool is run, the results in Table 5.10 are obtained for maximum system efficiency of System 2. The optimum input variables are shown in "Opt $\eta_{en,system}$" column. It is possible to achieve a system energy efficiency of 36% if the input parameters are set as shown.

If the system exergy efficiency is desired to be maximized, the variable values and the final results in Table 5.10 are obtained. Maximum system exergy efficiency is 44% when solar radiation is 500.1 W/m2, solar system fluid mass flow rate is 0.9 kg/s, ammonia-water and steam Rankine cycle mass flow rates is 0.5 kg/s, pressure ratio on the ammonia-water and steam Rankine cycles is 150 and the ambient temperature is 17.3°C. These optimum variable values are shown in "Opt $\eta_{ex,system}$" column.

Table 5.10 Independent variables of System 2 for efficiency maximization

Variable	**Min**	**Max**	**Opt** $\eta_{en,system}$	**Opt** $\eta_{ex,system}$	**Opt** $\eta_{ex,sc}$
Solar radiation (G), W/m^2	0	1000	99.8	500.1	1000
Ambient temperature (T_0),°C	10	35	16.9	17.3	17
Ammonia-water Rankine cycle pressure ratio (PR)	20	150	150	150	100
Steam Rankine cycle pressure ratio (PRR)	20	150	150	150	100
Solar cycle mass flow rate ($\dot{m}_{oil}$), kg/s	0.5	5	1.564	0.9	1.1
Ammonia-water Rankine cycle mass flow rate ($\dot{m}_r$), kg/s	0.5	5	5	0.5	2.5
Steam Rankine cycle mass flow rate ($\dot{m}_{st}$), kg/s	0.5	5	5	0.5	2.14
Maximum Power Output, kW			36%	44%	35%

Maximum energy efficiency in the solar cycle can also be maximized with the same variables but with different values. As shown in Table 5.10, a maximum efficiency of 35% can be

obtained by setting the input parameters. The optimum variable values to reach maximum solar cycle efficiency are given in "Opt $\eta_{ex,sc}$" column.

After optimizing system and solar cycle efficiencies, steam and ammonia-water Rankine cycle efficiencies can be maximized using the same method. The same input parameters, bound and guess values are chosen in the model as in the previous section. The results of steam and ammonia-water Rankine cycles optimization can be found in Table 5.11. "Min" and "Max" columns show minimum and maximum bound values for the parameters, respectively. "Opt $\boldsymbol{\eta_{en,st}}$" column shows the optimum values to achieve maximum steam Rankine cycle energy efficiency. "Opt $\boldsymbol{\eta_{ex,st}}$" column shows the optimum values to achieve maximum steam Rankine cycle exergy efficiency. "Opt $\boldsymbol{\eta_{en,rc}}$" column shows the optimum values to achieve maximum ammonia-water Rankine cycle energy efficiency. Finally "Opt $\boldsymbol{\eta_{ex,rc}}$" column shows the optimum values to achieve maximum ammonia-water Rankine cycle exergy efficiency. The rows contain the input variables. The last row shows the maximum efficiency value obtained from the optimization tool.

Table 5.11 Independent variables of System 2 for efficiency maximization

Variable	**Min**	**Max**	**Opt $\boldsymbol{\eta_{en,st}}$**	**Opt $\boldsymbol{\eta_{ex,st}}$**	**Opt $\boldsymbol{\eta_{en,rc}}$**	**Opt $\boldsymbol{\eta_{ex,rc}}$**
Solar radiation (G), W/m^2	0	1000	660	660	660	660
Ambient temperature (T_0),°C	10	35	35	35	35	35
Ammonia-water Rankine cycle pressure ratio (PR)	20	150	150	20	150	150
Steam Rankine cycle pressure ratio (PRR)	20	150	150	150	150	150
Solar cycle mass flow rate ($\dot{m}_{oil}$), kg/s	0.5	5	1.12	1.58	1.16	1.1
Ammonia-water Rankine cycle mass flow rate ($\dot{m}_r$), kg/s	0.5	5	1	0.84	0.5	0.5
Steam Rankine cycle mass flow rate ($\dot{m}_{st}$), kg/s	0.5	5	0.52	0.54	1.11	1.06
Maximum Efficiency			17%	90%	15%	80%

When the optimization tool is run for steam Rankine cycle energy efficiency, it is found that the optimization is done in 106 iterations, 6.6 seconds and a maximum value of 17.02% is found. The optimum variable values to reach maximum steam Rankine cycle energy efficiency are given in "Opt $\eta_{en,st}$" column.

To find maximum exergy efficiency of steam Rankine cycle, it took the optimization tool 105 iterations and 7.1 seconds. As a result, an efficiency value of 89.88% is found. The optimum variable values to reach maximum steam Rankine cycle energy efficiency are listed in "Opt $\eta_{ex,st}$" column.

Maximum efficiency of the ammonia-water Rankine cycle is calculated as 14.6% by the optimization tool as shown in Table 5.11. The optimum variable values to reach maximum ammonia-water Rankine cycle energy efficiency are listed in "Opt $\eta_{en,rc}$" column.

Obtaining the maximum exergy efficiency of the ammonia-water Rankine cycle is done using the same parameters. The final result of the maximum efficiency and the parameter values are listed in "Opt $\eta_{ex,rc}$" column.

- **Cost Minimization**

Cost minimization is performed using the EES Minimization/Maximization program. A minimum cost of $160,596 is determined following the evaluation. The calculation is achieved using 274 equations in 204 blocks and 213 iterations in 10.5 seconds. The results are shown in Table 5.12. The independent variables that effect the cost are; solar radiation, ambient temperature, ammonia-water Rankine cycle pressure ratio, steam Rankine cycle pressure ratio, solar cycle mass flow rate, ammonia-water Rankine cycle mass flow rate and steam Rankine cycle mass flow rate. The minimum and maximum values of each of the variables is shown in Table 5.12. These values define the boundaries for each variable. The optimum values for each variable are shown in the "Opt Cost" column of Table 5.12. To minimize the cost, output from the system also has to be minimized. The variable values found confirm this.

Table 5.12 Independent variables of System 2 for cost minimization

Variable	**Min**	**Max**	**Opt Cost**
Solar radiation (G), W/m^2	100	1000	100
Ambient temperature (T_0),°C	10	35	10
Ammonia-water Rankine cycle pressure ratio (PR)	2	150	150
Steam Rankine cycle pressure ratio (PRR)	2	150	16
Solar cycle mass flow rate ($\dot{m}_{oil}$), kg/s	0.5	5	0.5
Ammonia-water Rankine cycle mass flow rate ($\dot{m}_r$), kg/s	0.5	5	1.6
Steam Rankine cycle mass flow rate ($\dot{m}_{st}$), kg/s	0.5	5	3.1
Minimum Cost			$160,596

- **CO_2 Reduction Maximization**

CO_2 reduction by the system is calculated by determining the CO_2 emissions of a system using fossil fuels which has the same outputs. When the solar radiation is 999 W/m^2, ambient temperature is 10°C, ammonia-water Rankine cycle pressure ratio is 150, steam Rankine cycle pressure ratio is 150, solar cycle mass flow rate is 5 kg/s, ammonia-water Rankine cycle mass flow rate is 0.5 kg/s, steam Rankine cycle mass flow rate is 0.5 kg/s, there is a reduction of 4873 tons of CO_2 per year. The evaluation is determined by the EES program in 13.5 seconds. 274 equations are solved in 204 blocks and 235 iterations.

Table 5.13 Independent variables of System 2 for CO_2 reduction maximization

Variable	**Min**	**Max**	**Opt CO_2**
Solar radiation (G), W/m^2	100	1000	999
Ambient temperature (T_0),°C	10	35	10
Ammonia-water Rankine cycle pressure ratio (PR)	2	150	150
Steam Rankine cycle pressure ratio (PRR)	2	150	150
Solar cycle mass flow rate ($\dot{m}_{oil}$), kg/s	0.5	5	5
Ammonia-water Rankine cycle mass flow rate ($\dot{m}_r$), kg/s	0.5	5	0.5
Steam Rankine cycle mass flow rate ($\dot{m}_{st}$), kg/s	0.5	5	0.5
CO2 reduction (tons/year)			4873

5.2.4 Sensitivity Analysis

In this section, the effect of independent variables on the optimization targets of efficiency, cost and CO_2 reduction is evaluated. The independent variables considered are solar radiation, ambient temperature, ammonia-water Rankine cycle pressure ratio, steam Rankine cycle pressure ratio, solar cycle mass flow rate, ammonia-water Rankine cycle mass flow rate and steam Rankine cycle mass flow rate.

- **Solar Radiation**

The effect of solar radiation on system exergy efficiency, cost and CO_2 reduction in System 2 is shown in Figure 5.33. Solar radiation has a minimum value of 150 W/m^2 and maximum of 1000 W/m^2. The primary axis on the left shows the system exergy efficiency, while the secondary axis on the right shows costs and CO2 reduction by System 2.

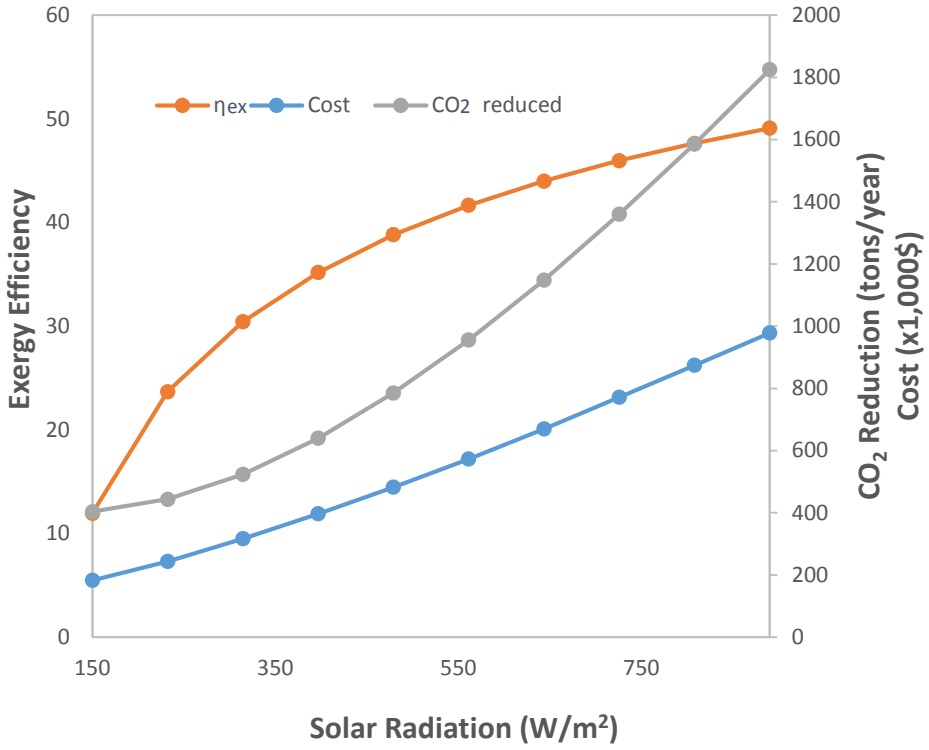

Figure 5.33 Effect of solar radiation on optimization targets

When solar radiation increases, all three variables increase. The increase in the system exergy efficiency is parabolic, with a tendency to stabilize. The system output increase is more than the system input increase hence the efficiency increases. CO_2 reduction increases as the system outputs increase. Cost increases for the same reason. A higher output requires a higher investment. The increase in the cost is straight, while CO_2 reduction is parabolic.

- **Ambient Temperature**

Although ambient temperature cannot be adjusted, it is a system input variable based on seasonal changes or during different climate considerations. The effect of ambient temperature on the optimization targets is shown in Figure 5.34. Ambient temperature varies between 10°C and 50°C. Efficiency values are on the left vertical axis, while CO_2 reduction and cost values are shown on the right vertical axis.

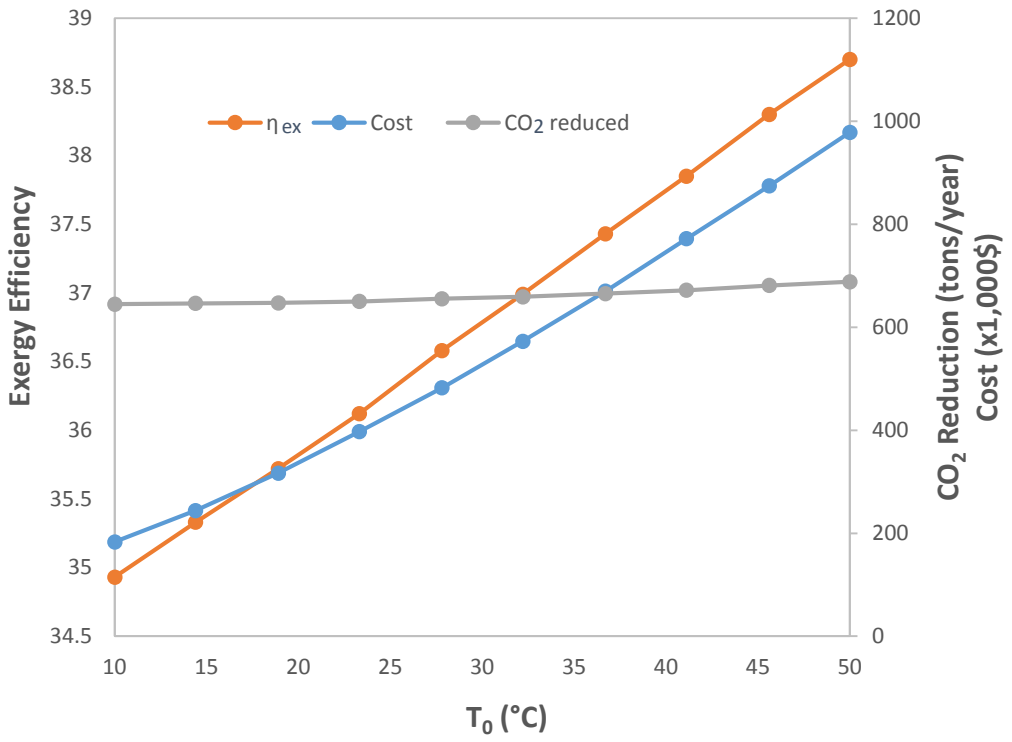

Figure 5.34 Effect of ambient temperature on optimization targets

Ambient temperature has no effect on the CO_2 reduction in the system, however as ambient temperature increases efficiency and cost increase as a straight line. This is to be expected as the two variables have the same trend. Increasing ambient temperature has a greater effect on output than input. The cost of the system increases because an increase in ambient temperature requires that the components be enlarged.

- **Ammonia-water Rankine Cycle Pressure Ratio**

The pressure ratio of the pump in ammonia-water Rankine cycle is an input variable of the system. Its effect on the system output is shown in Figure 5.35. Ammonia-water Rankine cycle pressure ratio is set to change between 25 and 145. The exergy efficiency value is shown on the primary vertical axis on the left, while CO_2 reduction and cost values are shown on the vertical axis on the right.

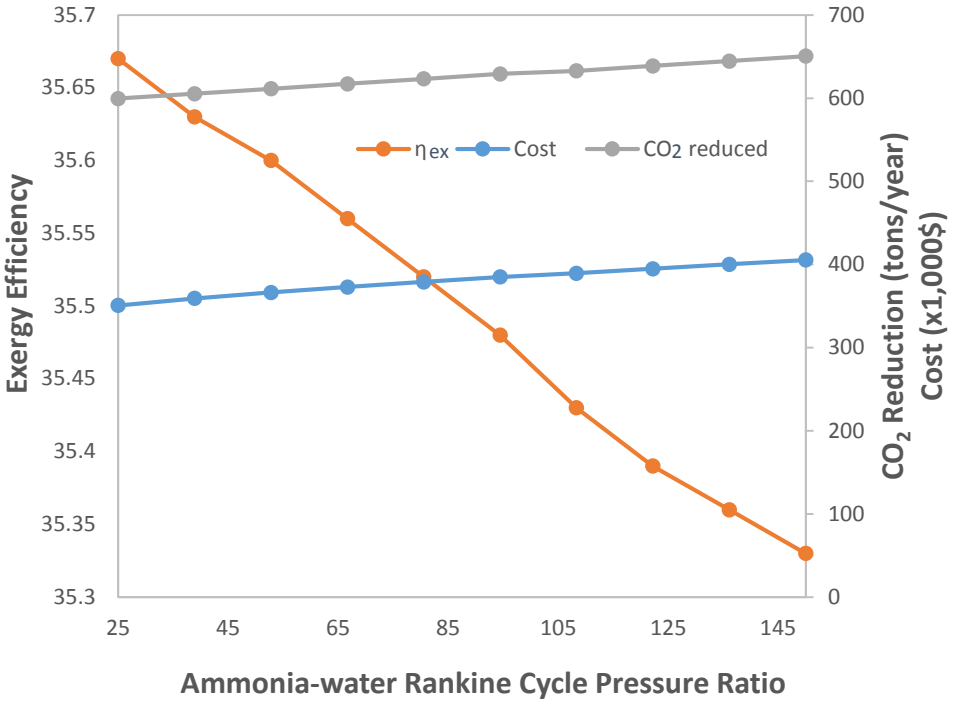

Figure 5.35 Effect of ammonia-water Rankine cycle pressure ratio on optimization targets

Increasing pressure ratio has an increasing effect on cost and CO_2 reduction. System output increases by the increase in the pressure ratio. As the capacity of the system increase, the cost of the system also increases. CO_2 reduction depends on the system output, hence the two curves are similar. The efficiency drops because the increase in the pressure ratio doesn't have enough effect to increase outputs of the system.

- **Steam Rankine Cycle Pressure Ratio**

Steam Rankine cycle pump pressure ratio has an effect on system efficiency, cost and CO_2 reduction. The result is shown in Figure 5.36. Minimum steam Rankine cycle pressure is 25 and maximum is 150. The left vertical axis shows exergy efficiency values, while the right axis shows cost and CO_2 reduction values.

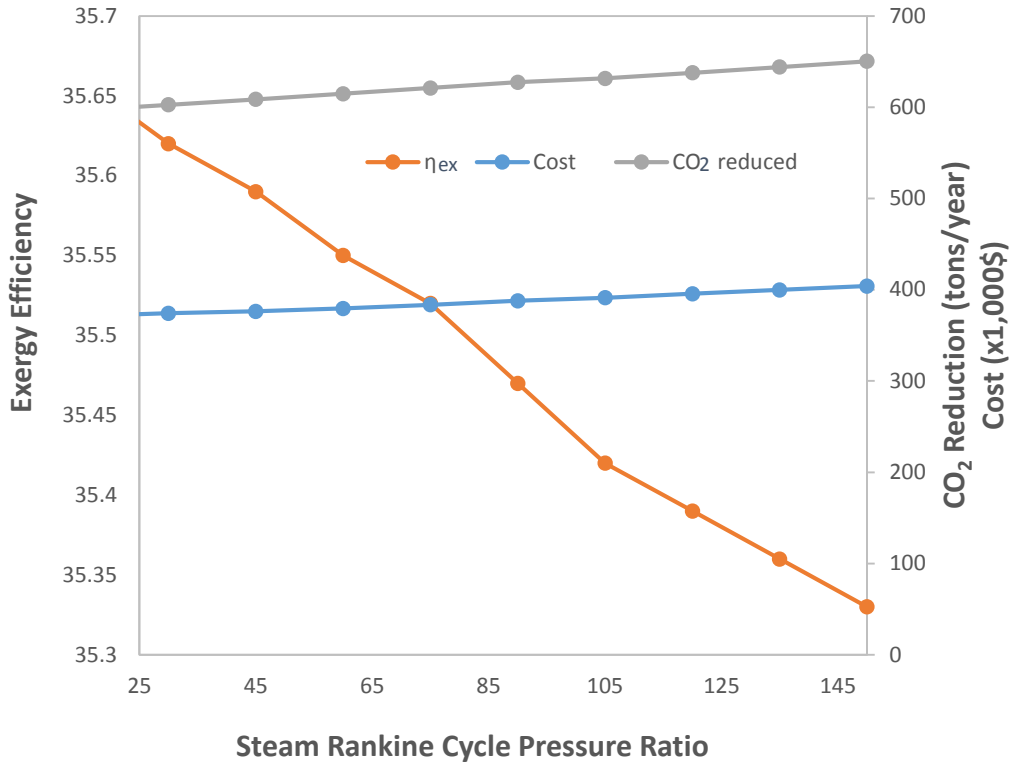

Figure 5.36 Effect of steam Rankine cycle pressure ratio on optimization targets

Steam Rankine cycle pressure ratio has the same effect on system optimization values as ammonia-water Rankine cycle pressure ratio. The graphs 5.35 and 5.34 are identical. Cost and CO_2 reduction increase with increasing steam Rankine cycle pressure ratio. Increased expenditure in equipment is needed for higher pressure ratio so that the output, cost and CO_2 reduction increase. The efficiency drops because as the increase in output is negated by the increase in the input.

- **Solar Cycle Mass Flow Rate**

In this section the effect of solar cycle mass flow rate on the system optimization values is evaluated. The results obtained from EES are shown in Figure 5.37. The solar cycle mass flow rate boundaries are set as 0.5 and 4.5 kg/s. The left vertical axis shows exergy efficiency, while right vertical axis shows cost and CO_2 reduction values.

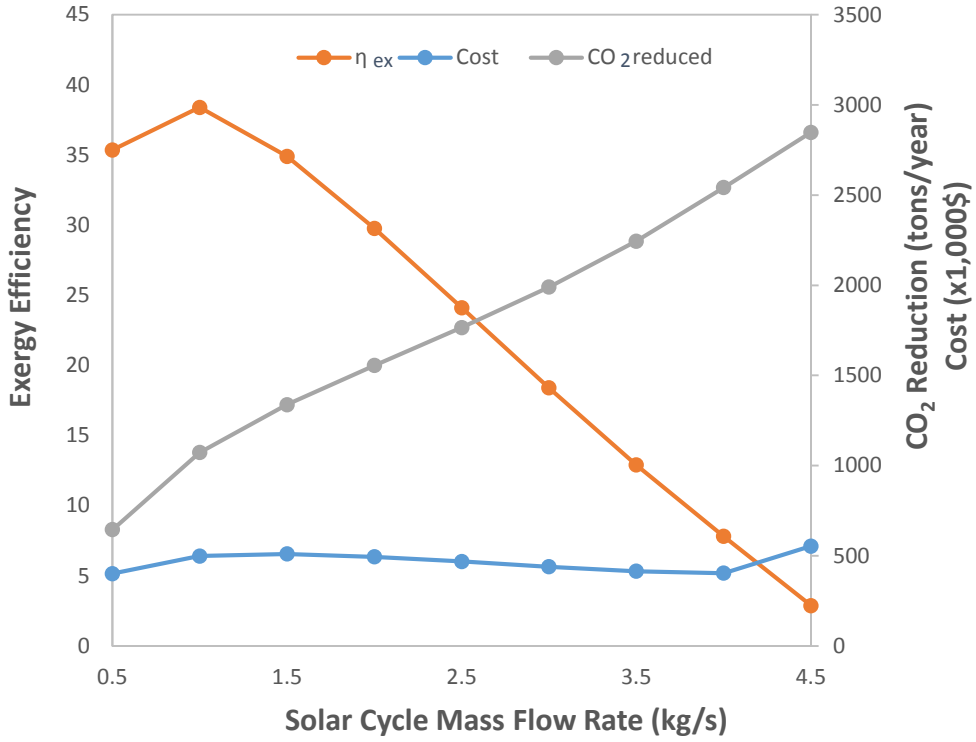

Figure 5.37 Effect of solar cycle mass flow rate on optimization targets

Solar cycle mass flow rate has different effects on the optimization targets. Cost of the system fluctuates but the variation is not large. Solar cycle mass flow rate doesn't have a significant effect on the cost of the system. CO_2 reduction increases with increasing solar cycle mass flow rate. This means output from the system increases. Exergy efficiency increases until it reaches approximately 1 kg/s, then it starts dropping. If the exergy efficiency is the primary target then lower values of solar cycle mass flow rate should be chosen.

- **Ammonia-water Rankine Cycle Mass Flow Rate**

The effect of ammonia-water Rankine cycle mass flow rate on cost, exergy efficiency and CO_2 reduction in the system is evaluated in this section. The result is shown in Figure 5.38. Ammonia-water Rankine cycle mass flow rate varies between 0.5 and 4.5 kg/s. The exergy efficiency value is shown on the left vertical axis, while the cost and CO_2 reduction values are shown on the right vertical axis.

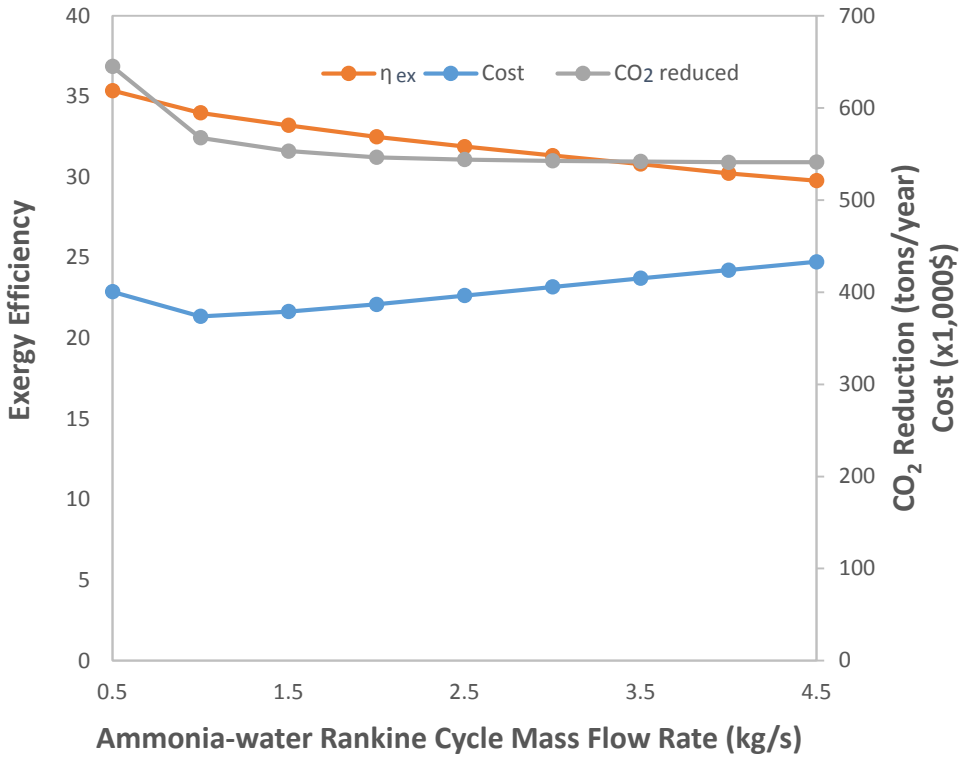

Figure 5.38 Effect of ammonia-water Rankine cycle mass flow rate on optimization targets

As ammonia-water Rankine cycle mass flow rate increases there is CO_2 reduction by the system however the exergy efficiency drops. CO_2 reduction stabilizes after 2 kg/s, while exergy efficiency continues dropping. As the output drops, CO_2 reduction drops. Exergy efficiency drops because the system output increase is negated by system input increase. Costs drops initially, then after 1 kg/s is reached it starts increasing. If the cost is the main design concern, than ammonia-water Rankine cycle mass flow rate should be 1 kg/s.

- **Steam Rankine Cycle Mass Flow Rate**

Steam Rankine cycle mass flow rate effect on system optimization values is discussed in this section. The resulting graph is shown in Figure 5.39. Steam Rankine cycle mass flow rate values are between 0.5 and 4.5 kg/s. The left hand side vertical axis shows exergy efficiency values, while the right hand axis shows cost and CO_2 reduction values.

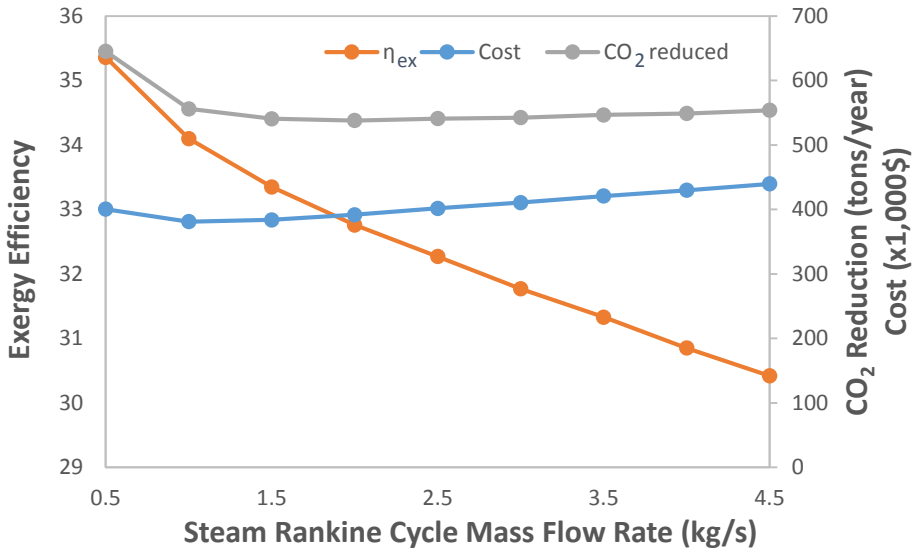

Figure 5.39 Effect of steam cycle mass flow rate on optimization targets

The system exergy efficiency drops with increasing steam Rankine cycle mass flow rate. System output increase is less than the system input increase. System costs drop initially, reaching a plateau at 1 kg/s, and then increases thereafter. As a result an optimum value of 1 kg/s steam Rankine cycle mass flow rate is suggested based on the cost graph analysis. CO_2 reduction drops after 2 kg/s and stabilizes thereafter. The steam Rankine cycle mass flow rate increase does not have an effect on the system outputs after 2 kg/s.

5.3 System 3

In this section, results of System 3 are analyzed and discussed. The assumptions and data considered, results and discussion and optimization are presented in the subsections.

5.3.1 Assumptions and Data Considered

The assumptions consisting all the systems are explained in section 5.1.1. The thermodynamic and cost analyses for System 3 are based on the following additional assumptions:

- States at points 31, 52 are saturated liquid.
- State at point 33, 55 are saturated vapor.

Table 5.14 shows input parameters used to model System 3. These are the input parameters for the system to operate. They are chosen by using the similar models in the literature or by using a smart design approach.

Table 5.14 Input parameters used to model System 3

Collector	
Width	2 m
Length	2 m
Absorber diameter	25 mm
Transparent envelope outer diameter	40 mm
Tube material	Stainless steel
Receiver efficiency	75% [91]
Solar system working fluid	Therminol 66
Thermal storage	
Insulation thickness	30 cm
Insulation material	Polyurethane [39]
Total surface area	6 m^2
Kalina cycle	
Working fluid	Ammonia-water
Absorption chiller	
Heat exchanger temperature difference	20°C
Generators temperature difference	15°C

5.3.2 Results of System 3

The results of System 3 are shown in Table 5.15. They are calculated by guessing the input variables. Depending on the application, better results can be achieved by optimization and more in-depth knowledge is provided in the following sections.

Table 5.15 Parameter values resulting from energy and exergy analyses of System 3

Maximum $\dot{Q}_{heating}$ (kW)	196
Maximum $\dot{Q}_{cooling,absorption}$ (kW)	164
Maximum $\dot{W}_{turbine}$ (kW)	118
Maximum η_{multi} (%)	47
Maximum ψ_{multi} (%)	88
Absorption chiller COP_{en}	2.0
Absorption chiller COP_{ex}	0.9
CO_2 emissions reduced (tons/year)	1786
Total exergy destruction rate (kW)	544

The exergy destruction in the system components and the system are shown in Figure 5.40. These values are calculated by using the model created in EES software and the equations shown in Table 4.7.

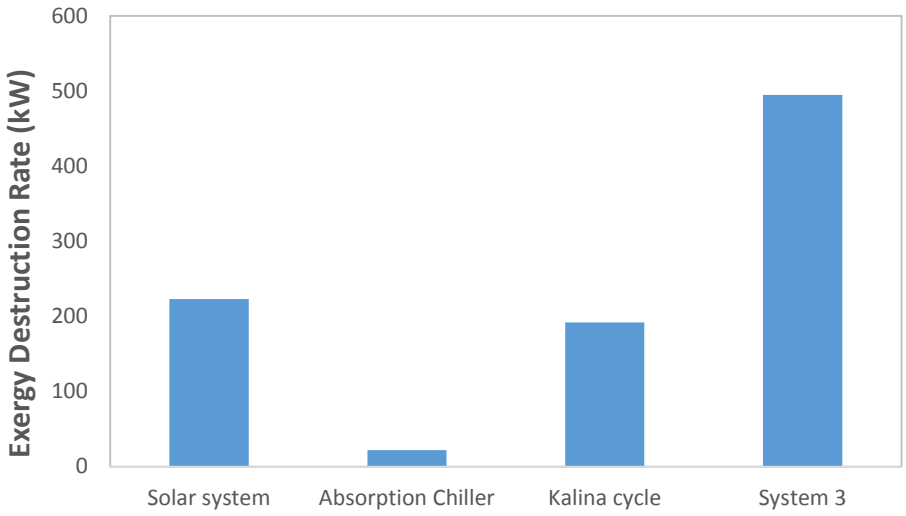

Figure 5.40 Exergy destruction rates in System 3

The highest destruction in System 3 is in the solar system, followed by the Kalina cycle and quadruple effect absorption chiller cycles. The main focus has to be given to the components where the exergy destruction rate is high to improve the system irreversibilities. The solar system has the highest irreversibility and as a result it has room to improve. The absorption chiller has the least irreversibility and so it is the most effective.

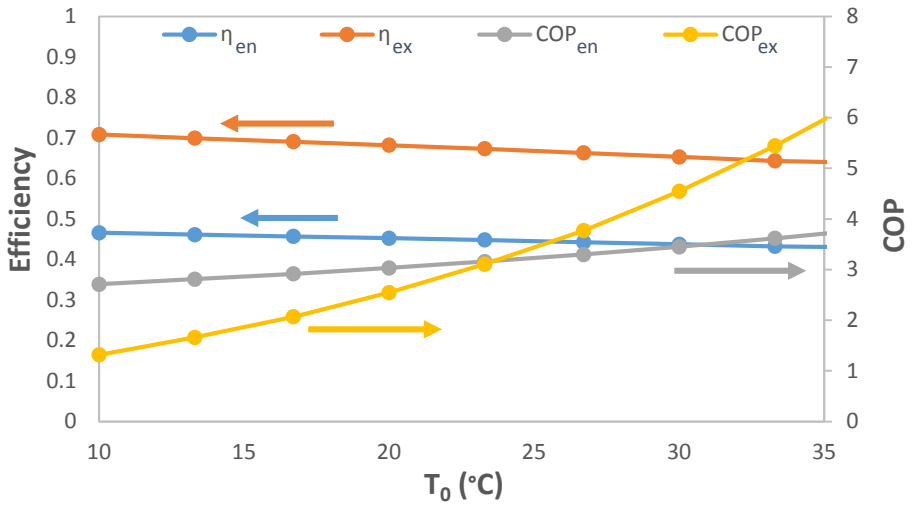

Figure 5.41 System energy and exergy efficiencies, energy and exergy COPs vs. ambient temperature

The energy and exergy efficiencies of the system both drop with the increasing ambient temperature as shown in Figure 5.41. The increase in the ambient temperature does not affect the output from the system so the same extent as it affects the outputs resulting the drop in the efficiencies. Coefficients of performance increase with the increasing ambient temperature. The increase is linear in energy COP, while it is logarithmic in exergy COP. Exergy COP is more affected by the change in ambient temperature because ambient temperature is a reference used in the equations. An increase in ambient temperature affects the absorption chiller to a greater extent than it affects its input so both of the COPs increase.

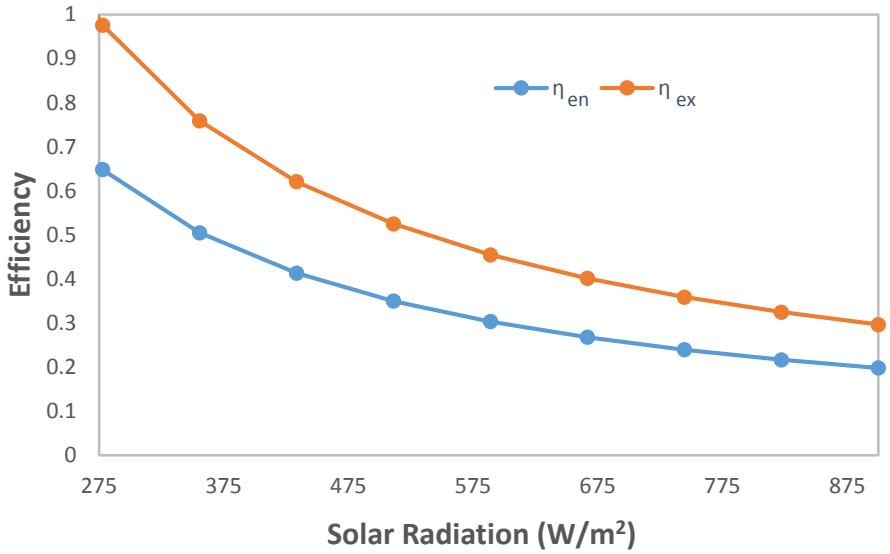

Figure 5.42 System energy and exergy efficiencies vs. solar radiation

Energy and exergy efficiencies drop with increasing solar radiation as shown in Figure 5.42. The rate of decrease is the same for both energy and exergy efficiencies of the system. Efficiencies drop by the increase in solar radiation because the increase in the output of the system is not as high as the increase in the input of the system which is solar radiation. This seems contradictory but an increase in solar radiation does not mean that the efficiency should also increase. The output from the system increases by the solar radiation increase but this increase is not enough to raise the efficiency.

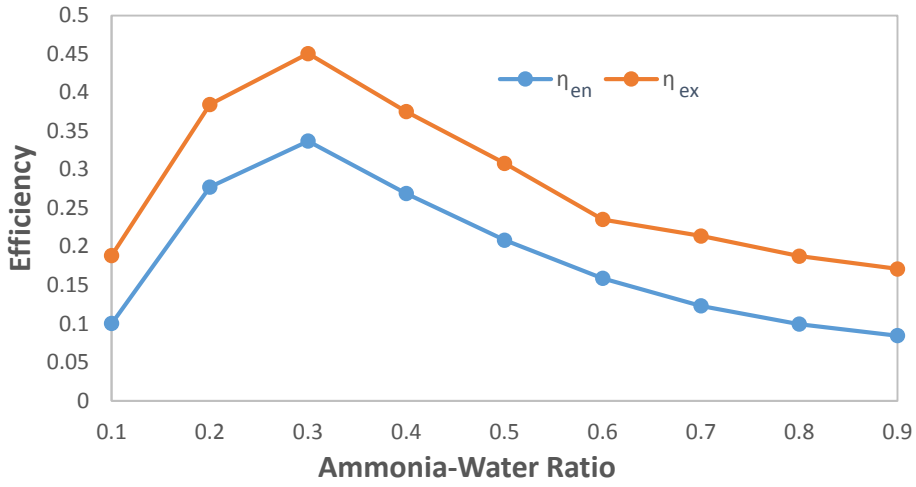

Figure 5.43 System energy and exergy efficiencies vs. Kalina cycle ammonia water ratio

In Figure 5.43 it can be seen that system energy and exergy efficiencies initially increase with the increasing ammonia-water mass fraction ratio in the Kalina cycle. They both reach a peak value at around 0.3 and then gradually drop. Both of the curves have the same slopes. By the help of this graph, the ammonia-water ratio can be set to reach the optimum system efficiency. Adding ammonia to the working fluid is the innovation in the Kalina cycle but it can be seen from the graphs that the fraction of ammonia-water should be determined carefully to obtain the desired result depending on the goal from the system.

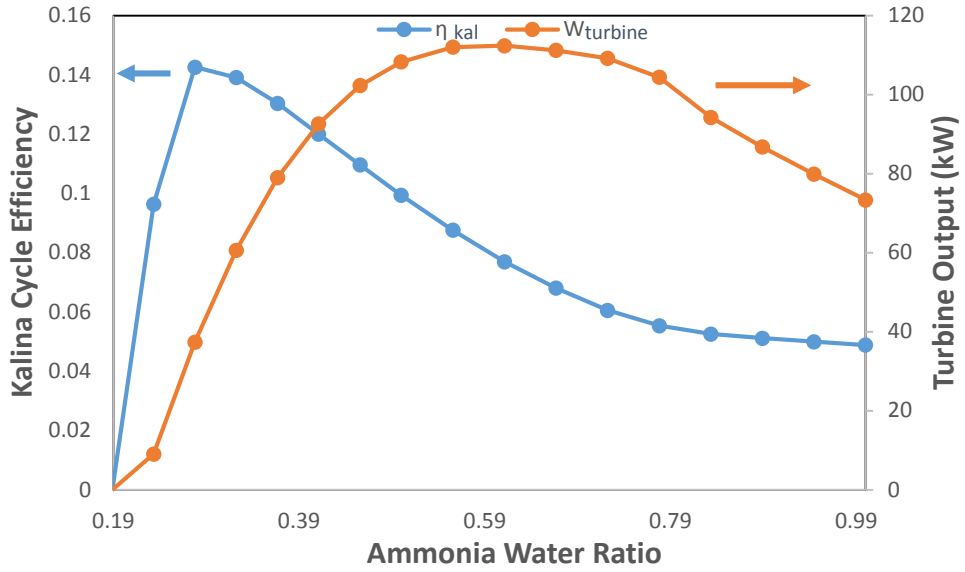

Figure 5.44 Kalina cycle efficiency and turbine output vs. ammonia-water ratio

Kalina cycle efficiency peaks at around 0.3 ammonia water mass ratio, then drops as shown in Figure 5.44. Turbine output power has a similar graph. Initially it increases with the increasing ammonia-water ratio. It reaches a peak at around 0.6 and then it starts dropping. Therefore, the maximum work output from the system can be achieved at an ammonia mass fraction ratio of 0.6. This graph shows that the optimum value of Kalina cycle ammonia-water ratio is different for maximum Kalina cycle efficiency and maximum Kalina cycle turbine output. The value of ammonia-water ratio for optimum Kalina cycle efficiency is almost the same as the value shown in Figure 5.43 for optimum system efficiency. However, if the main concern is power output from the system, a higher ammonia-water ratio should be chosen.

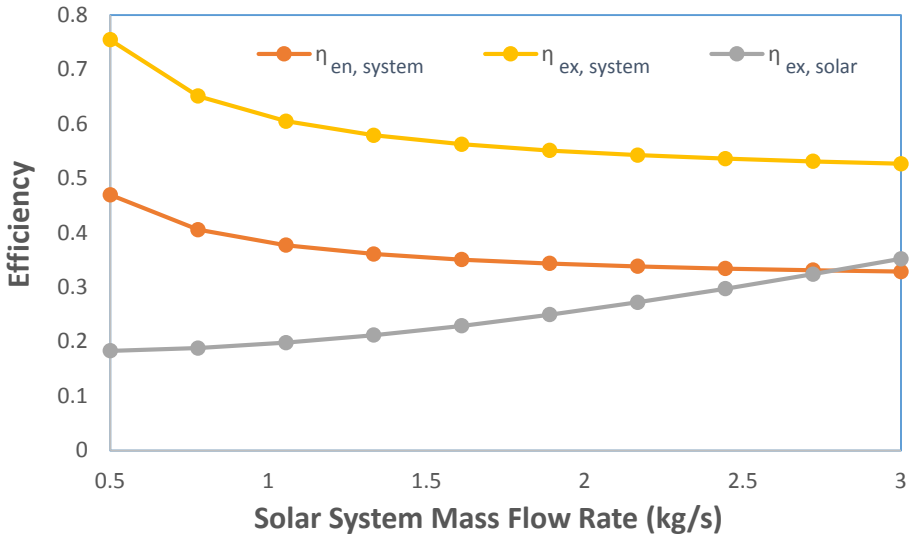

Figure 5.45 System and solar cycle efficiencies vs. solar system mass flow rate

Figure 5.45 shows that system energy and exergy efficiencies both drop with increasing solar system mass flow rate. The rate of drop is the same for both. Initially the drop is sharp, however it stabilizes. Solar system exergy efficiency increases with increasing solar system mass flow rate. It is a parabolic curve pointing upwards. Higher flow rate of solar system fluid decrease the system efficiencies but increases the solar system exergy efficiency. This is to be expected because the solar system mass flow rate affects the solar system efficiency directly, while the effect on the system efficiencies is indirect.

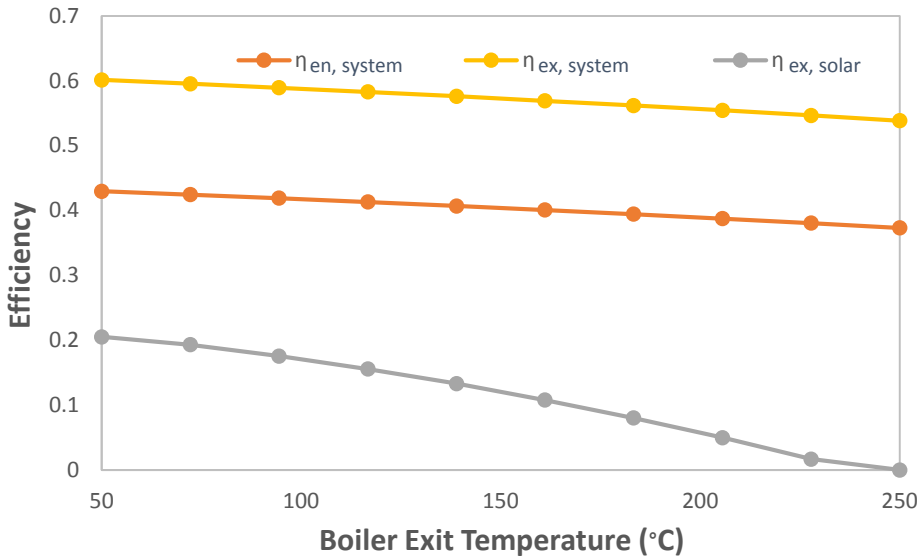

Figure 5.46 System and solar cycle efficiencies vs. boiler exit temperature

All the efficiencies drop with increasing boiler exit temperature as shown in Figure 5.46. System efficiency curves are parallel. The drop in solar system efficiency is very fast. The reason for the drop in the efficiencies is that when boiler exit temperature increases, less heat is transferred to Kalina cycle hence there is less turbine output. If the goal is to increase efficiency, then lower boiler exit temperature should be chosen.

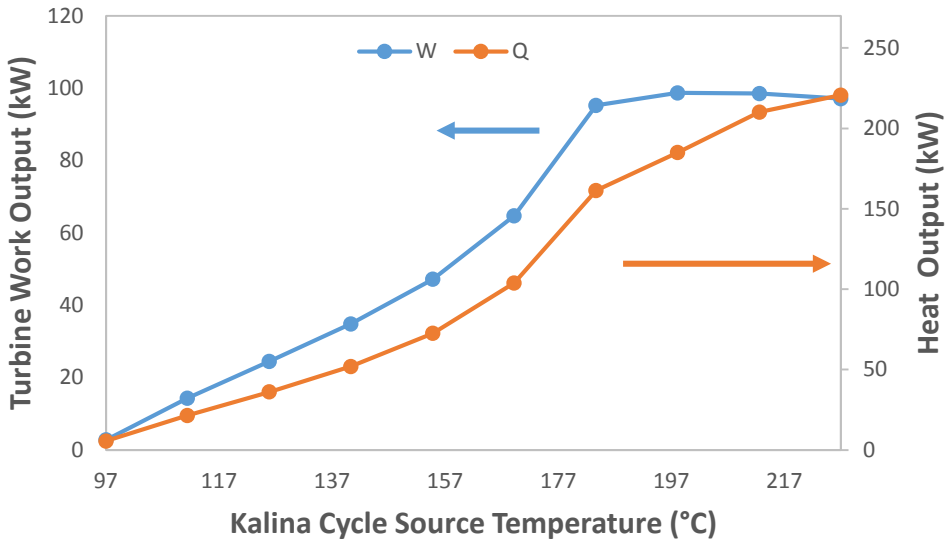

Figure 5.47 Kalina cycle work and heat outputs vs. source temperature

Turbine work and heat output both increase with the increasing source temperature as it can be seen in Figure 5.47. The increase flattens at around 180°C and reaches a peak at around 200°C for the work output graph. Heat output continues increasing but rate of increase slows down after 180°C. It can be concluded from this graph that increasing the source temperature indefinitely does not increase the work and heat outputs of the system as expected. After 180°C, there is no need to increase source temperature more. This shows that Kalina cycle is a perfect choice for low temperature sources.

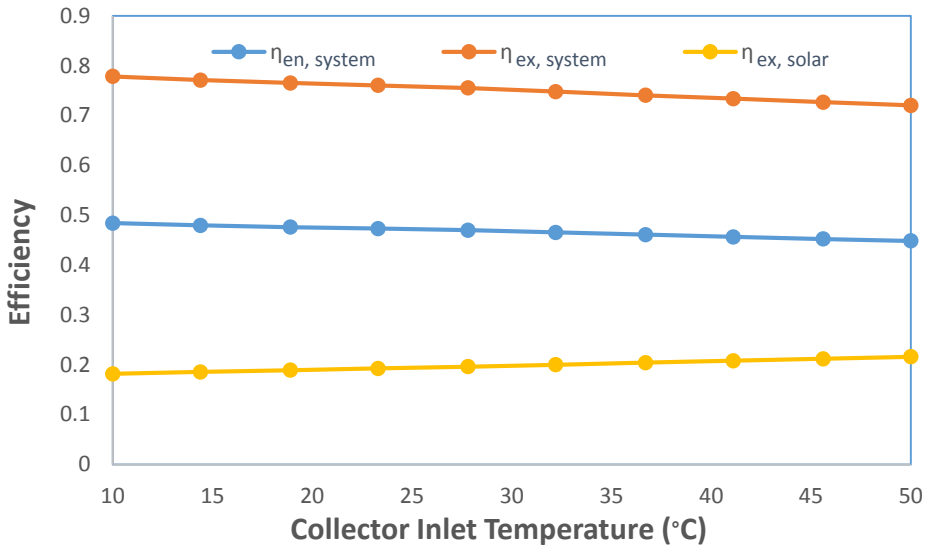

Figure 5.48 System and solar cycle efficiencies vs. collector inlet temperature

Figure 5.48 shows that the system energy and exergy efficiencies both drop with increasing collector inlet temperature. The rate of decrease is the same for both energy and exergy efficiency. The reason for the drop in efficiencies is because by increasing the collector inlet temperature, less heat is transferred to Kalina cycle hence reducing the turbine output and the efficiencies. Solar system exergy efficiency increases with increasing collector inlet temperature. The reason for this is as less heat is transferred to Kalina cycle, heat is preserved in the solar cycle, hence increasing the efficiency.

System efficiencies increased in a straight line as absorption chiller mass flow rate increased as shown in Figure 5.49. Exergy COP initially increased, reached a peak at around 3 kg/s and started decreasing slowly thereafter. Energy COP decreased as a straight line. The absorption

chiller mass flow rate increase affects the system outputs more than it affects the system inputs therefore efficiencies increase.

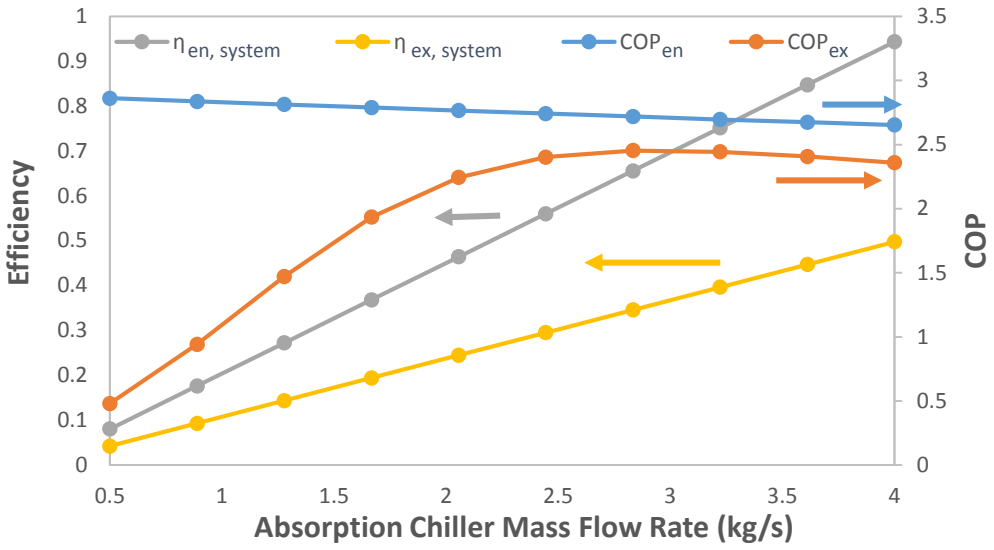

Figure 5.49 System efficiencies and absorption chiller COPs vs. absorption chiller mass flow rate

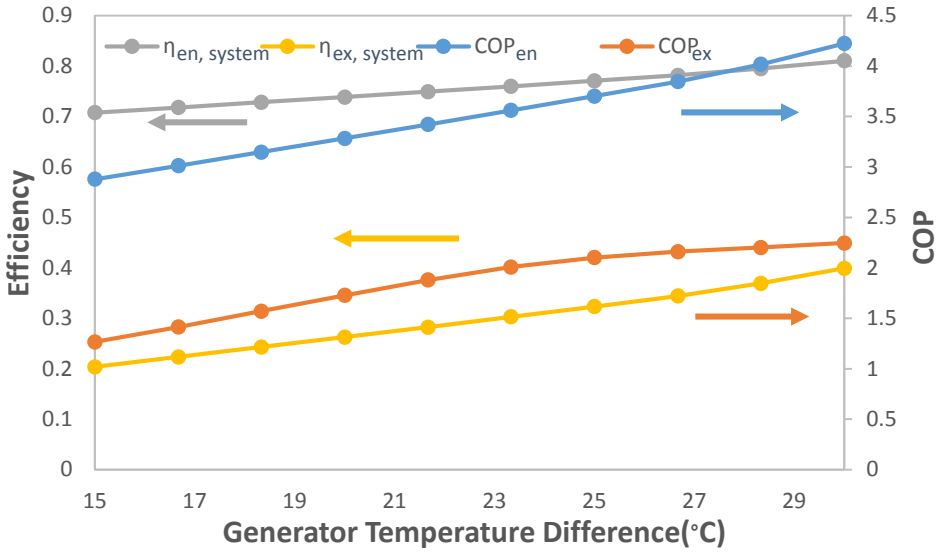

Figure 5.50 System efficiencies and absorption chiller COPs vs. generator temperature difference

The temperature difference of the 4 generators (very high temperature, high temperature, medium temperature, low temperature) in the quadruple effect absorption chiller affects COPs and efficiencies. As Figure 5.50 shows, energy COP increases are straight. Exergy COP increases in a slow rate and then stabilizes at around 30°C. System energy and exergy efficiencies increase in a straight line. The rate of increase is higher in system energy efficiency graph. Generator

temperature difference is a parameter that affects the efficiencies and COPs in a positive direction. In the absorption chiller higher generator temperature difference lets the generators work more effectively hence increasing the COPs and system performance. Higher temperature difference is integral if the main goal is efficiency and COP maximization.

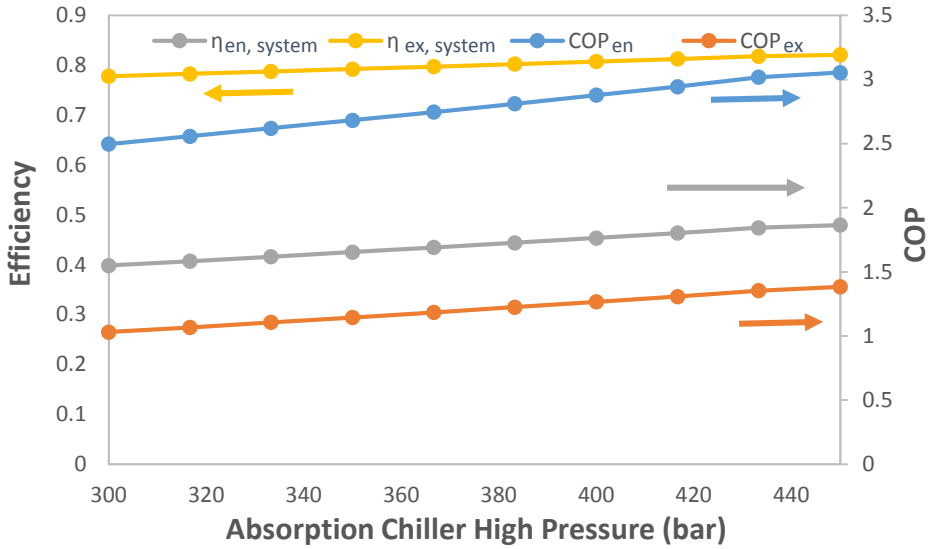

Figure 5.51 System efficiencies and absorption chiller COPs vs. absorption chiller high pressure

The system efficiencies and absorption chiller COPs all increase with increasing absorption chiller high pressure as it can be seen in Figure 5.51. System energy and exergy efficiencies have parallel graphs. Energy COP increases with the highest rate. All of the lines are straight. An absorption chiller pressure increase results in an increase in the system efficiencies and COPs, therefore higher pressure will produce the most benefits. As this affects the cost, an optimization should be done as introduced in sections 5.3.3 and 5.3.4.

The efficiencies and COPs all increase with increasing condenser heat in the absorption chiller as shown in Figure 5.52. The system energy and exergy efficiency graphs are parallel. Energy and exergy COP have curves with higher slopes than efficiency curves. Energy COP has the highest slope hence it is affected most by the condenser heat increase. As the condenser heat increases, more heat is rejected by the absorption chiller, increasing COPs and system efficiencies.

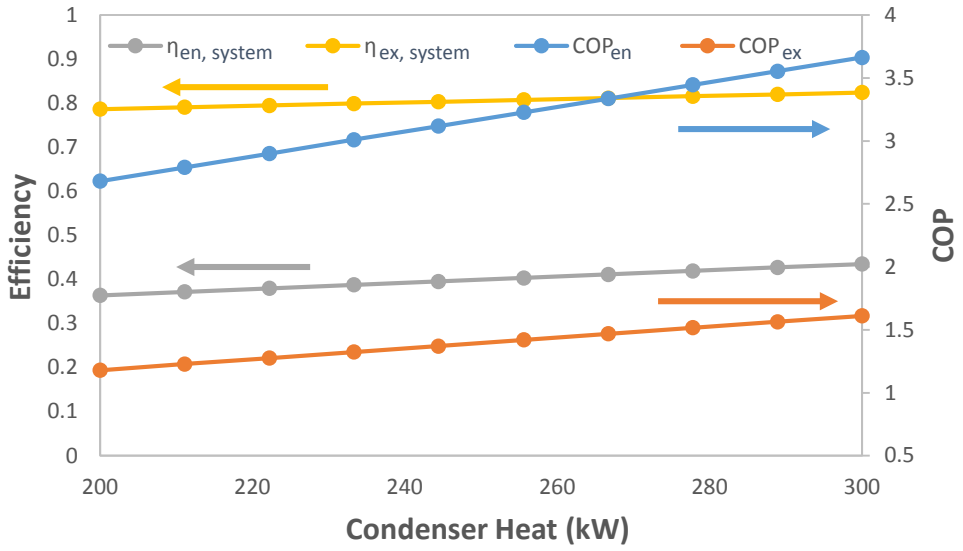

Figure 5.52 System efficiencies and absorption chiller COPs vs. absorption chiller condenser heat

5.3.3 Optimization

In this section, optimization for the important system outputs such as work ouput, system energy and exergy efficiencies, cost and reduced amount of CO_2 are performed using the EES optimization tool. The values of the independent variables (solar radiation, ambient temperature, solar cycle mass flow rate, absorption chiller mass flow rate, Kalina cycle ammonia mass fraction, boiler exit temperature) that affect the outputs are determined.

- **Power Output Maximization**

The work output is a system output that can be optimized. By setting the input variables, maximum output from System 3 can be achieved by using optimization tool of EES.

Input variables and their minimum and maximum bounds are shown in Table 5.16. These bounds have to be set initially in order to proceed towards optimization. Failure to set bounds initially would render it impossible to achieve an optimization. In addition, there are physical and economical boundaries for every input. When the input variables are set as in Table 5.16 to maximize turbine power output, a power of 118.4 kW can be obtained from the system. The variables, bounds and optimum values are shown in the table.

Table 5.16 Independent variables of System 3 for efficiency maximization

Variable	**Min**	**Max**	**Opt** $\dot{W}_{out}$	**Opt** $\dot{Q}_{eva}$
Solar radiation (G), W/m^2	0	1000	800	800
Ambient temperature (T_0), °C	10	35	20.4	17
Solar cycle mass flow rate ($\dot{m}_{oil}$), kg/s	0.5	5	1.42	2.5
Absorption chiller mass flow rate ($\dot{m}_1$), kg/s	1	3	1	1
Kalina cycle ammonia mass fraction (x)	0	1	0.75	0.5
Boiler exit temperature (T_{44}), °C	50	150	122.7	102
Maximum Output, kW			118	164

For maximum absorption chiller output, optimization tool is used and the results in Table 5.16 are obtained. Optimum values of the input variables can be found in "Opt $\dot{Q}_{eva}$" column.

- **Efficiency Maximization**

The system energy and exergy efficiencies are maximized by trial and error using approximate values for the input parameters such as solar radiation, ambient temperature, absorption chiller mass flow rate, solar cycle mass flow rate, Kalina cycle ammonia mass fraction and boiler exit temperature in this subsection. Bound values are determined depending on the physical limits. Then the optimum values for each parameter is determined to reach maximum efficiency as shown in Table 5.17.

Table 5.17 Independent variables of System 3 for efficiency maximization

Variable	**Min**	**Max**	**Opt** $\eta_{en,system}$	**Opt** $\eta_{ex,system}$
Solar radiation (G), W/m^2	0	1000	500	500
Ambient temperature (T_0), °C	10	35	17	10
Absorption chiller mass flow rate ($\dot{m}_1$), kg/s	1	3	2	3
Solar cycle mass flow rate ($\dot{m}_{oil}$), kg/s	0.5	5	2.49	2.28
Kalina cycle ammonia mass fraction (x)	0	1	0.27	0.27
Boiler exit temperature (T_{44}), °C	50	150	102	102
Maximum Efficiency			47%	88%

If the input parameters are set to the optimum values shown in "Opt $\eta_{en,system}$" column, a maximum system energy efficiency of 47% can be obtained.

When the same parameters are used in the optimization tool for system exergy efficiency, 88.2% can be achieved. This optimization took 42.6 seconds and result is obtained in 171 iterations. The optimum variable values can be found in "Opt $\eta_{ex,system}$" column.

- **Cost Minimization**

Cost minimization is performed in EES in 31.5 seconds. 502 equations are solved in 381 blocks and 138 iterations. A minimum cost of $133,029 is calculated when solar radiation is 100 W/m^2, ambient temperature is 17°C, absorption chiller mass flow rate is 1 kg/s, solar cycle mass flow rate is 2.5 kg/s, Kalina cycle ammonia mass fraction is 0 and boiler exit temperature is 102°C. The results are shown in Table 5.18. Minimum and maximum bounds are provided in the table.

Table 5.18 Independent variables of System 3 for cost minimization

Variable	**Min**	**Max**	**Opt Cost**
Solar radiation (G), W/m^2	0	1000	100
Ambient temperature (T_0), °C	10	35	17
Absorption chiller mass flow rate ($\dot{m}_1$), kg/s	1	3	1
Solar cycle mass flow rate ($\dot{m}_{oil}$), kg/s	0.5	5	2.5
Kalina cycle ammonia mass fraction (x)	0	1	0
Boiler exit temperature (T_{44}), °C	50	150	102
Minimum Cost			$133,029

- **CO_2 Reduction Maximization**

CO2 reduction is calculated by estimating the emission of a fossil fuel system with the same output values. Table 5.19 shows the results of the optimization. The minimum, maximum bound values and optimum values of each independent variable are shown. The independent variables that affect CO2 reduction are; solar radiation, ambient temperature, absorption chiller

Table 5.19 Independent variables of System 3 for CO_2 reduction maximization

Variable	**Min**	**Max**	**Opt CO_2**
Solar radiation (G), W/m^2	0	1000	1000
Ambient temperature (T_0), °C	10	35	17
Absorption chiller mass flow rate ($\dot{m}_1$), kg/s	1	3	3
Solar cycle mass flow rate ($\dot{m}_{oil}$), kg/s	0.5	5	2.5
Kalina cycle ammonia mass fraction (x)	0	1	0.88
Boiler exit temperature (T_{44}), °C	50	150	102
CO_2 reduction (tons/year)			2897

mass flow rate, solar cycle mass flow rate, Kalina cycle ammonia mass fraction and boiler exit temperature. The output from the system has to be maximized in order to maximize the amount of CO_2 reduction. More fossil fuels have to be consumed in the fossil fuel system in order to produce more output.

5.3.4 Sensitivity Analysis

The sensitivity analysis of System 3 is performed in this section. The effect of independent variables such as ambient temperature, solar radiation, absorption chiller mass flow rate, solar cycle mass flow rate and Kalina cycle ammonia mass fraction on the optimization targets is evaluated. Optimization targets are; system exergy efficiency, system cost and CO_2 reduction by the system using renewable energy instead of fossil fuels.

- **Ambient Temperature**

The effect of ambient temperature on optimization targets is evaluated in this section. Although ambient temperature is not a variable that can be set in a similar manner to other variables, it is important to see the effects, in order to select the location of the system depending on the climate. The results are shown in Figure 5.53.

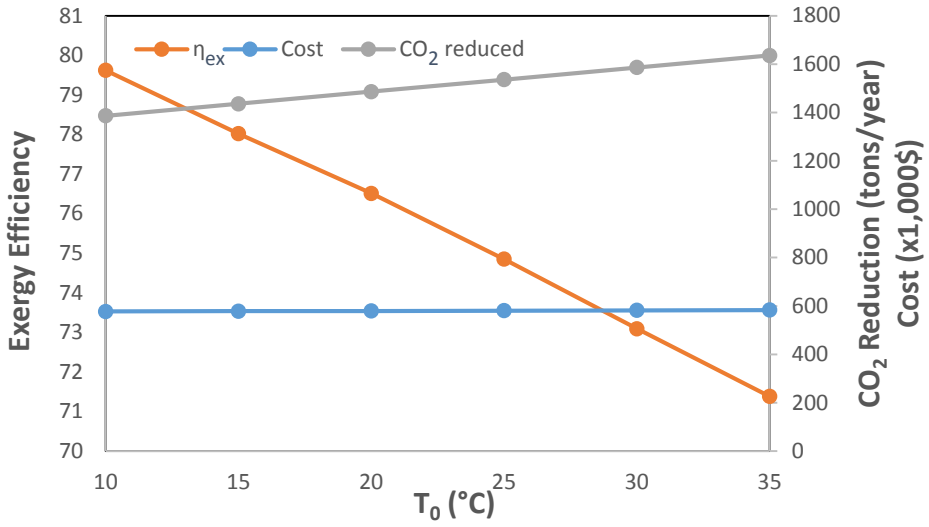

Figure 5.53 Effect of ambient temperature on optimization targets

The cost of the system increases slightly by the increase in the ambient temperature. CO_2 reduction increases as a result of the increase in the system outputs. The exergy efficiency drops because the increase in the ambient temperature does not affect the outputs as much as it affects the inputs.

- **Solar Radiation**

Solar radiation varies depending on the latitude, season and time of the day. With the assistance of sensitivity analysis, optimum solar radiation can be found depending on the optimization target. The result is shown in Figure 5.54. Solar radiation effect between 100 and 1000 W/m^2 is evaluated. The values in the vertical axis on the left show the system exergy efficiency values, while the values on the right vertical axis show the cost and CO_2 reduction.

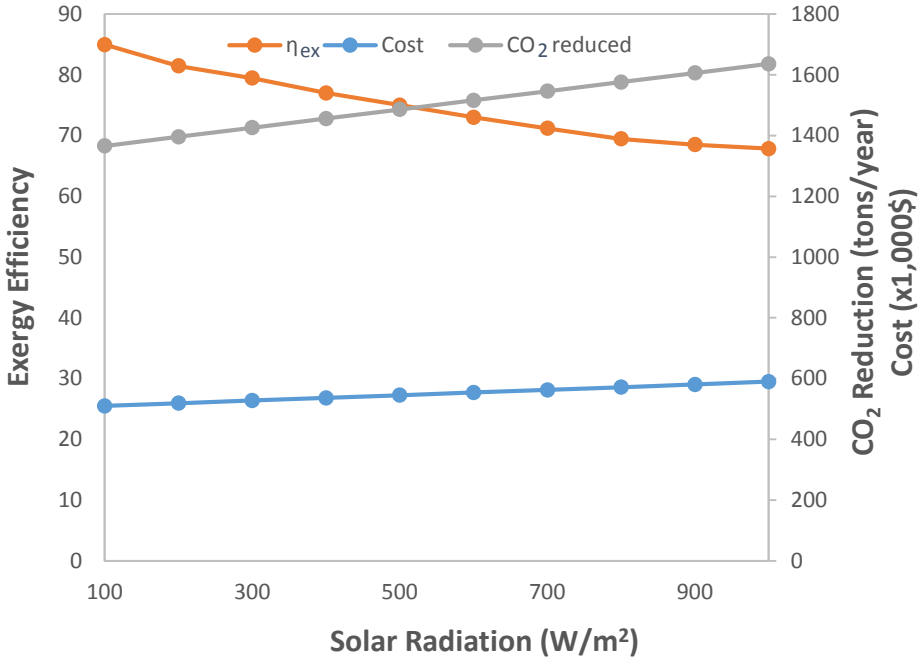

Figure 5.54 Effect of solar radiation on optimization targets

The cost of the system increases as the solar radiation increases. As the system component sizes increase, the cost increases. CO_2 reduction by the system increases. System outputs increase, therefore it follows that an equivalent system that uses fossil fuels would emit more CO_2. Exergy efficiency drops by the increase in solar radiation. Output increase is lower than the input increase therefore efficiency drops.

- **Absorption Chiller Mass Flow Rate**

The mass flow rate of quadruple effect absorption chiller is adjustable and its effect on optimization targets is evaluated in this section. The results are shown in Figure 5.55. On the graph the absorption chiller mass flow rate has a minimum value of 1 kg/s and maximum value of 3 kg/s. The primary vertical axis on the left shows efficiency values and the secondary vertical axis on the right shows cost and CO_2 reduction.

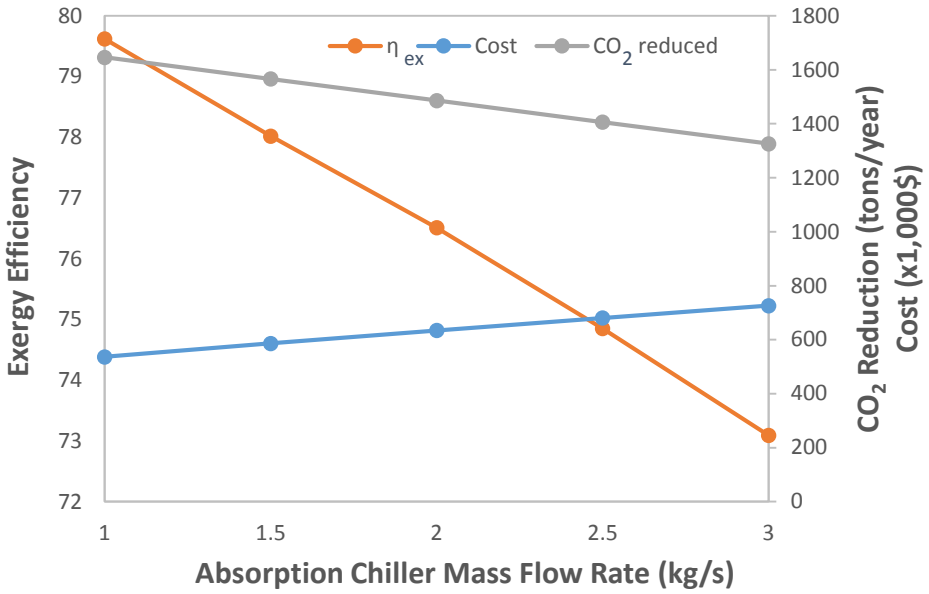

Figure 5.55 Effect of absorption chiller mass flow rate on optimization targets

An increase in the absorption chiller mass flow rate increases the cost of the system. The component sizes increase, as a result costs also increase. CO_2 reduction drops as the increase in absorption chiller mass flow rate decreases the turbine output. For the same reason, system exergy efficiency also drops. The output increase far exceeds the system input increase.

- **Solar Cycle Mass Flow Rate**

Solar cycle mass flow rate effect on system exergy efficiency, system cost and CO_2 reduction by the system are evaluated in this section. The resulting curves are shown in Figure 5.56. Solar cycle mass flow rate between 1 kg/s and 5 kg/s is selected. The vertical axis on the left shows the exergy efficiency values, while the right vertical axis shows cost and amount of CO_2 reduction.

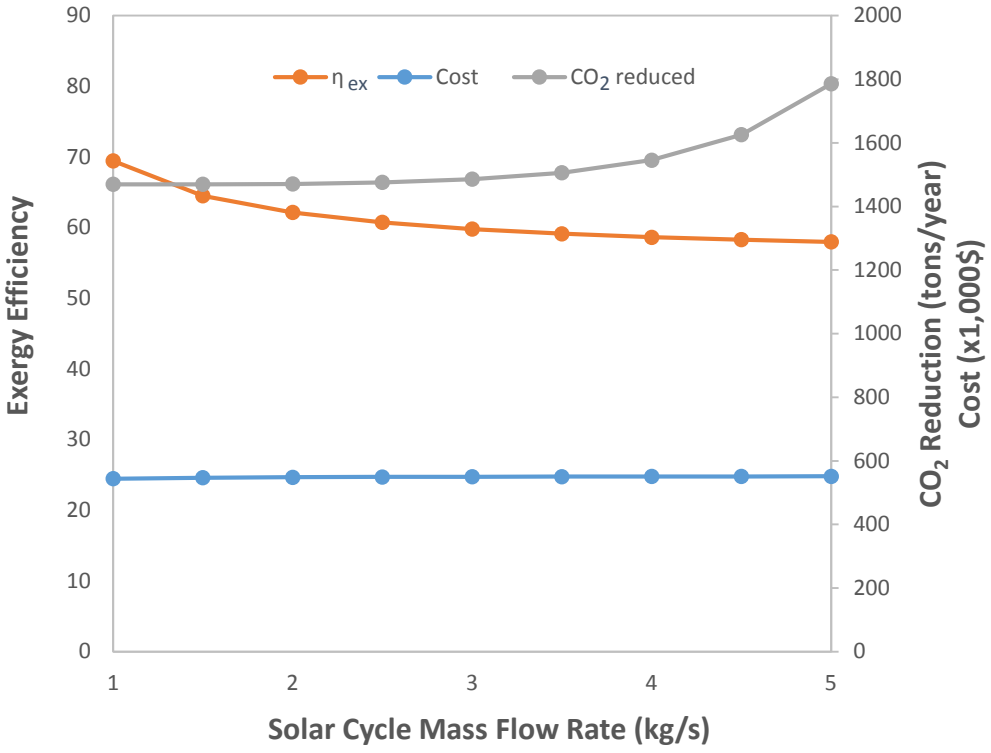

Figure 5.56 Effect of solar cycle mass flow rate on optimization targets

When the solar cycle mass flow rate is increased, CO_2 reduction by the system also increases (as a result of a jump in the system outputs). The cost of the system increases slightly as a result of the system components size increase. If system cost is a concern, solar cycle mass flow rate will not materially affect the results. CO_2 reduction by the system increases parabolic after 3 kg/s, respectively.

- **Kalina Cycle Ammonia Mass Fraction**

Kalina cycle ammonia mass fraction is an important variable as it affects the power cycle performance hence the outputs from the system. The effect on system exergy efficiency, cost and CO_2 reduction are shown in Figure 5.57. The primary vertical axis on the left shows system exergy efficiency values and the secondary vertical axis on the right shows cost and the amount of CO_2 reduction by the system.

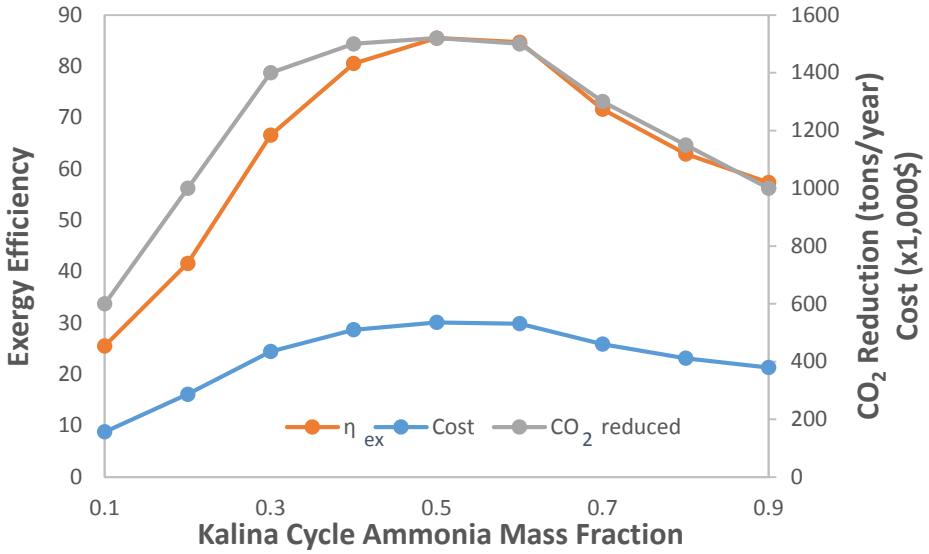

Figure 5.57 Effect of Kalina cycle ammonia mass fraction on optimization targets

Kalina cycle ammonia mass fraction effect allows the designer to select a design point, as all three curves have peak points. CO_2 reduction increases and reaches a peak at an ammonia mass fraction of approximately 0.5 kg/s. The costs of the system increases until it reaches the same peak point of 0.5 kg/s, then starts decreasing. System exergy efficiency has a similar trend and has a maximum efficiency of 85% at 0.5 kg/s.

5.4 Comparison with Experiment Results

In order to compare theoretical results with experimental data, trigeneration system setup designed and built by Tarique [105] is used.

Two systems (Systems 1 and 3) have outputs same as the experimental setup. The calculations of the initial and final conditions in these systems are compared with the experimental results. The results for System 2 are also showed for comparison reasons. The results of the experiments are important and provide a deeper understanding of the processes. This also allows for validation of the thermodynamic analysis results.

In order to utilize low-grade heat to generate power, cooling effect and hot water, a test bench is being built. A trigeneration system uses ammonia-water as a working fluid. The test bench consists of an expander, an air cooled condenser, a compressor, an evaporator, shell and tube heat exchanger, and auxiliary components. This integrated system combines power and cooling cycles, where the source heat is used to generate power through a scroll expander and a

portion of the heat is used in an ejector cooling system. The residual heat, which is normally released to the environment in this type of power cycle, is captured for hot water heating or space heating [99]. State points and components of the experimental setup is shown in Figure 5.58.

To accomplish the targets in the Ph.D. study by means of testing ammonia-water mixtures in the bench, first an appropriate scroll compressor is selected and converted into a scroll expander by operating in reverse direction so as to generate electric power. Source temperature is adjustable between 100-140°C. Temperature and pressure are measured at the inlet and outlet of each component which will be compared with findings of the analysis.

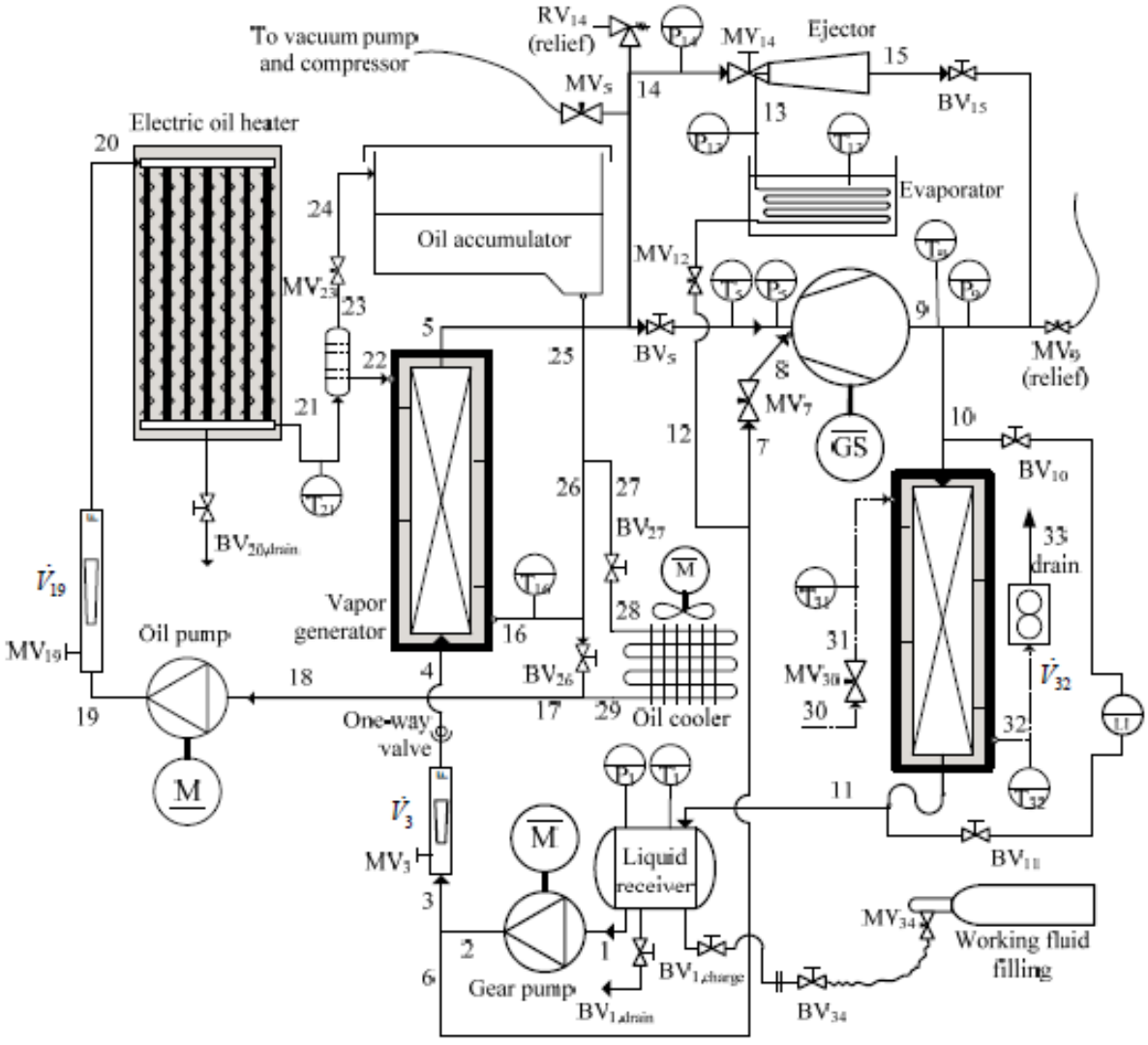

Figure 5.58 Ammonia – water based trigeneration system as built (adapted from [99])

After the procurement of the main components of the system such as scroll expander, pump and generator, the auxiliary components such as condenser, supports, heat exchangers, flanges, pipes etc. are manufactured in the machine shop.

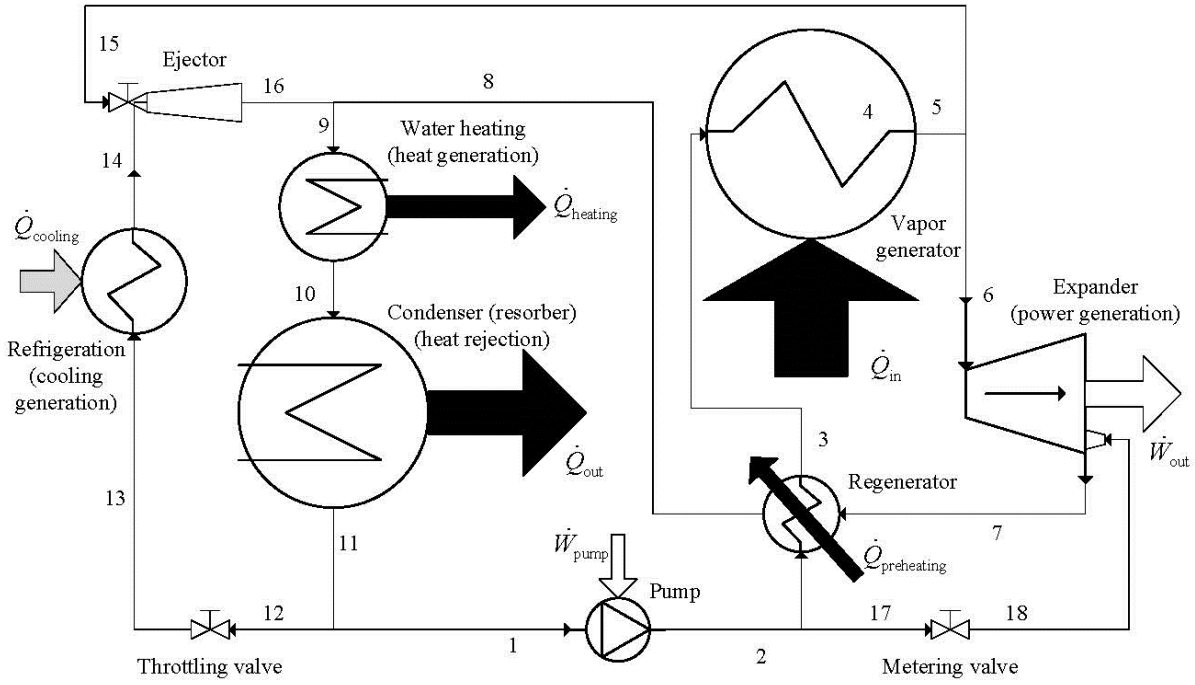

Figure 5.59 Trigeneration system with ammonia-water for power, heating and cooling (adapted from [105])

The simplified configuration of the experimental setup with the state points is shown in Figure 5.59. Black arrows signify heat fluxes, grey arrow signifies cooling and white arrow signifies power.

The processes in the system are explained in Table 5.20.

The comparison of the outputs from the experimental setup and the systems designed are shown in Table 5.21. As the quantity of the inputs (heat inputs) are different, each result is given as a percentage of the heat input.

In the systems, energy is distributed to system components in different proportions. Heating, cooling, electricity or other outputs can be favored depending on the application. The same system can be run to demonstrate different outputs. This is one of the reasons that the output of the systems and experimental setup do not necessarily match.

Table 5.20 Ammonia-water based trigeneration system with Rankine and ejector cycle integration

Process	Description
1-2	Pressurization of liquid (pumping)
2-3	Preheating (regenerator)
3-4-5	Vapor generation
5-6-15	Flow splitting of superheated vapor (#5 toward expander, #15 toward ejector)
6-7	Vapor expansion
7-8	Regeneration (heat release from two-phase flow)
8-9-16	Mixing of streams #8 and #16
9-10	Ammonia resorption and incomplete condensation
10-11	Complete condensation and heat rejection
11-1-12	Liquid flow splitting (#1 toward pump, #12 toward throttling valve)
13-14	Evaporation and heat absorption from cooling process
14-15-16	Ejector process (14-16 compression, 15-16 expansion)
17-18	Cold liquid injection for lubrication

Source: [105]

The research literature information is used to define the efficiencies of the components in the system. This is based on the average of the efficiencies of the same components from different systems or the manufacturer's data. The efficiencies of the components in the experimental setup can be different than the assumed efficiencies.

The losses in the pipes or flow restricting devices are calculated on an average basis. The losses in the experimental setup may be different than the model losses.

Finally the proposed systems and the experimental setup have similar outputs but with some major changes. For example in System 1 wind energy and electrolyzer differ from the experimental setup. System 2 has different outputs. System 3 has Kalina cycle, which differs substantially from the Rankine cycle. In addition, in the experimental setup, there is a quadruple effect absorption chiller which is different than a single effect absorption chiller. System input parameters other than heat input can be adjusted to achieve the same result as the experimental results.

Due to unprocessed data, efficiencies, heat losses and different system configurations, the results do not match.

Table 5.21 Performance comparison of trigeneration system with systems

Quantity	Experimental Value	System 1 (% of input)	System 2 (% of input)	System 3 (% of input)
Net generated work	69.1 kJ/kg (2.6%)	21.83 kJ/kg (6.2%)	37.52 kj/kg (9.7%)	54.87 kJ/kg (15%)
Generated heat	1,930 kJ/kg (73%)	53.39 kJ/kg (15%)	67.93 kj/kg (17.5%)	95.7 kJ/kg (27%)
Generated cooling	226 kJ/kg (11%)	27.94 kJ/kg (8%)	-	53.9 kJ/kg (15%)
Heat input	2,105 kJ/kg	331 kJ/kg	371 kJ/kg	297 kJ/kg
Energy input	537.1 kJ/kg	17.37 kJ/kg	17.01 kJ/kg	15.17 kJ/kg
Generated heat exergy	176 kJ/kg (8.4%)	9 kJ/kg (2.7%)	9 kJ/kg (2.4%)	22.76 kJ/kg (7.7%)
Exergy of cooling effect	-19.13 kJ/kg (1%)	-1.8 (0.5%)	-	-5.67 kJ/kg (2%)
Energetic COP	1.06	0.80	-	2.35
Exergetic COP	0.49	0.31	-	2.81

Source: [105]

5.5 Case Study

In this section a case study is performed to visualize the systems studied. A requirement for a building is defined and the cost, exergy efficiency and CO_2 reduction are calculated.

5.5.1 Definition of the Need

The major outputs from multigeneration systems are heating, cooling and electricity. System 1 and System 3 are able to supply these needs. Note that System 2 does not have an absorption chiller and some systems have other outputs where comparisons have been attempted.

As discussed in section 4.6 and shown in table 4.4, annual electricity, heating/domestic hot water and cooling loads of a suite are 8609, 9287 and 929 kWh respectively. The data is interpreted from a study made by Binkley [96]. In her study the average number of suites per building is 188 therefore the same data is utilized. The annual electricity, heating/domestic hot water and cooling loads of a 188 suite are 1618, 1746 and 175 MWh respectively. The annual and instant loads are shown in Table 5.22.

Table 5.22 Loads for the case study

Electricity Load		Heating/Domestic Hot Water		Cooling	
Annual (MWh)	Instant (kW)	Annual (MWh)	Instant (kW)	Annual (MWh)	Instant (kW)
1618	185	1746	199	175	20

5.5.2 Results from the Systems

When the annual loads of a 188 suite building are used as the goal of the three systems, the results in Table 5.23 are achieved.

Table 5.23 Results of the case study

Systems	Cost ($)	Exergy Efficiency (%)	CO_2 reduction (tons/year)
System 1	680,000	26	3936
System 2	956,000	49	1774
System 3	580,000	75	1486

The results in the table shows that system 3 has the lowest cost and the highest exergy efficiency. Most CO_2 is reduced by system 1. As a result System 1 and System 3 seem to be the most favorable systems.

It should be noted that although System 2 has no cooling effect, cooling load is added to the heating load in order to make a comparison between the systems. As the heating load of System 2 is higher than the other systems, it is necessary to include the cooling load as well.

There are other outputs from the systems as well as heating, cooling and electricity. For example system 1 produces hydrogen, system 2 produces hydrogen and desalinated water and system 3 produces hydrogen. These are additional outputs from the systems that affect the results. The reason why system 2 is ranked behind the other systems is because of the additional desalinated water it produces.

Chapter 6: Conclusions and Recommendations

6.1 Conclusions

Multigeneration energy systems attract a lot of attention due to simultaneous production of heating, cooling, electricity, hydrogen, hot water and fresh water from a common energy source. Multigeneration systems utilize the waste heat of a power plant to improve overall thermal performance, essentially utilizing the “free” energy available via the waste energy.

The high usage of fossil fuel has led to ozone layer depletion and global warming problems. Fossil fuels when used release harmful gasses such as CO_2, NO_x, and SO_x etc. which are not only harmful to living creatures but also to the nature. Due to the effects of using fossil fuels in the nature, researchers have started looking into the use of alternative fuels. One of the renewable sources of energy is solar energy. The solar flux arriving on the earth surface contains lots of energy which can be used for producing power or heat.

This thesis focused on developing three novel multigeneration energy systems using solar and wind energy to meet all the energy requirements of a multi-unit building. In order to provide a comparison with deeper detail, these three novel multigeneration energy systems are considered for system performance assessment. Exergy, economic and environmental impact analysis of the systems are conducted to gain a better insight into this study.

In the first system, solar energy is used to produce electricity, domestic heating water, cooling and hydrogen. There is a wind turbine to supply the system and measure the effects. The system utilizes a Rankine cycle, absorption chiller and electrolyzer. This system has 43% maximum energy efficiency and 65% maximum exergy efficiency. Maximum turbine output is 48 kW, while cooling effect is 28 kW and heating effect is 298.5 kW. 5079 tons per year of CO_2 is reduced by System 1 at a minimum cost of $236,024. System 1 is capable of supplying 49 suites.

In the second system there is only solar energy support. Outcomes from System 2 are heating, desalination, electricity and hydrogen. There are two Rankine cycles to increase efficiency. It has a maximum energy efficiency of 36% and maximum exergy efficiency of 44%. Maximum total turbine output is 116 kW and CO_2 reduction is 4873 tons per year at a minimum cost of $160,596. It can produce 0.04 kg/s desalinated water. System 2 is capable of supplying 106 suites.

In the third system solar energy is converted into electricity, heating load, cooling load, hydrogen and energy. A four stage absorption chiller is chosen for use in the cooling system to increase efficiency. There is a Kalina cycle to generate electricity and subsequently to produce hydrogen with the help of the electrolyzer. Maximum energy efficiency of System 3 is 47%, while maximum exergy efficiency is 88%. It produces a maximum power of 118 kW and has a maximum cooling effect of 164 kW at a minimum cost of $133,029. It saves 2897 tons of CO_2 per year compared to a conventional system to produce the same outputs. System 3 is capable of supplying 108 suites.

The modeling of the systems is performed by in the Engineering Equation Solver (EES) program. Optimization of the systems and sensitivity analysis is done to find the behavior of the systems under different conditions. The effects of ambient temperature, solar radiation, cycle mass flow rates, boiler exit temperature, pump pressure ratio, ammonia-mass fraction on cost, system output, system efficiencies, and environmental impact are evaluated.

A case study has been performed to compare the three systems. It has been determined that System 3 is the most efficient with 75% exergy efficiency, has the lowest cost with $580,000 and based on the needs of a Toronto, ON, 188 suite building system 1 reduced the most CO_2 by 3936 tons/year.

Systems are compared with the outputs of a trigeneration system developed in the lab. Due to the unprocessed data and different outputs, the results don't match 100%. However, it is seen that by using multigeneration, efficiency of a system is higher than combined efficiency of a system with separate units.

By the help of this thesis, the same or similar systems can be built and used to achieve higher efficiencies by using renewable sources to serve multi-unit buildings or districts. The future energy solutions have to contain renewable sources as an alternative to fossil fuels. Other similar hybrid energy generating systems can be analyzed with a fair degree of accuracy using the proposed technique.

6.2 Recommendations

The results of this thesis should be used to design new multigeneration systems or develop these systems to achieve better results in the future. The following studies should be conducted:

- The systems developed in this study should be prtotyped, built and tested experimentally.

- Exergoenvirosustainability analysis tools should be used to analyze these systems to cover the sustainability dimensions.
- The actual climatic data (including solar intensity, temperature pressure, wind speed, relative humidity, etc.) for different locations should be used to investigate how well these systems will perform.
- More sophisticated global optimization techniques like Nelder-Maed Simplex method, Direct algorithm or the Generic method should be applied to compare results and achieve better outcomes.
- The thermal energy storage options should be incorporated in these newly developed systems to offset the mismatch between demands and supplies.
- Other types of renewable energy resources, such as geothermal, biomass and ocean thermal energy conversion should be incorporated in the present systems, depending on the local availability of resources.

References

[1] Dincer I, Rosen MA, Energy, environment and sustainable development, *Applied Energy*, 64 (1999) 427-440

[2] Cuda P, Exergoeconomic Analysis and Optimization of Organic Rankine Cycles, M.Sc. Thesis, Faculty of Engineering and Applied Science, UOIT, Oshawa, ON, 2012.

[3] Ahmadi P, Dincer I, Rosen M, Exergo-environmental analysis of an integrated organic Rankine Cycle for trigeneration. *Energy Conversion and Management*, 64 (2012) 447–453.

[4] Dincer I, Rosen M, Thermodynamic aspects of renewables and sustainable development. *Renewable and Sustainable Energy Reviews*, 9 (2005) 169–189.

[5] Fernandez-Garca A, Zarza E, Valenzuela L, Prez M, Parabolictrough solar collectors and their applications. *Renewable and Sustainable Energy Reviews*, (2010) 14 (7), 1695–1721.

[6] Hosseini M, Investigation of Energy Storage Options for Sustainable Energy Systems, Ph.D. Thesis, Faculty of Engineering and Applied Science, UOIT, Oshawa, Ontario, 2013.

[7] Al-Sulaiman F, Dincer I, Hamdullahpur F, Exergy modeling of a new solar driven trigeneration system. *Solar Energy*, 2011; 85(9): 2228-2243.

[8] Ahmadi P: Modeling, Analysis and Optimization of Integrated Energy Systems for Multigeneration Purposes, Ph.D. Thesis, Faculty of Engineering and Applied Science, UOIT, Oshawa, Ontario, 2013.

[9] Dincer I, Rosen M, Exergy as a drive for achieving sustainability, *International Journal of Green Energy*, 1(1) (2004) 1–19.

[10] Ahmadi P, Dincer I, Rosen MA, Exergy, exergoeconomic and environmental analyses and evolutionary algorithm based multi-objective optimization of combined cycle power plants, *Energy*, 36 (2011) 5886-5898

[11] Ahmadi P, Dincer I, Rosen MA, Energy and exergy analyses of hydrogen production via solar-boosted ocean thermal energy conversion and PEM electrolysis, *International Journal of Hydrogen Energy*, 38 (2013) 1795-1805

[12] Dincer I, Rosen MA: Exergy: energy, environment and sustainable development. Elsevier Science; 2012.

[13] Ahmadi P, Dincer P, Thermodynamic and exergoenvironmental analyses, and multi-objective optimization of a gas turbine power plant, *Applied Thermal Engineering*, 31 (2011) 2529-2540

[14] Cengel YA, Boles MA, Kanoğlu M: Thermodynamics: an engineering approach. McGraw-Hill New York; 2011.

[15] Abusoglu A, Kanoglu A, Exergoeconomic analysis and optimization of combined heat and power production: A review. *Renewable and Sustainable Energy Reviews*, 13 (2009) 2295-2308.

[16] Ahmadi P, Dincer I, Exergoenvironmental analysis and optimization of a cogeneration

plant system using Multimodal Generic Algorithm. *Energy,* 35 (2010) 5161-5172.

[17] Pavlas M, Stehlík P, Oral J, Šikula J, Integrating renewable sources of energy into an existing combined heat and power system. *Energy*, 31-13 (2006) 2499-2511.

[18] Al-Sulaiman FA, Dincer I, Hamdullahpur F, Energy analysis of a trigeneration plant based on solid oxide fuel cell and organic Rankine Cycle. *International Journal of Hydrogen Energy,* 35 (2010) 5104-5113.

[19] Al-Sulaiman FA, Dincer I, Hamdullahpur F, Energy and exergy analyses of a biomass trigeneration system using an organic Rankine Cycle. *Energy*, 45 (2012) 975-985.

[20] Khaliq A, Exergy analysis of gas turbine trigeneration system for combined production of power heat and refrigeration. *International Journal of Refrigeration*, 32 (2009) 534-545.

[21] Ahmadi P, Rosen M, Dincer I, Greenhouse gas emission and exergo-environmental analyses of a trigeneration energy system. *International Journal of Greenhouse Gas Control*, 5 (2011) 1540-1549.

[22] Al-Suleiman FA, Hamdullahpur F, Dincer I, Performance comparison of three trigeneration systems using organic rankine cycles. *Energy*, (2011) 5741-5754.

[23] Temir G, Bilge D, Thermodynamic analysis of a trigeneration system. *Applied Thermal Engineering,* 24 (2004) 2689-2699.

[24] Delisle V, Kummert M, A novel approach to compare building-integrated photovoltaics/thermal air collectors to side-by-side PV modules and solar thermal collectors, *Solar Energy,* 100 (2014)50-65

[25] Brogren M, Optical efficiency of low-concentrating solar energy systems with parabolic reflectors, Ph.D. Thesis, Faculty of Science and Technology, Uppsala University, Uppsala, Sweden, 2004.

[26] Kodama T, Gokon N, Thermochemical cycles for high-temperature solar hydrogen production. *Chemical Reviews,* 107 (2007) 4048-4077.

[27] Wang ZL, Naterer GF, Gabriel KS, Secnik E, Gravelsins R, Daggupati VN, Thermal design of a solar hydrogen plant with a copper-chlorine cyle and molten salt energy storage. *International Journal of Hydrogen Energy*, 36 (2001) 11258-11272.

[28] Ghandehariun S, Rosen MA, Naterer GF, Wang Z, Comparison of molten salt heat recovery options in the Cu-Cl cycle of hydrogen production, *International Journal of Hydrogen Energy*, 36 (2011) 11328-11337.

[29] Ratlamwala TAH, Dincer I, Aydin M, Energy and exergy analyses and optimization study of an integrated solar heliostat field system for hydrogen production. *International Journal of Hydrogen Energy,* 37 (2012) 18704-18712.

[30] Ozturk M, Dincer I, Thermodynamic analysis of a solar-based multi-generation system with hydrogen production. *Applied Thermal Engineering,* 51 (2013) 1235-1244.

[31] Ratlamwala TAH, Gadalla MA, Dincer I, Performance assessment of an integrated PV/T and triple effect cooling system for hydrogen and cooling production, *International Journal*

of Hydrogen Energy, 36 (2011) 11282-11291

[32] Xu C, Wang Z, Li X, Sun F, Energy and exergy analysis of solar power tower plants. *Applied Thermal Engineering*, 31 (2011) 390-413.

[33] Ratlamwala TAH, Dincer I, Gadalla MA, Kanoglu M, Thermodynamic analysis of a new renewable energy based hybrid system for hydrogen liquefaction, *International Journal of Hydrogen Energy*, 37 (2012) 12108-18117

[34] Wang J, Dai Y, Gao L, Ma S, A new combined cooling heating and power system driven by solar energy, *Renewable Energy*, 34 (2009) 2780-2788

[35] Ozcan, H, and Dincer, I, Energy and exergy analyses of a solar driven Mg–Cl hybrid thermochemical cycle for co-production of power and hydrogen, *International Journal of Hydrogen Energy*, 39(28) (2014) 15330-15341.

[36] Ozturk M, Dincer I, Thermodynamic assessment if an integrated solar power tower and coal gasification system for multi-generation purposes, *Energy Conversion and Management*, 76 (2013) 1061-1072

[37] Chua KJ, Yang WM, Wong TZ, Ho CA: Integrating renewable energy technologies to support building trigeneration, *Renewable Energy*, 41 (2012) 358-367

[38] Gardner P, Garrad A, Jamieson P, Snodin H and Tindal A., Wind Energy – The Facts; Volume 1: Technology

[39] Desmukh MK, Desmukh SS, Modeling of hybrid renewable energy systems. *Renewable and Sustainable Energy Reviews*, 12 (2008) 235-249.

[40] Celik AN, Techno-economic analysis of autonomous PV-wind hybrid energy systems using different sizing methods. *Energy Conversion and Management*, 44 (2003) 1951-1968.

[41] Nema P, Nema RK, Rangnekar S, A current and future state of art development of hybrid energy system using wind and PV-solar: A review. *Renewable and Sustainable Energy Reviews*, 13 (2009) 2096-2103.

[42] Agustin JLB, Dufo-Lopez R, Simulation and optimization of stand-alone hybrid renewable energy systems. *Renewable Sustainable Energy Reviews*, 13 (2009) 2111-2118.

[43] Notton G, Diaf S, Stoyanov L, Hybrid Photovoltaic/Wind Energy Systems for Remote Locations. *Energy Procedia*, 6 (2011) 666-677.

[44] Caliskan H, Dincer I, Hepbasli A: Exergoeconomic and environmental impact analyses of a renewable energy based hydrogen production system, *International Journal of Hydrogen Energy*, (2013) 1-8

[45] Kaabeche A, Belhamel M, Ibtiouen R: Techno-economic valuation and optimization of integrated photovoltaic/wind energy conversion system, *Solar Energy*, 85 (2011) 2407-2420

[46] Celik AN: Techno-economic analysis of autonomous PV-wind hybrid energy systems using different sizing methods, *Energy Conversion and Management*, 44 (2003) 1951-1968

[47] Deshmukh MK, Deshmukh SS: Modeling of hybrid renewable energy systems,

Renewable and Sustainable Energy Reviews, 12 (2008) 235-249

[48] Erdinc O, Uzunoglu M: Optimum design of hybrid renewable energy systems: Overview of different approaches, *Renewable and Sustainable Energy Review*, 16 (2012) 1412-1425

[49] Wang ZL, Naterer GF, Gabriel KS, Secnik E, Gravelsins R, Daggupati VN, Thermal design of a solar hydrogen plant with a copper-chlorine cyle and molten salt energy storage. *International Journal of Hydrogen Energy*, 36 (2001) 11258-11272.

[50] Ratlamwala TAH, Dincer I, Gadalla MA, Thermodynamic analysis of an integrated geothermal based quadruple effect absorption system for multigenerational purposes. *Thermochimica Acta*, 535 (2012) 27-35.

[51] Coskun C, Oktay Z, Dincer I, Thermodynamic analyses and case studies of geothermal based multi-generation systems. *Journal of Cleaner Production*, 32 (2012) 71-80.

[52] Desideri U, Bidini G, Study of possible optimization criteria for geothermal power plants. *Energy Conversion Management*, 38-15-17 (1997) 1681-1691.

[53] Ozgener L, Hepbasli A, Dincer I, Rosen MA, Exergoeconomic analysis of geothermal district heating systems: A case study, *Applied Thermal Engineering*, 27 (2007) 1303-1310

[54] Ratlamwala TAH, Gadalla MA, Dincer I, Thermodynamic analyses of an integrated PEMFC-TEARS-geothermal system for sustainable buildings, *Energy and Buildings*, 44 (2012) 73-80

[55] Ratlamwala TAH, Dincer I, Gadalla MA, Performance analysis of a novel integrated geothermal-based system for multi-generation applications, *Applied Thermal Engineering*, 40 (2012) 71-79

[56] Ratlamwala TAH, Dincer I, Comparative efficiency assessment of novel multi-flash integrated geothermal systems for power and hydrogen production, *Applied Thermal Engineering*, 48 (2012) 359-366

[57] Aybar HS, Akhatov JS, Avezova NR, Halimov AS, Solar powered RO desalination: Investigations on pilot project of PV powered RO desalination system, *Applied Solar Energy*, 46-4 (2010) 275-284

[58] Khawaji AD, Kutubkhanah IK, Wie JM, Advances in seawater desalination technologies. *Desalination*, 221 (2008) 47-69.

[59] Cap DP, Von Arx AV, Solar desalinization plant, US Patent 2011 0048921 A1, Mar. 3, 2011.

[60] Fernández-López C, Viedma A, Herrero R, Kaiser AS, Seawater integrated desalination plant without brine discharge and powered by renewable energy systems. *Desalination*, 235 1–3, (2009) 179–198

[61] Houcine I, BenAmara M, Guizani A, Maalej M, Pilot plant testing of a new solar desalination process by a multiple-effect-humidification technique. *Desalination*, 196 (2006) 105-124.

[62] Yildirim C, Solmus I, A parametric study in a humidification-dehumidification (DH)

desalination unit powered by solar air and water heaters, *Energy Conversion and Management*, 86 (2014) 568-575

[63] Franchini G, Perdichizzi A, Modeling of a solar driven HD (Humidification-Dehumidification) desalination system, *Energy Procedia*, 45 (2014) 588-597

[64] Trieb F, Muller-Steinhagen H, Concentrating solar power for seawater desalination in the Middle East and North Africa, *Desalination*, 220 (2008) 165-183

[65] Trieb F, Muller-Steinhagen H, Kern J, Scharfe J, Kabariti M, Al Taher A, Technologies for large scale seawater desalination using concentrated solar radiation, *Desalination*, 235 (2009) 33-43

[66] Mabrouk AA, Nafey AS, Fath HES, Thermoeconomic analysis of some existing desalination processes, *Desalination*, 205 (2007) 354-373

[67] Sharqawy MH, Lienhard VJH, Zubair SM, On exergy calculations of seawater with applications in desalination systems, *International Journal of Thermal Science*, 50 (2011) 187-196

[68] Marston CH,Parametric Analysis of the Kalina Cycle, *Journal of Engineering for Gas Turbines and Power*, 112 (1990) 107-116

[69] Nag PK, Gupta AVSSKS, Exergy Analysis of the Kalina Cycle, *Applied Thermal Engineering*, 18-6 (1998) 427-439

[70] Wall G, Chuang CC, Ishida M, Exergy Study of the Kalina Cycle, *Analysis of Design and Energy Systems*, 10-3 (1989) 73-77

[71] Jones DA: A Study of the Kalina Cycle System 11 for the Recovery of Industrial Waste heat with Heat Pump Augmentation, M.Sc. Thesis, Auburn University, Auburn, Alabama, 2011

[72] Lolos OA, Rogdakis ED, A Kalina power cycle driven by renewable energy sources, *Energy*, 34 (2009) 457-464

[73] Ogriseck S, Integration of Kalina cycle in a combined heat and power plant, a case study, *Applied Thermal Engineering*, 29 (2009) 2843-2848

[74] Wang J, Yan Z, Zhou E, Dai Y, Parametric analysis and optimization of a Kalina cycle driven by solar energy, *Applied Thermal Engineering*, 50 (2013) 408-415

[75] Zhang X, He M, Zhang Y: A review of research on the kalina cycle, *Renewable and Sustainable Energy Reviews*, 16 (2012) 5309-5318

[76] Wang J, Yan Z, Zhou E, Dai Y, Parametric analysis and optimization of a Kalina Cycle driven solar energy. *Applied Thermal Engineering*, 50 (2013) 408-415.

[77] U.S. Department of Energy, Energy Efficiency & Renewable Energy, Advanced Manufacturing Office, Steam tip Sheet #14

[78] Palacios-Bereche R, Gonzales R, Nebra SA, Exergy calculation of lithium bromide–water solution and its application in the exergetic evaluation of absorption refrigeration

systems LiBr-H2O, *International Journal of Energy Research*, 36 (2012) 166-181

[79] Marc O, Anies G, Lucas F, Castaing-Lasvignottes J, Assessing performance and controlling operating conditions of a solar driven absorption chiller using simplified numerical models, *Solar Energy*, 86 (2012) 223102239

[80] Chua HT, Toh HK, Ng KC, Thermodynamic modeling of an ammonia-water absorption chiller, *International Journal of Refrigeration* 25, (2002) 896-906.

[81] Kim DS and Infante Ferreira CA: Air-cooled Libr-water absorption chillers for solar air conditioning in extremely hot weathers, *Energy Conversion and Management*, 50 (2009) 1018-1025

[82] Farshi LG, Mahmoudi SMS, Rosen MA, Yari M, Amidpour M, Exergoeconomic analysis of double effect absorption refrigeration. *Energy Conversion and Management*, 65 (2013) 13-25.

[83] Adewusi SA, Zubair M, Second law based thermodynamic analysis of ammonia–water absorption system, *Energy Conservation and Management*, 45 (2004) 2355–2369.

[84] Chua HT, Toh HK, Ng KC, Thermodynamic Modeling of an ammonia-water absorption chiller, *International Journal of Refrigeration*, 25 (2002) 896-906.

[85] Shokati N, Ranjbar F, Yari M, A comparative analysis of rankine and absorption power cycles from exergoeconomic viewpoint, *Energy Conversion and management*, 88 (2014) 657-668

[86] Colonna P, Gabrielli P: Industrial trigeneration using ammonia-water absorption refrigeration systems (AAR), *Applied Thermal Engineering*, 23 (2003) 381-396

[87] Huicochea A, Rivera W, Gutierrez-Urueta G, Bruno JC, Coronas A: Thermodynamic analysis of a trigeneration system consisting of a micro gas turbine and a double effect absorption chiller, *Applied Thermal Engineering*, 31 (2011) 3347-3353

[88] Haji Abedin A, Thermochemical energy storage systems: modelling, analysis and design, M.Sc. Thesis, University of Ontario Institute of Technology, Oshawa, ON, 2010

[89] Dincer I, Dost S, Li X, Performance analyses of sensible heat storage systems for thermal applications, *International Journal of Energy Research*, 21 (1997) 1157–1171

[90] Ozlu S, Dincer I, Development and analysis of a solar and wind energy based multigeneration system, *Solar Energy*, (2015) (In review)

[91] Ozlu S, Dincer I, Performance assessment of a new solar energy-based system, *Energy*, (2015) (In review)

[92] Ozlu S, Dincer I, Analysis and evaluation of a new solar energy-based multigeneration system, *Energy Conversion and Management*, (2015) (In review)

[93] Tsatsaronis G, Application of thermoeconomics to the design and synthesis of energy plants. *Energy, Energy System Analysis, and Optimization*.

[94] Dincer I, Colpan CO, Kadioglu F, Causes, Impacts and Solutions to Global Warming,

Springer, New York, 2013

[95] United States Environmental Protection Agency Clean Energy web page retrieved on February 01, 2015 http://www.epa.gov/cleanenergy/energy-and-you/affect/air-emissions.html

[96] Binkley C, Energy consumption trends of multi-unit residential buildings in the city of Toronto, M.Sc. Thesis, Department of Civil Engineering, University of Toronto, Toronto, Ontario, 2012

[97] Heating Degree days, Toronto Hydro

[98] Duffie JA, Beckman WA, *Solar Engineering of Thermal Processes.* John Wiley & Sons, Inc.; 2006

[99] M.S. Sodha, I. Chrysis, Optimal insulation of solar hot water tanks, *Applied Energy,* 19-1 (1985) 73-75.

[100] Peters MS, Timmerhaus KD, West RE, Timmerhaus K, West R: *Plant design and economics for chemical engineers.* McGraw-Hill New York; 1968.

[101] Lian Z, Chua K, Chou S, A thermoeconomic analysis of biomass energy for trigeneration. *Applied Energy* 87 (2010) 84-95.

[102] Genç G, Çelik M, Serdar Genç M, Cost analysis of wind-electrolyzer-fuel cell system for energy demand in Pınarbaşı-Kayseri, *International Journal of Hydrogen Energy* (2012).

[103] F-Chart Software Engineering Equation Solver program overview web page, retrieved on May 16, 2015, http://www.fchart.com/ees/

[104] Kalogirou S, Solar Energy Engineering, Elsevier; 2014

[105] Tarique MA, Design, Analysis and Experimental Investigation of a New Scroll Expander Based Tri-Generation System, Ph.D. Thesis, Faculty of Engineering and Applied Science, UOIT, Oshawa, Ontario, 2014.

Appendix

A.1 EES Codes for the systems:

For System 1:

```
T[0] = 273 + 25 [C]
P[0] = 1 [bar];
s[0] = entropy (water, T=T[0], P=P[0])
h[0] = enthalpy (water, T=T[0], P=P[0])
omega_air=0.0153
h_0_air=Enthalpy(AirH2O,T=T[0],w=omega_air,P=P[0])
s_0_air=Entropy(AirH2O,T=T[0],w=omega_air,P=P[0])
m_dot_oil=0.5 "kg/s"
Q_solar=NS*Q_s
Q_s=A_ap*F_r*(S-((A_r/A_ap)*U_l*(T[33]-T[0]))) "W"
NS=2.5
w_col=2 "m"
D_o=0.040 "m"
A_ap=(w_col-D_o)*L "m2"
L=2 "m"
S=G_b*eta_r
G_b=400 "W/m2"
eta_r=0.765
A_r=pi*D_o*L
F_1=(1/U_l)/(1/U_l+D_o/(h_cr*D_i)+(D_o/(2*k)*ln(D_o/D_i)))
U_l=15 "W/mK"
D_i=0.025 "m"
h_cr=200 "W/m2K"
k=16"W/m C"
F_r=m_dot_oil*cp_salt/(A_r*U_l)*(1-exp(-1/m_dot_oil*cp_salt/(A_r*U_l*F_1)))
Ex_d_solar_cycle=Ex_dot_solar_cell-Q_in*(1-T[0]/T_boiler)-Q_out_dwh*(1-T[0]/T_out_dwh)-
Q_abs_g*(1-T[0]/T_abs_g)
Ex_d_solar_cell=Ex_dot_solar_cell+Ex_dot[33]-Ex_dot[35]
Ex_dot_solar_cell=Q_solar*(1-ConvertTemp (C,K,T[0])/ConvertTemp (C,K,T_sun))
T_sun=5778 "K"

Eta_en_solar=(Q_in+Q_out_dwh+Q_abs_g)/Q_solar
Eta_ex_solar=(Q_in*(1-T[0]/T_boiler)+Q_out_dwh*(1-T[0]/T_out_dwh)+Q_abs_g*(1-
T[0]/T_abs_g))/Ex_dot_solar_cell

Z_solar=310*L*w_col
T[33]=T[0]+5
cp_salt=Cp(Therminol_66, T=T[33])
P[33]=100 "bar"
h[33]=Enthalpy(Therminol_66, T=T[33], P=P[33])
s[33]=Entropy(Therminol_66, T=T[33])
Ex_dot[33]=m_dot_oil*((h[33]-h[0])-T[0]*(s[33]-s[0]))
P[35]=P[33]
```

```
Q_solar=m_dot_oil*(h[35]-h[33])
h[35]=Enthalpy(Therminol_66, T=T[35], P=P[35])
s[35]=Entropy(Therminol_66, T=T[35])
Ex_dot[35]=m_dot_oil*((h[35]-h[0])-T[0]*(s[35]-s[0]))

//Hot Storage
h_oa=0.1 "W/m2C" "heat transfer coefficient oil air"
eta_ins=0.3 "m" "insulation thickness"
k_pf=0.016 "W/mC" "polyurethane foam thermal conductivity"
1/U_hs=1/h_oa+eta_ins/k_pf "overall heat transfer coefficient"
A_hs=3 "m2" "cold storage surface area"
Q_hs=U_hs*(T[35]-T[0])*A_hs
m_dot_oil*(h[35]-h[29])=Q_hs
P[29]=P[33]
h[29]=Enthalpy(Therminol_66, T=T[29], P=P[29])
s[29]=Entropy(Therminol_66, T=T[29])
Ex_dot[29]=m_dot_oil*((h[29]-h[0])-T[0]*(s[29]-s[0]))
Z_hs=27*Q_hs

//Boiler
Ex_dot_in=Ex_dot[29]-Ex_dot[30]
Q_in=m_dot_oil*(h[29]-h[30])
T_boiler=(T[29]+T[30]+T[20]+T[21])/4
P[30] = P[33]
h[30]=Enthalpy(Therminol_66, T=T[30], P=P[30])
s[30]=Entropy(Therminol_66, T=T[30])
Ex_dot[30]=m_dot_oil*((h[30]-h[0])-T[0]*(s[30]-s[0]))
A_boiler=Q_in/(U_boiler*delta_t_ln_boiler)
U_boiler=2  "kW/m2K"
delta_T_ln_boiler=((T[29]-T[21])-(T[30]-T[20]))/(ln(abs(((T[29]-T[21])/(T[30]-T[20])))))
T[30] = 273 + 100

//Hot Water
Q_out_dwh=m_dot_oil*(h[30]-h[17])
Q_out_dwh=m_dwh*cp_water*(T[32]-T[31])
cp_water=Cp(Water,T=(T[31]+T[32])/2,P=P[0])
T[31]=T[0]
T[32]=273 + 60
Ex_dot[31]=m_dwh*cp_water*(T[31]-T[0])
Ex_dot[32]=m_dwh*cp_water*(T[32]-T[0])
Ex_dot_dwh=Ex_dot[30]-Ex_dot[17]
T_out_dwh=(T[17]+T[30]+T[31]+T[32])/4
h[17]=Enthalpy(Therminol_66, T=T[17], P=P[17])
s[17]=Entropy(Therminol_66, T=T[17])
Ex_dot[17]=m_dot_oil*((h[17]-h[0])-T[0]*(s[17]-s[0]))
P[17]=P[33]
T[17]=T[30]-30


//Generator
h[18]=Enthalpy(Therminol_66, T=T[18], P=P[18])
```

```
s[18]=Entropy(Therminol_66, T=T[18])
Ex_dot[18]=m_dot_oil*((h[18]-h[0])-T[0]*(s[18]-s[0]))
P[18]=P[33]
Q_abs_g=m_dot_oil*(h[17]-h[18])
Ex_dot_abs_g=Ex_dot[17]-Ex_dot[18]

//Cold Storage
1/U_cs=1/h_oa+eta_ins/k_pf "overall heat transfer coefficient"
m_dot_oil*(h[18]-h[33])=Q_cs
A_cs=6 "m2" "hot storage surface area"
Z_cs=27*Q_cs

"LiBr - H2O ABSORPTION"
LL=1                                          "number of the first state of absorption"

"Parameters to be changed"
T_abs_e=273+7[K]                              "evaporator temperature"
T_abs_c=273+35[K]                             "condenser temperature"
T_abs_a=273+40[K]                             "absorber temperature"
T_abs_g=273+80[K]                             "genarator temperature"
Q_abs_g=35 [MW]                               "COOLING LOAD"
epsilon_abs=0.8                               "Heat exchanger effectiveness for solution heat
exchanger"
epsilon_hex=0.85                              "Heat exchanger effectiveness"

"Temperatures"
T[LL]=T_abs_a
T[LL+1]=T[LL]
"T[L+2]="epsilon_abs=((T[LL+2]-T[LL]))/((T[LL+3]-T[LL]))
T[LL+3]=T_abs_g
"T[L+4]="epsilon_abs=(T[LL+3]-T[LL+4])/(T[LL+3]-T[LL])"effectiveness of counter flow HEX is used
to determine T[L+4]"
T[LL+5]=T[LL+4]
T[LL+6]=T_abs_g
T[LL+7]=T_abs_c
T[LL+8]=T_abs_e
T[LL+9]=T[LL+8]
T[LL+10]=273+18.6                             "Cooling water inlet temperature"
T[LL+11]=273+10                               "Cooling water exit temperature"
T[LL+12]=T[0]+2                               "Heat rejection - water inlet temperature"
T[LL+13]=T[0]+5                               "Heat rejection - water outlet temperature"
T[LL+14]=T[0]                                 "Ambient air inlet temperature for drying
process"
T[LL+15]=273+50 [K]                           "Drying air temperature - Variable"

Q_abs_e/epsilon_hex=m[LL+10]*(h[LL+10]-h[LL+11])"To calculate mass flow rate of coolingwater"
Q_abs_a/epsilon_hex=m[LL+12]*(h[LL+13]-h[LL+12])


"Pressure at each point"
```

```
P[LL+7]=P_sat(Water,T=T[LL+7])                    "Pressure of condenser, saturation presure at T_abs_c"
P[LL+8]=P_sat(Water,T=T[LL+8])                    "Pressure of evaporator, saturation presure at T_abs_e"

P[LL]=P[LL+8]
P[LL+1]=P[LL+7]
P[LL+2]=P[LL+7]
P[LL+3]=P[LL+7]
P[LL+4]=P[LL+7]
P[LL+5]=P[LL+8]
P[LL+6]=P[LL+7]
P[LL+9]=P[LL+8]

"LiBr mass fractions"
x_LiBr[LL]=x_LiBrH2O(T[LL],P[LL])
x_LiBr[LL+3]=x_LiBrH2O(T[LL+3],P[LL+3])
x_LiBr[LL+1]=x_LiBr[LL]
x_LiBr[LL+2]=x_LiBr[LL]
x_LiBr[LL+4]=x_LiBr[LL+3]
x_LiBr[LL+5]=x_LiBr[LL+3]
x_LiBr[LL+6]=0
x_LiBr[LL+7]=0
x_LiBr[LL+8]=0
x_LiBr[LL+9]=0

"Mass flow rates"
m[LL]=m[LL+1]
m[LL+1]=m[LL+2]
m[LL+3]=m[LL+4]
m[LL+4]=m[LL+5]
m[LL]=m[LL+5]+m[LL+9]
m[LL]*x_LiBr[LL]=m[LL+5]*x_LiBr[LL+5]+m[LL+9]*x_LiBr[LL+9] "LiBr mass balance, applied to the absorber"
m[LL+6]=m[LL+7]
m[LL+7]=m[LL+8]
m[LL+8]=m[LL+9]

"Quality"
x[LL+7]=0
x[LL+9]=1

"Specific heat"
Cp_X2=Cp_LiBrH2O(T[LL+1],x_LiBr[LL+1])    "specific heat at point 2 considering L=1"
Cp_X4=Cp_LiBrH2O(T[LL+3],x_LiBr[LL+3])    "specific heat at point 4 considering L=1"

"Enthalpy values"
h[LL]=h_LiBrH2O(T[LL],x_LiBr[LL])
h[LL+1]=h_LiBrH2O(T[LL+1],x_LiBr[LL+1])
h[LL+2]=h_LiBrH2O(T[LL+2],x_LiBr[LL+2])
h[LL+3]=h_LiBrH2O(T[LL+3],x_LiBr[LL+3])
```

```
h[LL+5]=h[Ll+4]
h[LL+6]=Enthalpy(Water,T=T[LL+6],P=P[LL+6])
h[LL+7]=Enthalpy(Water,x=x[LL+7],P=P[LL+7])
h[LL+8]=h[LL+7]
h[LL+9]=Enthalpy(Water,x=x[LL+9],P=P[LL+9])
h[LL+10]=Enthalpy(Water,T=T[LL+10],P=P[0])
h[LL+11]=Enthalpy(Water,T=T[LL+11],P=P[0])
h[LL+12]=Enthalpy(Water,T=T[LL+12],P=P[0])
h[LL+13]=Enthalpy(Water,T=T[LL+13],P=P[0])
h[LL+14]=Enthalpy(AirH2O,T=T[LL+14],w=omega_air,P=P[0])
h[LL+15]=Enthalpy(AirH2O,T=T[LL+15],w=omega_air,P=P[0])

"Entropy values"
s[LL]=s_LiBrH2O(T[LL],x_LiBr[LL])
s[LL+1]=s_LiBrH2O(T[LL+1],x_LiBr[LL+1])
s[LL+2]=s_LiBrH2O(T[LL+2],x_LiBr[LL+2])
s[LL+3]=s_LiBrH2O(T[LL+3],x_LiBr[LL+3])
s[LL+4]=s_LiBrH2O(T[LL+4],x_LiBr[LL+4])
s[LL+5]=s_LiBrH2O(T[LL+5],x_LiBr[LL+5])
s[LL+6]=Entropy(Water,T=T[LL+6],P=P[LL+6])
s[LL+7]=Entropy(Water,T=T[LL+7],x=x[LL+7])
s[LL+8]=Entropy(Water,T=T[LL+8],h=h[LL+8])
s[LL+9]=Entropy(Water,T=T[LL+9],x=x[LL+9])
s[LL+10]=Entropy(Water,T=T[LL+10],P=P[0])
s[LL+11]=Entropy(Water,T=T[LL+11],P=P[0])
s[LL+12]=Entropy(Water,T=T[LL+12],P=P[0])
s[LL+13]=Entropy(Water,T=T[LL+13],P=P[0])
s[LL+14]=Entropy(AirH2O,T=T[LL+14],w=omega_air,P=P[0])
s[LL+15]=Entropy(AirH2O,T=T[LL+15],w=omega_air,P=P[0])

"Exergy of flow for each state"
h_0_X1=h_LiBrH2O(T[0],x_LiBr[LL])          "Enthalpy at ambient condition for strong
solution"
s_0_X1=s_LiBrH2O(T[0],x_LiBr[LL])          "Entropy at ambient condition for strong
solution"
h_0_X4=h_LiBrH2O(T[0],x_LiBr[LL+3])        "Enthalpy at ambient condition for weak
solution"
s_0_X4=s_LiBrH2O(T[0],x_LiBr[LL+3])        "Entropy at ambient condition for weak
solution"
ex[LL]=(h[LL]-h_0_X1)-T[0] *(s[LL]-s_0_X1)
ex[LL+1]=(h[LL+1]-h_0_X1)-T[0] *(s[LL+1]-s_0_X1)
ex[LL+2]=(h[LL+2]-h_0_X1)-T[0] *(s[LL+2]-s_0_X1)
ex[LL+3]=(h[LL+3]-h_0_X4)-T[0] *(s[LL+3]-s_0_X4)
ex[LL+4]=(h[LL+4]-h_0_X4)-T[0] *(s[LL+4]-s_0_X4)
ex[LL+5]=(h[LL+5]-h_0_X4)-T[0] *(s[LL+5]-s_0_X4)
ex[LL+6]=(h[LL+6]-h[0])-T[0] *(s[LL+6]-s[0])
ex[LL+7]=(h[LL+7]-h[0])-T[0] *(s[LL+7]-s[0])
ex[LL+8]=(h[LL+8]-h[0])-T[0] *(s[LL+8]-s[0])
ex[LL+9]=(h[LL+9]-h[0])-T[0] *(s[LL+9]-s[0])
ex[LL+10]=(h[LL+10]-h[0])-T[0] *(s[LL+10]-s[0])
ex[LL+11]=(h[LL+11]-h[0])-T[0] *(s[LL+11]-s[0])
```

```
ex[LL+12]=(h[LL+12]-h[0])-T[0] *(s[LL+12]-s[0])
ex[LL+13]=(h[LL+13]-h[0])-T[0] *(s[LL+13]-s[0])
ex[LL+14]=(h[LL+14]-h_0_air)-T[0] *(s[LL+14]-s_0_air)
ex[LL+15]=(h[LL+15]-h_0_air)-T[0] *(s[LL+15]-s_0_air)

"Energy balance equation"
Q_abs_e=m[LL+9]*(h[LL+9]-h[LL+8])                    "Cooling load - in order to find MASS FLOW
RATE OF WATER"
W_abs=m[LL]*(h[LL+1]-h[LL])                          "work of pump"
Q_abs_a=m[LL+5]*h[LL+5]+m[LL+9]*h[LL+9]-
m[LL]*h[LL]
m[LL+1]*(h[LL+2]-h[LL+1])=m[LL+3]*(h[LL+3]-
h[LL+4])
Q_abs_g=m[LL+3]*h[LL+3]+m[LL+6]*h[LL+6]-
m[LL+2]*h[LL+2]
Q_abs_c=m[LL+6]*(h[LL+6]-h[LL+7])                    "condenser"

"Exergy balance equations"
m[LL+9]*(ex[LL+9]-ex[LL+8])+Q_abs_e*(1-
T_abs_e/T[0])=Ex_d[LL]
    "EVAPORATOR - to be changed"
m[LL+5]*ex[LL+5]+m[LL+9]*ex[LL+9]=m[LL]*ex[LL]+Q_abs_a*(1-
T[0]/T_abs_a)+Ex_d[LL+1]
m[LL+3]*(ex[LL+3]-ex[LL+4])=m[LL+1]*(ex[LL+2]-
h[LL+1])+Ex_d[LL+2]
    "solution heat exchanger"
Q_abs_g*(1-T[0]/ConvertTemp
(C,K,T_abs_g))+m[LL+2]*ex[LL+2]=m[LL+3]*ex[LL+3]+m[LL+6]*ex[LL+6]+Ex_d[LL+3]

m[LL+6]*(ex[LL+6]-ex[LL+7])=Q_abs_c*(1-
T[0]/T_abs_c)+Ex_d[LL+4]
    "condenser"

"COP Calculations"
COP_abs=Q_abs_e/Q_abs_g
COP_ex_abs=(Q_abs_e*(1-T_abs_e/T[0]))/(Q_abs_g*(1-T[0]/T_abs_g))

CRF=(i*(1+i)^n)/((1+i)^n-1)
i=0.02 "interest rate"
n=25 "total operating period of the system in years"
OH=5000 "annual number of operation hours"

//Rankine
PR=137
pthrottle=pcond*PR
pcond=1
etaturb=0.9
etapump=0.85
x=0.2
Q_in=m_dot_he*(h[21]-h[20])
m_dot_he=1
```

"Inlet of turbine"
T[21]=Tthrottle
p[21]=pthrottle
CALL NH3H2O(123,T21,P21,x: T[21],P[21],x[21],h[21],s[21],u[21],v[21],q[21])

"Inlet of condenser"
CALL NH3H2O(235,P[22],x,s[21]: T22s,P22s,x22s,h22s,s22s,u22s,v22s,q22s)
p[22]=pcond
h[22]=h[21]-etaturb*(h[21]-h22s)
CALL NH3H2O(234,P22,x,h22: T[22],P[22],x[22],h[22],s[22],u[22],v[22],q[22])
"Inlet of pump"
p[19]=p[22]
q[19]=0
CALL NH3H2O(238,P19,x,q19: T[19],P[19],x[19],h[19],s[19],u[19],v[19],q[19])
Tcond=T[19]

"Inlet of boiler"
p[20]=pthrottle
CALL NH3H2O(235,P[20],x,s[19]: T20s,P20s,x20s,h20s,s20s,u20s,v20s,q20s)
h[20]=h[19]+(h20s-h[19])/etapump
CALL NH3H2O(234,P20,x,h20: T[20],P[20],x[20],h[20],s[20],u[20],v[20],q[20])

"Work and heat calculations"
wout=h[21]-h[22]
win=h[20]-h[19]
qin=h[21]-h[20]
W_out=m_dot_he*(h[21]-h[22])
W_in=m_dot_he*(h[20]-h[19])

"Thermal efficiency"
eta=(wout-win)/qin

"2nd law efficiency -- i.e. relative to Carnot"
etaCarnot=1-(converttemp('K','R',Tcond))/(converttemp('K','R',Tthrottle))
epsilon=eta/etaCarnot

Ex_dot_rankine=Q_in*(1-T[0]/T_in)-Q_out*(1-T[0]/T_out)-W_out+W_in
Eta_en_rankine=(W_out-W_in)/Q_in
Eta_ex_rankine=(Q_out*(1-T[0]/T_out)+W_out-W_in)/(Q_in*(1-T[0]/T_in))
T_in=(T[20]+T[21])/2

//Condenser
Q_out=m_dot_he*(h[22]-h[19])
Q_out=mw*4.185*dTw
dTw=45
T[26]=T[0]
T[27]=273+60
V_dot_w=mw/1*60
T_out=(T[22]+T[19])/2

```
Z_condenser=280.74*(Q_out/(2200*delta_T_ln))+746*mw
delta_T_ln=(delta_T_in-delta_T_out)/ln(abs(delta_t_in/delta_t_out))
delta_t_in=T[22]-T[27]
delta_t_out=T[19]-T[26]

//Electrolyzer
m_dot_h2=eta_electrolyzer*w_out/hhv_h2
eta_electrolyzer=0.6
hhv_h2=142.18e6 "J/kg"
Ex_dot_h2=m_dot_h2*(ex_h2_ch+ex_h2_ph)
ex_h2_ch=253153/MW_h2
MW_h2=MolarMass(H2) "kg/kmol"
ex_h2_ph=((h_h2-h[0])-T[0])*(s_h2-s[0])
h_h2=Enthalpy(H2,T=T[0])
s_h2=Entropy(H2,T=T[0],P=P[0])
Z_electrolyzer=1000*(W_out)
//33.4 kilowatt hours is also equivalent (in energy) to one kilogram of hydrogen gas
P_h2=33400*M_dot_h2

//Wind Turbine
P_w=ro_air*A_wt*C_p_wt*(V_wind^3)/2000 "kW"
Ex_d_wind=(1/C_p_wt-1)*P_w
A_wt=pi*D_wt^2
D_wt=34 "m"
ro_air=1.225 "kg/m3"
C_p_wt=0.593
V_wind=4.19 "m/s"
Ex_dot_wind=ro_air*A_wt*(V_wind^3)/2000 "kW"
Eta_ex_wind=P_w/Ex_dot_wind
Z_wind=5000*P_w

eta_en_system=(W_out+P_w)/(Q_solar+P_w)
eta_ex_system=(W_out+Q_out*(1-T[0]/T[27])+(Q_abs_e*(1-T_abs_e/T[0]))+Q_out_dwh*(1-
T[0]/T[32])+P_w)/(Ex_dot_wind+Ex_dot_solar_cell)
Ex_dot_system=Ex_dot_solar_cell+ro_air*A_wt*(V_wind^3)/2000-Q_out_dwh*(1-T[0]/T_out_dwh)-
Q_abs_e*(1-T_abs_e/T[0])-Q_out*(1-T[0]/T[19])-ex_dot_h2
Ex_d_rankine=Q_in*(1-T[0]/T_boiler)-Q_out*(1-T[0]/T[19])-W_out+W_in
Q_heating=Q_out+Q_out_dwh
Ex_heating= Q_out*(1-T[0]/T[19])+Ex_dot_dwh
```

For System 2:

```
//Solar Cycle
T[0]=273+15
P[0]=1
s[0] = entropy (water, T=T[0], P=P[0])
h[0] = enthalpy (water, T=T[0], P=P[0])
m_dot_oil=0.5 "kg/s"

//Boiler
```

```
P[20]=100 "bar"
h[20]=Enthalpy(Therminol_66, T=T[20], P=P[20])
s[20]=Entropy(Therminol_66, T=T[20])
Ex_dot[20]=m_dot_oil*((h[20]-h[0])-T[0]*(s[20]-s[0])) "kW"
Ex_dot_in=Ex_dot[20]-Ex_dot[21] "kW"
Q_he=m_dot_oil*(h[20]-h[21])
T[21]=273+100
P[21] = P[20]
h[21]=Enthalpy(Therminol_66, T=T[21], P=P[21])
s[21]=Entropy(Therminol_66, T=T[21])
Ex_dot[21]=m_dot_oil*((h[21]-h[0])-T[0]*(s[21]-s[0]))
U_boiler=2  "kW/m2K"

//Collector
Q_solar=m_dot_oil*(h[19]-h[18])
Q_solar=NS*Q_s
Q_s=A_ap*F_r*(SE-A_r/A_ap*U_l*(T[18]-T[0])) "W"
NS=2.5
w_col=2 "m"
D_o=0.040 "m"
A_ap=(w_col-D_o)*L "m2"
L=2 "m"
SE=G_b*eta_r
G_b=400 "W/m2"
eta_r=0.765
A_r=pi*D_o*L
F_1=(1/U_l)/(1/U_l+D_o/(h_cr*D_i)+(D_o/(2*k)*ln(D_o/D_i)))
U_l=15 "W/mK"
D_i=0.025 "m"
h_cr=200 "W/m2K"
k=16"W/m C"
F_r=m_dot_oil*cp_salt/(A_r*U_l*F_1)*(1-exp(-1/m_dot_oil*cp_salt/(A_r*U_l*F_1)))*F_1
T[18]=T[0]+5
P[18]=P[20]
h[18]=Enthalpy(Therminol_66, T=T[18], P=P[18])
s[18]=Entropy(Therminol_66, T=T[18])
Ex_dot[18]=m_dot_oil*((h[18]-h[0])-T[0]*(s[18]-s[0]))
Z_solar=310*L*w_col
cp_salt=Cp(Therminol_66, T=T[18])
T_sun=5778"K"

//Hot Storage
h_oa=1 "W/m2C" "heat transfer coefficient oil air"
eta_ins=0.3 "m" "insulation thickness"
k_pf=0.016 "W/mC" "polyurethane foam thermal conductivity"
1/U_hs=1/h_oa+eta_ins/k_pf "overall heat transfer coefficient"
A_hs=6 "m2" "cold storage surface area"
Q_hs=U_hs*(T[19]-T[0])*A_hs
m_dot_oil*(h[19]-h[20])=Q_hs
h[19]=Enthalpy(Therminol_66, T=T[19], P=P[19])
s[19]=Entropy(Therminol_66, T=T[19])
```

```
Ex_dot[19]=m_dot_oil*((h[19]-h[0])-T[0]*(s[19]-s[0]))
P[19]=P[20]
Z_hs=27*Q_hs

//Hot Water
Q_out_dwh=m_dot_oil*(h[21]-h[18])
Q_out_dwh=m_dwh*cp_water*(T[23]-T[22])
cp_water=Cp(Water,T=(T[22]+T[23])/2,P=P[0])
T[22]=T[0]
T[23]=273+60
Ex_dot[22]=m_dwh*cp_water*(T[22]-T[0])
Ex_dot[23]=m_dwh*cp_water*(T[23]-T[0])
Ex_dot_dwh=Ex_dot[21]-Ex_dot[18]
T_out_dwh=(T[18]+T[21]+T[22]+T[23])/4
Z_out_dwh=0.3*m_dwh
T_solar=(T[18]+T[19])/2
T_he=(T[2]+T[3]+T[20]+T[21])/4

Ex_dot_solar_cell=Q_solar*(1-ConvertTemp (C,K,T[0])/ConvertTemp (C,K,T_sun))
Eta_en_solar=(Q_he+Q_out_dwh)/Q_solar
Eta_ex_solar=(Q_he*(1-T[0]/T_he)+Q_out_dwh*(1-T[0]/T_out_dwh))/Ex_dot_solar_cell
Ex_d_solar_cycle=Ex_dot_solar_cell-Q_he*(1-T[0]/T_he)-Q_out_dwh*(1-T[0]/T_out_dwh)

//Two Stage Steam Cycle
Tthrottle2=400
PRR=137
pmedium2=pthrottle2/7
pcond2=1
etaturb=0.7
etapump=0.85
m_st=0.5
Q_he=m_st*(h[3]-h[2])

"Inlet of high pressure turbine"
p[3]=pthrottle2
T[3]=temperature(steam, h=h[3], P=P[3])
s[3]=entropy(steam,T=T[3],P=p[3])


"Inlet of low pressure turbine"
s4s=s[3]
p[4]=pmedium2
h4s=enthalpy(steam,S=s4s,P=p[4])
h[4]=h[3]-etaturb*(h[3]-h4s)
T[4]=temperature(steam,H=h[4],P=p[4])
s[4]=entropy(steam,H=h[4],P=p[4])
x[4]=quality(steam,H=h[4],P=p[4])

"Inlet of condenser"
s5s=s[4]
p[5]=pcond2
```

```
h5s=enthalpy(steam,S=s5s,P=p[5])
h[5]=h[4]-etaturb*(h[4]-h5s)
T[5]=temperature(steam,H=h[5],P=p[5])
s[5]=entropy(steam,H=h[5],P=p[5])
x[5]=quality(steam,H=h[5],P=p[5])

"Inlet of pump"
p[1]=p[5]
h[1]=enthalpy(steam,P=p[1],X=0)
s[1]=entropy(steam,P=p[1],X=0)
T[1]=temperature(steam,P=p[1],X=0)
Tcond2=T[1]

"Inlet of boiler"
s2s=s[1]
p[2]=pthrottle2
h2s=enthalpy(steam,S=s2s,P=p[2])
h[2]=h[1]+(h2s-h[1])/etapump
T[2]=temperature(steam,H=h[2],P=p[2])
s[2]=entropy(steam,H=h[2],P=p[2])

"Work and heat calculations"
wout2=h[3]-h[5]
qout2=h[5]-h[1]
win2=h[2]-h[1]
qin2=h[3]-h[2]

"Thermal efficiency"
eta2=(wout2-win2)/qin2
etaCarnot2=1-(converttemp('K','R',Tcond2))/(converttemp('K','R',Tthrottle2))
epsilon2=eta2/etaCarnot2
Q_condenser1=m_st*(h[5]-h[1])
T_condenser1=(T[1]+T[5]+T[8]+T[9])/4
Ex_dot_steam=Q_he*(1-T[0]/T_he)-Q_condenser1*(1-T[0]/T_condenser1)-W_dot_ee-
W_dot_ell+W_dot_pumpp
Eta_en_steam=(W_dot_ee+W_dot_ell-W_dot_pumpp)/Q_he
Eta_ex_steam=(Q_condenser1*(1-T[0]/T_condenser1)+W_dot_ee+W_dot_ell-
W_dot_pumpp)/(Q_he*(1-T[0]/T_he))
P[2]=P[1]*PRR
h[3]=h[4]+w_ee
m_st*w_ee=W_dot_ee
h[4]=h[5]+w_ell
m_st*w_ell=W_dot_ell
W_dot_pumpp=m_st*win2

//Two Stage Rankine Cycle
pthrottle=PR*pcond
PR=137
pmedium=20
pcond=1
x=0.2
```

```
m_r=0.5
Q_condenser1=m_r*(h[9]-h[8])

"Inlet of turbine"
T[9]=Tthrottle
p[9]=pthrottle
CALL NH3H2O(123,T9,P9,x: T[9],P[9],x[9],h[9],s[9],u[9],v[9],q[9])

"Inlet of low pressure turbine"
CALL NH3H2O(235,P[10],x,s[9]: T10s,P10s,x10s,h10s,s10s,u10s,v10s,q10s)
p[10]=pmedium
h[10]=h[9]-etaturb*(h[9]-h10s)
CALL NH3H2O(234,P10,x,h10: T[10],P[10],x[10],h[10],s[10],u[10],v[10],q[10])

"Inlet of condenser"
p[11]=pcond
h[11]=h[10]-etaturb*(h[10]-h11s)
CALL NH3H2O(234,P11,x,h11: T[11],P[11],x[11],h[11],s[11],u[11],v[11],q[11])
CALL NH3H2O(235,P[11],x,s[10]: T11s,P11s,x11s,h11s,s11s,u11s,v11s,q11s)

"Inlet of pump"
p[7]=p[11]
q[7]=0
CALL NH3H2O(238,P7,x,q7: T[7],P[7],x[7],h[7],s[7],u[7],v[7],q[7])
Tcond=T[7]

"Inlet of boiler"
CALL NH3H2O(235,P[8],x,s[7]: T8s,P8s,x8s,h8s,s8s,u8s,v8s,q8s)
h[8]=h[7]+(h8s-h[7])/etapump
CALL NH3H2O(234,P8,x,h8: T[8],P[8],x[8],h[8],s[8],u[8],v[8],q[8])

"Work and heat calculations"
wout=h[9]-h[11]
qout=h[10]-h[7]
win=h[8]-h[7]
qin=h[9]-h[8]

"Thermal efficiency"
eta=(wout-win)/qin
etaCarnot=1-(converttemp('F','R',Tcond))/(converttemp('F','R',Tthrottle))
epsilon=eta/etaCarnot
T[13]=273+60
Q_out=m_r*(h[11]-h[7])
T_out=(T[7]+T[11]+T[12]+T[13])/4
Ex_dot_rankine=Q_condenser1*(1-T[0]/T_condenser1)-Q_out*(1-T[0]/ConvertTemp (C,K,T_out))-
W_dot_e-W_dot_el+W_dot_pump
Eta_en_rankine=(W_dot_e+W_dot_el-W_dot_pump)/Q_condenser1
Eta_ex_rankine=(Q_out*(1-T[0]/T_out)+W_dot_e+W_dot_el-W_dot_pump)/(Q_condenser1*(1-
T[0]/T_condenser1))
P[8]=P[7]*PR
h[9]=h[10]+w_e
```

```
m_r*w_e=W_dot_e
P[13]=P[7]
CALL NH3H2O(123,T[13],P[13],x: Tc13,Pc13,x[13],h[13],s[13],u[13],v[13],q[13])
h[10]=h[11]+w_el
m_r*w_el=W_dot_el
W_dot_pump=m_r*win

//Desalination
T[12]=273+18 [C] "sea water temperature"
T_h=T[11]
N=15
S=35 [g/kg]
l_v=(SW_LatentHeat(T_b1-273,S)+SW_LatentHeat(T_bN-273,S))/2000
c=(SW_SpcHeat(T_b1-273,S)+SW_SpcHeat(T_bN-273,S))/2000

Percent_recovery=m_f/m_d
m_f/m_d=l_v/(c*delta_f)+(N-1)/(2*N)
//m_d=mass rate of distillate (kg/h)
//m_f=mass rate of feed (kg/h)
//l_v=average latent heat of vaporization (kJ/kg)
//c=mean specific heat under constant pressure for all liquid streams (kJ/kg-K)
//N=total number of stages or effects
delta_f=(T_b1-T_bN)*N/(N-1)
//T_b1=temperature of brine in first effect (K)
//T_bN=temperature of brine in the last effect (K)
T_b1=T[13]
T_bN=T[16]
T[16]=273+35 [C]
Q_out=m_d*l_v*(t_h-T[12])/delta_f
//t_h=top brine temperature
Z_desalination=m_f*24*2000

//Electrolyzer
m_dot_h2=eta_electrolyzer*(W_e+W_el)/hhv_h2
m_dot_h2_daily=m_dot_h2*3600*24
eta_electrolyzer=0.6
hhv_h2=142.18e6 "J/kg"
Ex_dot_h2=m_dot_h2*(ex_h2_ch+ex_h2_ph)
ex_h2_ch=253153/MW_h2
MW_h2=MolarMass(H2) "kg/kmol"
ex_h2_ph=((h_h2-h[0])-T[0])*(s_h2-s[0])
h_h2=Enthalpy(H2,T=T[0])
s_h2=Entropy(H2,T=T[0],P=P[0])
Z_electrolyzer=1000*(W_e+W_el)

//33.4 kilowatt hours is also equivalent (in energy) to one kilogram of hydrogen gas
P_h2=33400*M_dot_h2

eta_en_system=(W_dot_e+W_dot_el+W_dot_ee+W_dot_ell)/(Q_solar+W_dot_pump+W_dot_pumpp)
```

```
eta_ex_system=(Q_out*(1-T[0]/ConvertTemp (C,K,T_out))+Q_out_dwh*(1-
T[0]/T_out_dwh)+W_dot_e+W_dot_el+W_dot_ee+W_dot_ell-W_dot_pump-
W_dot_pumpp)/Ex_dot_solar_cell
Ex_dot_system=Ex_dot_solar_cell-Q_out_dwh*(1-
T[0]/T_out_dwh)+W_dot_e+W_dot_el+W_dot_ee+W_dot_ell
CRF=(i*(1+i)^ny)/((1+i)^ny-1)
i=0.02 "interest rate"
ny=25 "total operating period of the system in years"
OH=5000 "annual number of operation hours"

W_total=W_dot_e+W_dot_el+W_dot_ee+W_dot_ell
```

For System 3:

```
//Solar Cycle
T[0]=273+23.3
P[0]=1
s[0] = entropy (water, T=T[0], P=P[0])
h[0] = enthalpy (water, T=T[0], P=P[0])
m_dot_oil=0.5 "kg/s"

//Boiler
P[43]=100 "bar"
h[43]=Enthalpy(Therminol_66, T=T[43], P=P[43])
s[43]=Entropy(Therminol_66, T=T[43])
Ex_dot[43]=m_dot_oil*((h[43]-h[0])-T[0]*(s[43]-s[0])) "kW"
Ex_dot_in=Ex_dot[43]-Ex_dot[44] "kW"
Q_he=m_dot_oil*(h[43]-h[44])
//Q_he=Q_solar/4 "kW"
T[44]=273+72.2


P[44] = P[43]
h[44]=Enthalpy(Therminol_66, T=T[44], P=P[44])
s[44]=Entropy(Therminol_66, T=T[44])
Ex_dot[44]=m_dot_oil*((h[44]-h[0])-T[0]*(s[44]-s[0]))

//Collector
Q_solar=m_dot_oil*(h[42]-h[48])
Q_solar=NS*Q_s
Q_s=A_ap*F_r*(SE-A_r/A_ap*U_l*(T[48]-T[0])) "W"
NS=1
w_col=2 "m"
D_o=0.040 "m"
A_ap=(w_col-D_o)*L "m2"
L=2 "m"
SE=G_b*eta_r
G_b=900 "W/m2"
eta_r=0.765
A_r=pi*D_o*L
```

```
F_1=(1/U_l)/(1/U_l+D_o/(h_cr*D_i)+(D_o/(2*k)*ln(D_o/D_i)))
U_l=15 "W/mK"
D_i=0.025 "m"
h_cr=200 "W/m2K"
k=16"W/m C"
F_r=m_dot_oil*cp_salt/(A_r*U_l*F_1)*(1-exp(-1/m_dot_oil*cp_salt/(A_r*U_l*F_1)))*F_1
T[48]=T[0]+5
//T[18]=273+40 [C]
P[48]=P[43]
h[48]=Enthalpy(Therminol_66, T=T[48], P=P[48])
s[48]=Entropy(Therminol_66, T=T[48])
Ex_dot[48]=m_dot_oil*((h[48]-h[0])-T[0]*(s[48]-s[0]))
Z_solar=310*L*w_col
cp_salt=Cp(Therminol_66, T=T[48])
T_sun=5778"K"


//Hot Storage
h_oa=1 "W/m2C" "heat transfer coefficient oil air"
eta_ins=0.3 "m" "insulation thickness"
k_pf=0.016 "W/mC" "polyurethane foam thermal conductivity"
1/U_hs=1/h_oa+eta_ins/k_pf "overall heat transfer coefficient"
A_hs=6 "m2" "cold storage surface area"
Q_hs=U_hs*(T[42]-T[0])*A_hs
m_dot_oil*(h[42]-h[43])=Q_hs
h[42]=Enthalpy(Therminol_66, T=T[42], P=P[42])
s[42]=Entropy(Therminol_66, T=T[42])
Ex_dot[42]=m_dot_oil*((h[42]-h[0])-T[0]*(s[42]-s[0]))
P[42]=P[43]
Z_hs=27*Q_hs "K. Nithyanandam, R. Pitchumani "

//Hot Water
Q_dot_htg=m_dot_oil*(h[44]-h[48])
T_he=(T[43]+T[44]+T54+T55)/4
Ex_dot_solar_cell=Q_solar*(1-ConvertTemp (C,K,T[0])/ConvertTemp (C,K,T_sun))
Eta_en_solar=(Q_he+Q_dot_htg)/Q_solar
Eta_ex_solar=(Q_he*(1-T[0]/T_he)+Q_dot_htg*(1-T[0]/T_htg))/Ex_dot_solar_cell
Ex_d_solar_cycle=Ex_dot_solar_cell-Q_he*(1-T[0]/T_he)-Q_dot_htg*(1-T[0]/T_htg)
OH=5000 "annual number of operation hours"

"Abs"
P[1]=250
Qua[1]=0.00
Call NH3H2O(238, ln1, x[4], Qua[1]: T[1], P[1]/100, x[1], h[1], s[1], u[1], v[1], Qu[1])
Q_dot_abs=m_dot[11]*h[11]+m_dot[16]*h[16]-m_dot[1]*h[1]
Ex_dot[16]=m_dot[16]*((h[16]-h[0])-T[0]*(s[16]-s[0]))
P[15]=P[2]
Call NH3H2O(234, ln100ab, x[12], In300bb: T[15], P[15]/100, x[15], h[15], s[15], u[15], v[15], Qu[15])
h[16]=h[15]
P[16]=P[1]
```

Call NH3H2O(234, ln100abb, x[12], In300bbb: T[16], P[16]/100, x[16], h[16], s[16], u[16], v[16], Qu[16])
T_abs=T[1]

EX_dot_abs_th=(1-(T_abs/T[0]))*Q_dot_abs

"Pump"
P[2]=400
x[2]=x[4]
T[2]=T[1]+0.4
Call NH3H2O(123, In10, In11, In12: T[2], P[2]/100, x[2], h[2], s[2], u[2], v[2], Qu[2])
W_dot_p=m_dot[2]*h[2]-m_dot[1]*h[1]

Ex_dot[1]=m_dot[1]*((h[1]-h[0])-T[0]*(s[1]-s[0]))
Ex_dot[2]=m_dot[2]*((h[2]-h[0])-T[0]*(s[2]-s[0]))
"LHX"
P[3]=P[2]
x[3]=x[4]
T[3]=T[19]+delta_T_HE
Call NH3H2O(123, In13, In14, In15: T[3], P[3]/100, x[3], h[3], s[3], u[3], v[3], Qu[3])
P[19]=P[2]
x[19]=x[2]
T[19]=T[2]
Call NH3H2O(123, In100a, In111b, In121c: T[19], P[19]/100, x[19], h[19], s[19], u[19], v[19], Qu[19])
P[14]=P[2]
Call NH3H2O(234, ln100a, x[12], In300a: T[14], P[14]/100, x[14], h[14], s[14], u[14], v[14], Qu[14])
m_dot[13]*h[13]+m_dot[23]*h[23]=m_dot[14]*h[14]
m_dot[19]*h[19]+m_dot[14]*h[14]=m_dot[3]*h[3]+m_dot[15]*h[15]
Ex_dot[14]=m_dot[14]*((h[14]-h[0])-T[0]*(s[14]-s[0]))
Ex_dot[3]=m_dot[3]*((h[3]-h[0])-T[0]*(s[3]-s[0]))
Ex_dot[19]=m_dot[19]*((h[19]-h[0])-T[0]*(s[19]-s[0]))
Ex_dot[15]=m_dot[15]*((h[15]-h[0])-T[0]*(s[15]-s[0]))

"HHX"
P[2]=P[20]
x[4]=x[20]
T[3]=T[20]
Call NH3H2O(123, In13a, In14a, In15a: T[20], P[20]/100, x[20], h[20], s[20], u[20], v[20], Qu[20])
P[2]=P[21]
x[4]=x[21]
T[3]=T[21]
Call NH3H2O(123, In13aa, In14aa, In15aa: T[21], P[21]/100, x[21], h[21], s[21], u[21], v[21], Qu[21])
m_dot[20]*h[20]+m_dot[12]*h[12]=m_dot[4]*h[4]+m_dot[13]*h[13]
P[13]=P[2]
Call NH3H2O(234, ln100, x[12], In300: T[13], P[13]/100, x[13], h[13], s[13], u[13], v[13], Qu[13])
Ex_dot[20]=m_dot[20]*((h[20]-h[0])-T[0]*(s[20]-s[0]))
Ex_dot[13]=m_dot[13]*((h[13]-h[0])-T[0]*(s[13]-s[0]))
Ex_dot[21]=m_dot[21]*((h[21]-h[0])-T[0]*(s[21]-s[0]))

"LTG"

P[22]=P[2]
Call NH3H2O(234, ln200, x[4], In400: T[22], P[22]/100, x[22], h[22], s[22], u[22], v[22], Qu[22])
P[23]=P[2]
x[23]=x[12]
T[23]=T[22]++delta_T_G
Call NH3H2O(123, In16a, In17a, In18a: T[23], P[23]/100, x[23], h[23], s[23], u[23], v[23], Qu[23])
P[6]=P[2]
Call NH3H2O(234, ln20abc, x[5], ln3001a: T[6], P[6]/100, x[6], h[6], s[6], u[6], v[6], Qu[6])
P[7]=P[2]
x[7]=x[5]
T[7]=T[22]-+delta_T_G
Call NH3H2O(123, In16aa, In17aa, In18aa: T[7], P[7]/100, x[7], h[7], s[7], u[7], v[7], Qu[7])
m_dot[22]*h[22]=m_dot[21]*h[21]+m_dot[18]*h[18]
-Q_dot_LTG=m_dot[22]*h[22]-m_dot[23]*h[23]-m_dot[7]*h[7]
m_dot[22]*h[22]+m_dot[5]*h[5]=m_dot[23]*h[23]+m_dot[7]*h[7]+m_dot[6]*h[6]
Ex_dot[22]=m_dot[22]*((h[22]-h[0])-T[0]*(s[22]-s[0]))
Ex_dot[23]=m_dot[23]*((h[23]-h[0])-T[0]*(s[23]-s[0]))

"HTG"
P[4]=P[2]
x[4]=0.6
T[4]=T[20]+delta_T_G
Call NH3H2O(123, In19, In20, In21: T[4], P[4]/100, x[4], h[4], s[4], u[4], v[4], Qu[4])
xa[5]=0.999
P[5]=P[2]
Call NH3H2O(234, ln20abd, xa[5], ln300bbc: T[5], P[5]/100, x[5], h[5], s[5], u[5], v[5], Qu[5])
P[12]=P[2]
x[12]=0.4
T[12]=T[4]+delta_T_G
Call NH3H2O(123, In25, In26, In27: T[12], P[12]/100, x[12], h[12], s[12], u[12], v[12], Qu[12])
-Q_dot_HTG=m_dot[4]*h[4]-m_dot[5]*h[5]-m_dot[12]*h[12]
Ex_dot[4]=m_dot[4]*((h[4]-h[0])-T[0]*(s[4]-s[0]))
Ex_dot[5]=m_dot[5]*((h[5]-h[0])-T[0]*(s[5]-s[0]))
Ex_dot[12]=m_dot[12]*((h[12]-h[0])-T[0]*(s[12]-s[0]))
T_HTG=(T[5]+T[4]+T[12])/3
EX_dot_HTG_th=(1-(T[0]/T_HTG))*Q_dot_HTG

"CHX"
P[17]=P[2]
x[17]=x[4]
T[17]=T[2]
Call NH3H2O(123, In10a, In11b, In12c: T[17], P[17]/100, x[17], h[17], s[17], u[17], v[17], Qu[17])
P[18]=P[2]
x[18]=x[4]
T[18]=T[17]+delta_T_HE
Call NH3H2O(123, In10aa, In11bb, In12cc: T[18], P[18]/100, x[18], h[18], s[18], u[18], v[18], Qu[18])
m_dot[6]*h[6]+m_dot[17]*h[17]=m_dot[8]*h[8]+m_dot[18]*h[18]
P[8]=P[2]
Call NH3H2O(234, ln20ab, x[5], ln3001: T[8], P[8]/100, x[8], h[8], s[8], u[8], v[8], Qu[8])
Ex_dot[6]=m_dot[6]*((h[6]-h[0])-T[0]*(s[6]-s[0]))
Ex_dot[17]=m_dot[5]*((h[17]-h[0])-T[0]*(s[17]-s[0]))

```
Ex_dot[18]=m_dot[18]*((h[18]-h[0])-T[0]*(s[18]-s[0]))

"cond"
Q_dot_con=Q_dot_htg-30
P[9]=P[2]
h[10]=h[9]
Call NH3H2O(234, In28a, x[5], In28c: T[9], P[9]/100, x[9], h[9], s[9], u[9], v[9], Qu[9])
Q_dot_con=m_dot[7]*h[7]+m_dot[8]*h[8]-m_dot[9]*h[9]
Ex_dot[7]=m_dot[7]*((h[7]-h[0])-T[0]*(s[7]-s[0]))
Ex_dot[8]=m_dot[8]*((h[8]-h[0])-T[0]*(s[8]-s[0]))
Ex_dot[9]=m_dot[9]*((h[9]-h[0])-T[0]*(s[9]-s[0]))
T_con=T[9]

EX_dot_con_th=(1-(T_con/T[0]))*Q_dot_con

"EVA"
P[10]=P[1]
Call NH3H2O(234, ln1001, x[5], In3001: T[10], P[10]/100, x[10], h[10], s[10], u[10], v[10], Qu[10])
P[11]=P[1]
x[11]=x[5]
T[11]=-13.5+273.15
Call NH3H2O(123, In4, In5, In6: T[11], P[11]/100, x[11], h[11], s[11], u[11], v[11], Qu[11])
Q_dot_eva=m_dot[11]*h[11]-m_dot[10]*h[10]
Ex_dot[11]=m_dot[11]*((h[11]-h[0])-T[0]*(s[11]-s[0]))
Ex_dot[10]=m_dot[10]*((h[10]-h[0])-T[0]*(s[10]-s[0]))
T_eva=(T[11]+T[10])/2

EX_dot_eva_th=(1-(T_eva/T[0]))*Q_dot_eva

"Mass"
m_dot[1]=1
m_dot[2]=m_dot[1]
m_dot[19]=0.8*m_dot[2]
m_dot[17]=0.2*m_dot[2]
m_dot[3]=m_dot[19]
m_dot[18]=m_dot[17]
m_dot[20]=0.8*m_dot[3]
m_dot[21]=0.2*m_dot[3]
m_dot[4]=m_dot[20]
m_dot[4]=m_dot[5]+m_dot[12]
m_dot[4]*x[4]=m_dot[5]*x[5]+m_dot[12]*x[12]
m_dot[13]=m_dot[12]
m_dot[14]=m_dot[13]+m_dot[23]
m_dot[22]=m_dot[21]+m_dot[18]
m_dot[22]=m_dot[7]+m_dot[23]
m_dot[6]=m_dot[5]
m_dot[8]=m_dot[5]
m_dot[9]=m_dot[7]+m_dot[8]
m_dot[10]=m_dot[9]
m_dot[11]=m_dot[10]
m_dot[15]=m_dot[14]
```

```
m_dot[16]=m_dot[15]
m_dot[22]*x[22]=m_dot[7]*x[7]+m_dot[23]*x[23]

COP=Q_dot_eva/(Q_dot_HTG+W_dot_p)
COP_EX=(EX_dot_eva_th/(EX_dot_HTG_th+W_dot_p))

eta_en_system=(W_net)/(Q_solar+W_pump)
eta_ex_system=(Q_dot_eva*(1-T[0]/ConvertTemp (C,K,T_eva))+W_net)/Ex_dot_solar_cell
Ex_dot_system=Ex_dot_solar_cell-Q_dot_eva*(1-T[0]/T_eva)+W_turb
```